/
Article / Book Information

(　)	
Title(English)	An experimental study of seepage-induced transport of fines in embankments
(　)	
Author(English)	Kazuki Horikoshi
(　)	：　　　　　　， ：　　　　　　　　　， ：　　9977　， ：2015　9　25　， ：　　　　， ：　　　，　　　　，　　　　，　　　，
Citation(English)	Degree:, Conferring organization: Tokyo Institute of Technology, Report number:　　9977　, Conferred date:2015/9/25, Degree Type:Course doctor, Examiner:,,,,
(　)	
Type(English)	Doctoral Thesis

An Experimental Study of Seepage-induced Transport of Fines in Embankments

Kazuki Horikoshi

Tokyo Institute of Technology

2015

An Experimental Study of Seepage-induced Transport of Fines in Embankments

Kazuki Horikoshi

DISSERTATION

submitted in partial fulfillment of the requirements for the degree of

DOCTOR OF PHILOSOPHY

at

TOKYO INSTITUTE OF TECHNOLOGY

Acknowledgements

Contens

LISTS OF FIGURES

Chapter 5

Chapter 6

Chapter 7

LIST OF PHOTOGRAPH

LISTS OF TABLE

NOTATION

a empirical material parameter

b empirical material parameter

B the bulk modulus

c empirical material parameter

CC the curvature coefficient

CU the uniformity coefficient

C_c the mass fraction of the coarse particles

$C_2^{''}$ the empirical parameter that depends on the packing coefficient

C_{ef} the fines concentration in fluid pore

d the particle diameter

$d*$ dimensionless diameter

D_{50} the median grain size

D_{10} the effective grain size

D_{15c} the diameter of the 15% mass passing the coarser fraction (filter material)

d_{15f} the diameter of the 15 %mass passing the finer fraction (base material)

d_{85f} the diameter of the 85% mass passing the finer fraction (base material)

d_1 empirical material parameter

d_2 empirical material parameter

D_r the relative density

Dr_s the relative density of the coarse skeleton

D_h^c the Kozeny effective diameter of coarse fraction

D_i^c the average diameter in the i-th interval of the particle size distribution curve of

coarse fraction

e the void ratio

e_c the void ratio of coarse particles

e_{max} the maximum void ratio

e_{min} the minimum void ratio fraction

E the solid discharge by unit surface area

E^* the dimensionless solid discharge

F the force

f_c the fines contents represented by volume ration

f_c'   The fines content contained both trapped fines in pore fluid and fines remaining in the soil skeleton by volume ration

f_{co} the initial fines content

$f_{c\infty}$ the ultimate fines content

FC the mass fraction of the fine particles

f_L the friction factors relating shear stress to the mean flow velocity under laminar flow conditions

f_T the friction factors relating shear stress to the mean flow velocity under turbulent flow conditions

F_i^c the weight of grains in the i-th interval of the particle size distribution curve of coarse fraction

G the gravity

G_s the specific gravity of the solid

h the head

i the hydraulic gradient

i_{cr} the critical hydraulic gradient defined by Terzaghi

i_{sc} the critical gradient for suffusion

k the hydraulic conductivity of the soil

k_{wu} the unsaturated hydraulic conductivity

K the intrinsic permeability

k_{er} the erosion coefficient

l the dimension

l_{us} empirical pore-connectivity parameter

m empirical parameter

m_w the mass of water

m_s the mass of soil particles

$\dot{m}_{ef}$ the rate of increase of the fines moving within a unit volume of the pore

n the porosity

n_c the porosity of skeleton

n_f the average porosity of fine particles

n_{VG} empirical parameter

p the pressure

q_s the function of transport rate of erosion per unit width

q_s^* the dimensionless sediment flux

$\overline{q}_e$ the mass of eroded fines per unit volume and time on boundary $\Gamma_{\rho e}$

Q the flow rate

Q_e the mass change of trapped fines into pore fluid in the soil element due to erosion per unit volume

r the diameter of the pipe

R the capillary radius

s the ratio of solid to fluid density

S_r the degree of saturation

S_e the effective saturation

t the time

T the surface tension

v the velocity

v_c the critical seepage velocity

v_r reference velocity (material parameter)

V the total volume V of soil

V_a the volume of air

V_w the volume of water

V_s the volume of solids

V_{sk} the volume of the solid in the soil skeleton

V_{sc} the volume of the coarse soil

V_{sf}	the volume of the fine soil
V_l	the volume of the fluid mixture
V_{ef}	the volume of trapped fines into fluid
V_v	the volume of voids
w	the water content
z	the position head
α	the stress reduction factor
α_D	the shape coefficient
α_{VG}	empirical parameter
β	the unitless proportionality coefficient
θ	the volume water content
θ_r	the residual water content
θ_s	the saturated water content
θ_{sl}	slope angle
$\dot{\varepsilon}_{er}$	the erosion rate (the mass of soil eroded per unit area and time)
μ	the viscosity
o_{50}	the average capillary tube diameter of the coarser fraction
ρ	the density
ρ_w	the density of water
ρ_s	the density of soil
ρ_t	the wet density of soil
ρ_{sg}	the density of sediment grain
ρ_e	the mass of trapped fines in pore fluid per unit volume
ρ_l	the mass of pore fluid per unit volume
ρ_f	the current the density of fines transported by the seepage flow in the soil element
σ'_f	portion of the effective stress on the fine particles
σ'_v	the vertical effective stress
τ	the shear stress between the flowing liquid and the soil
τ_c	the critical shear stress

τ^* the dimensionless shear stress

ϕ the internal friction angle

Chapter 1   Introduction

1.1. Background

In recent earthquakes which occurred in the mountain area, such as the 2007 Noto Hanto Earthquake, most of the damages of houses, roads and railways were associated with the failure of fills built on catchment topography.   The past earthquakes have underscored the vulnerability of valley fills.   The 2009 Suruga Bay Earthquake inflicted social loss due to a valley fill collapse in the Tomei Expressway, one of the busiest expressways in Japan. Moreover, the 2011 Great East Japan Earthquake caused failure of the valley fills in many places.   Fills built on catchment topography such as valley and swamp areas had been subjected to convergent flow.   It is possible that those fills had suffered from years of erosion inside of soil, which chronically loosened the soil packing.   Indeed, numerous soil structure failures reported in the literatures may have been attributed to soil erosion. Erosion-induced convergent flow sometime forms "pipe" or conduits which is called "macropores" in hydrology literature, where the channel part of matrix flow is relatively rapid than adjacent areas.   The existence of local large void or relatively-rapid channel causes the washing out of fines (Yamamoto *et al.* 2009; Shido 1993).   This fines erosion might lead to significantly increasing hydraulic conductivity and decreasing soil strength (Ke and Takahashi, 2012).   Ground disasters caused by fines loss have not only occurred in valley fill, but also in reclaimed land (Khomenko, 2006; Kuwano *et al.*, 2012) and hydraulic structure.

The detachment or migration of fines inside the void of a coarse skeleton by seepage inside ground is called "suffusion," one of the modes of internal erosion, in geotechnical engineering.   Suffusion is known as one of the causes of the deterioration of the hydraulic structure, in severe cases, triggering the failure of the hydraulic structure.   Costa (1985) showed that major cause of failure of fill dams was piping and seepage.   According to the statistical analysis on dam failures by Foster *et al.* (2000), approximately half embankment dam failure or damage are related to internal erosion including suffusion.   Fry *et al.* (2012)

presented similar statistics by using the 47 failures collected from February 2010 to April 2012.

The process of dam failure by internal erosion and piping is classified into four phases: initiation and continuation of erosion, progression to form a pipe, and formation of a breach (Foster and Fell, 1999). Foster and Fell (1999) described this erosion process by detailed event trees. Some of these processes show failure initiated by suffusion in embankment or foundation, which is the target of this study.

Suffusion might develop for phases of initiation and continuation of erosion in the failure scenarios initiated by suffusion. This phenomenon is a potential risk for long-term stability of the hydraulic structure over a period of years. In these phases, the performance of hydraulic structure, e.g. hydraulic and mechanical characteristics, might deteriorate progressively. On the other hand, time scale for phases related to piping, progression to form a pipe phase and formation of a breach phase, are relatively short, compared with time scale for phases of initiation and continuation of erosion. In other words, the hydraulic structure is in phases of these initiation or continuation of erosion for most of the service life. However, currently, the detail process of suffusion inside a hydraulic structure is not fully understood. Therefore, this study focuses on suffusion development phase includes initiation and continuation of erosion phases.

1.2. Objectives

The goal of this dissertation is to examine the seepage-induced suffusion process in an embankment with foundations during the phases of initiation and continuation of erosion for prediction of failure of a hydraulic soil structure. To achieve the goal, objectives of this dissertation are:

1. Firstly, to reproduce the seepage-induced suffusion with the small-scaled model in the laboratory.
2. Secondly, to identify the seepage-induced suffusion process in embankment with foundation and to demonstrate the applicability and limitations of existing erosion model, a series of physical model tests on the seepage-induced suffusion on a small-scaled homogeneous model embankment is conducted, and then the physical model test is numerically simulated.

3. Finally, to investigate the cause of redeposition of fines and its consequences on the suffusion process, a series of physical model tests on the small-scaled model embankment on foundation ground with different fines contents is performed.

1.3. Layout of the dissertation

This dissertation is composed of 8 chapters.

Chapter 1 is the current chapter which introduces the background of the research.

Chapter 2 summarizes previous studies on internal erosion (suffusion).

Chapter 3 presents reviews existing scaling laws and states limitations of small-scaled physical model tests.

Chapter 4 explores ways to reproduce suffusion in small model and determines experimental conditions for tests in Chapters 5 and 7.

Chapter 5 identifies the seepage-induced suffusion process in a homogenous embankment through the physical model tests with homogenous embankment model.

Chapter 6 presents numerically simulation of the physical model tests described in Chapter 5 and points out the applicability and limitations of existing erosion models.

Chapter 7 investigates the cause of redeposition of fines and its consequences on the suffusion process through the physical model tests with two layers foundation.

Conclusions and recommendations of this study are presented in Chapter 8.

REFFERENCES

Costa, J. E. 1985. Floods from dam failures, U.S. Geological Survey Open-File Report, U.S. Geological Survey.

Foster, M. & Fell, R. 1999. A framework for estimating the probability of failure of embankment dams by internal erosion and piping using event tree methods, UNICIV reports, 377, University of New South Wales.

Foster, M., Fell, R. & Spannagle, M. 2000. The statistics of embankment dam failures and accidents. *Canadian Geotechnical Journal,* 37(5)**,** pp. 1000-1024.

Fry, J. J., Vogel, A., Royet, P. & Courivaud, J. R., Dam failures by erosion: lessons from ERINOH data bases. *Proceedings of the 6th International Conference on Scour and Erosion.* 2012, Paris, pp. 273-280.

Ke, L. & Takahashi, A. 2012. Strength reduction of cohesionless soil due to internal erosion induced by one-dimensional upward seepage flow. *Soils and Foundations,* 52(4)**,** pp. 698-711.

Khomenko, V. P. Suffosion hazard: Today's and tomorrow's problem for cities. 10th IAEG International Congress, 2006 Nottingham. pp. 1-8.

Kuwano, R., Kohata, Y. & Sato, M. A case study of ground cave-in due to large scale subsurface erosion in old land fill, *Proceedings of the 6th International Conference on Scour and Erosion* 2012, Paris. pp. 265-271.

Shindo, S. 1993. Convergent flow of subsurface water concerned with slope failure. *The Quaternary Research,* 35(5)**,** pp. 315-322. (In Japanese).

Yamamoto, T., Nakai, T., Maruki, Y., Kodaka, T., Kishida, K. & Ohnishi, Y. 2009. Health assessment of the slopes along the roads introducing the long-term degradation concept. *Japanese Geotechnical Journal,* 4(1)**,** pp. 21-33. (In Japanese).

Chapter 2   Literature review

2.1. Introduction

The aim of this Chapter is to review previous studies on seepage-induced problem in the geotechnical engineering.   Section 2.2 describes the internal erosion, which is a focus of this study.   Section 2.3 discusses the internal erosion process in a hydraulic structure according to several investigation on dam's failure or damage.   In Section 2.4, controlling factors of internal erosion, especially suffusion, are summarized from previous elemental seepage test on internal instability of soils.   Hydraulic characteristics after suffusion are described in Section 2.5.   Finally in Sections 2.6 and 2.7, modeling studies considering the geometry of a real structure in suffusion problem are introduced.

2.2. Terminologies for seepage-induced problems in geotechnical engineering

Internal erosion, as its name indicates, is erosion in the ground.   This phenomenon is well-known as a potential risk for the long-term stability of hydraulic soil structure, such as dams and levees.   Types of internal erosion include concentrated leak erosion, contact erosion, backward erosion, and suffusion (Fry, 2012; Fell and Fry, 2013).   Concentrated leak erosion is driven by seepage flow in the opening (crack or cavity).   It detaches particles from the sides of the opening (Fig. 2-1).   Contact erosion is the erosion of particles at the interface between fine and coarse layers due to a quasi-horizontal groundwater flow as shown Fig. 2-2(a).   There are several types of configurations according to interface, gravity and flow direction (Fig.2-2 (b)).   Backward erosion describes the erosion of soil particles at the exit end of a seepage path, such as leaking through the downstream surface due to a high exit velocity or hydraulic gradient.   Suffusion describes the phenomenon that finer particles are eroded through the voids between the coarse particles by seepage flow as shown Fig.2-3.   It is also described as "a special case of backward erosion peculiar to gap graded soil" (Richards and Reddy, 2014).   This dissertation focuses on the suffusion phenomenon.   Suffusion occurs at a hydraulic gradient of about one-third to one-fifth of Terzaghi's critical gradient method for homogeneous granular soil (Skempton and Brogan, 1994).

Moffat *et al*. (2011) defined suffusion as the phenomenon that "the finer fraction of an internally unstable soil moves within the coarser fraction without any loss of matrix integrity or change in total volume," whereas for suffosion, "particle migration yields a reduction in total volume and a consequent potential for collapse of the soil matrix". In this dissertation, the widely accepted term "suffusion" is used.
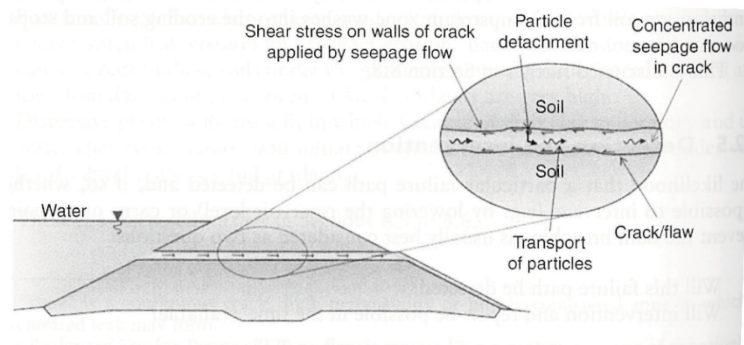
Figure 2-1   Diagram of detachment transport of particles in concentrated leak erosion

(Fell *et al*.2014)
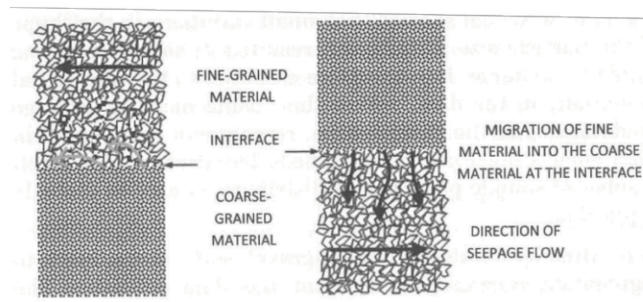
(a)   Diagram of contact erosion (Fell and Fry, 2013)

(b) Diagram of different base contact erosion (Philippe *et al*.,2013)

Figure 2-2   Diagram of contact erosion
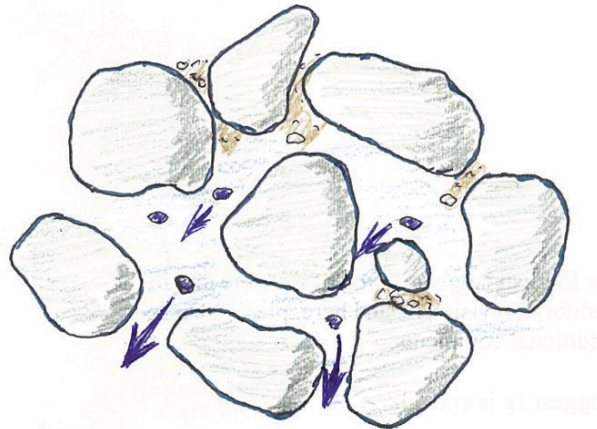
Figure 2-3   Illustration of the concept of suffusion

2.3. Statistical investigation on internal erosion process

The process of dam failure by internal erosion and piping is classified into four phases: initiation and continuation of erosion, progression to form a pipe, and formation of a breach (Foster and Fell, 1999).   Foster and Fell (1999) described this erosion process by detailed event trees.   Some of these processes show failure initiated by suffusion in embankments or foundations, which is the target of this study.   Figure 2-4 shows an example of these event trees initiated by suffusion in embankment.
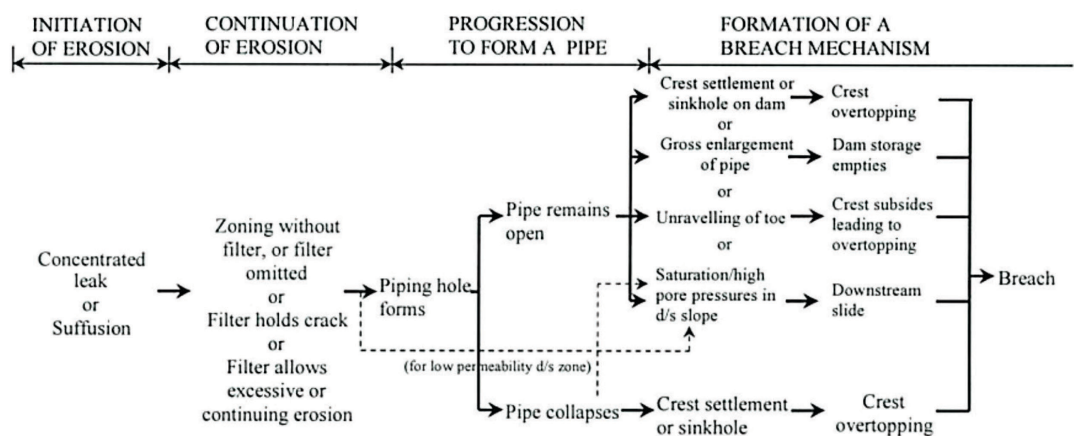
(a)   Event trees of failure of dams initiated by suffusion (Foster and Fell, 1999)
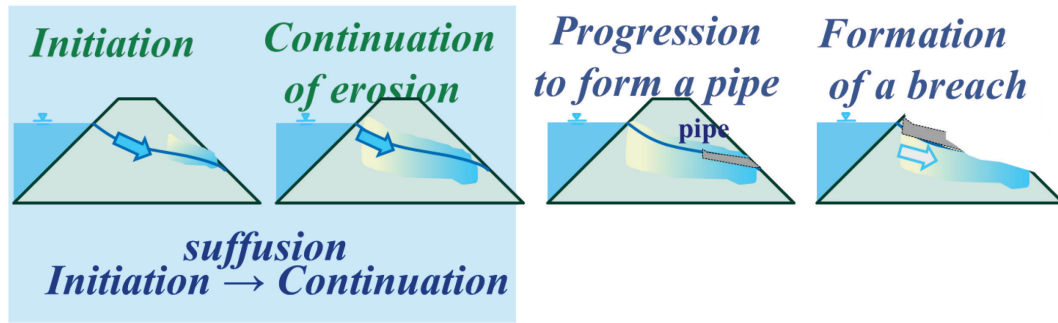
(b)   Illustration of failure of dams initiated by suffusion

Figure 2-4   Process of dam's failure by internal erosion (Foster and Fell, 1999)

Suffusion might be developed in phases of initiation and continuation of erosion in the failure scenarios (Foster and Fell, 1999). If suffusion occurs in the filling, the hydraulic (Bendahmane *et al.*, 2006, 2008; Sail *et al.*, 2011; Marot *et al.*, 2011; Moffat *et al.*, 2011; Luo *et al.*, 2012) and mechanical (Miur Wood *et al.*, 2010; Ke and Takahahi, 2012, 2014a, 2014b, 2015; Chang and Zhang, 2013, 2014; Shire *et al.* 2014; Sato, 2014) characteristics of soil are rapidly altered. That is deterioration of hydraulic structure, which is firstly developed in initiation phase. This phenomenon is known as a potential risk for long-term stability of the hydraulic structure over a period of years (Fell *et al.* 2001, 2003). In continuation phase, the performance of a hydraulic structure, e.g. hydraulic and mechanical characteristics, might deteriorate progressively. On the other hand, the time scale for phases related to piping, progression to form a pipe phase and formation of a breach phase, are relatively short, compared with the time scale for phases of initiation and continuation of erosion (Fell *et al.* 2001, 2003). In other words, the hydraulic structure is in phases of the initiation or continuation of erosion for most of its service life. Therefore, this study focuses on the suffusion development phase that includes initiation and continuation of erosion phases. The concept diagram of temporal deterioration of hydraulic structure is shown in Fig. 2-5.
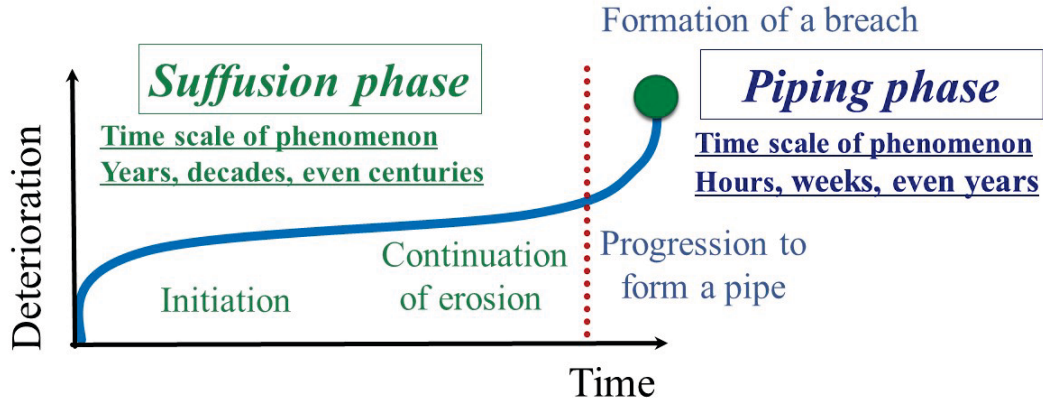
Figure 2-5   Diagram of temporal deterioration of hydraulic structure

2.4. Study for predicting initiation of internal erosion (suffusion)

2.4.1.   Over review of current studies on suffusion

For the initiation phase in the failure process of embankment dams, there are many suffusion and internal instability researches based on one-directional upwards or downwards seepage experiments; the initiation of this phenomenon depends on the particle size ratio between finer fraction and coarse fraction (*e.g.* Honjo *et al.*, 1996; Terzaghi, 1939), particle size distribution (*e.g.* Kenney and Lau, 1985; Li and Fannin, 2008; Wan and Fell, 2008; Chang and Zhang, 2013; Moraci *et al.*, 2014), particle shape (Marot *et al.*, 2012), the confining pressure (*e.g.* Bendahmane *et al.*, 2008; Moffat and Fannin, 2011), hydraulic gradient (*e.g.* Skempton and Brogan, 1994; Sterpi, 2003), flow velocity (Perzlmaier *et al.*, 2007), and seepage angle (Richards and Reddy, 2012, 2014), among the other factors.   Richards and Reddy (2014) suggested a methodology based on kinetic energy to predict suffusion and backward erosion initiation potential and performed analyses of factors of safety against these phenomena for a homogenous embankment model with a foundation.

2.4.2.   Particle size, Grain shape

Terzaghi (1939) proposed following filter criteria to prevent the migration of material into other zones of dam (Eq. 2.1) and to suppress the development of excess pore pressure in the dam (Eq. 2.2).

$$\frac{D_{15c}}{d_{85f}} < 4 \tag{2.1}$$

9

$$\frac{D_{15c}}{d_{15f}} > 4 \qquad (2.2)$$

Here, D_{15c} is the diameter of the 15% mass passing the coarser fraction (filter material), d_{85f} and d_{15f} are the diameter of the 15 and 85% mass passing the finer fraction (base material). The first criterion (Eq. 2.1) was applied for assessment of internal instability of soil by dividing material into its finer fraction and coarser fraction (Kezdi, 1979). Kenney and Lau (1985, 1986) deducted criterion based on shape of grain size distribution for the assessment of soil internal instability based on grain size distribution. Based on these criteria, further geometric criteria have been developed according to the results of the one-directional upwards or downwards seepage tests.

2.4.3. Hydraulic constraint (Hydraulic gradient, flow velocity)

Terzaghi defined the well-known critical hydraulic gradient to cause piping failure in homogeneous granular soil as follows:

$$i_{cr} = \frac{G_s - 1}{1 + e} \qquad (2.3)$$

where, G_s is the density of soil particles. This critical hydraulic gradient does not always fit with all soils. For internal instability of soils, suffusion occurs at a hydraulic gradient of about one-third to one-fifth of Terzaghi's critical gradient (*e.g.* Skempton and Brogan, 1994). Therefore, several studies presented the critical hydraulic gradient for initiation of suffusion (Skempton and Brogan, 1994; Monnet, 1998 (referred in Bonelli, 2012); Li and Fannin, 2012). Some studies focused on the flow velocity (Perzlmaier *et al.*, 2007) and they showed threshold velocity for fines migration.

2.4.4. Effects of stress state

Ke and Takahashi (2014) carried out a series of one-dimensional downward seepage tests on gap-graded soil with fines contents of 35% under the several confining pressures and showed erosion potential decreases with an increasing in confining pressure. Bendahmane *et al.* (2008) also showed a similar tendency on different internally instable soil. Moffat *et al.* (2011) and, Moffat and Fannin (2011) demonstrated that an increase in effective confining pressure would cause an increase in the critical hydraulic gradient for erosion (Fig. 2-6). Tomlinson and Vaid (2000) investigated effect of the confining pressure on the initiation of piping experimentally. Their results indicate that (a) the confining pressure has a certain

influence on internal stability if the particle size ratio D_{15c}/d_{85f} between coarse particles and fines is not so large and (b) the particle size ratio D_{15c}/d_{85f} is the most important parameter for the initiation of piping.
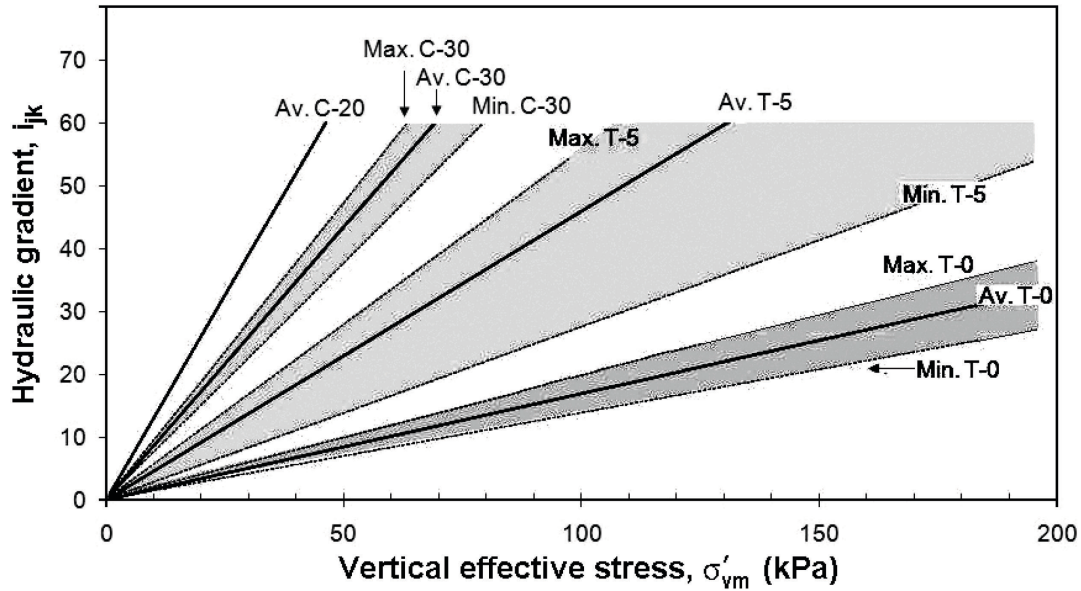
Figure 2-6   Hydromechanical boundaries

in stress–gradient space (Moffat and Fannin, 2011)

2.5.   Studies on progression of suffusion

In the continuation erosion phase, the development of erosion depends on the presence or absence of an adequate filter or transition zone (Foster and Fell, 1999).   Moffat et al. (2011) showed spatial and temporal progression of seepage-induced internal instability, which included suffusion and suffosion from initiation to progression in a one-dimensional seepage field.   They observed the specimen condition through the transparent wall and measured the local hydraulic gradient in the specimen.   However, one-dimensional seepage tests by Bendahmane et al. (2006) and Bendahmane et al. (2008) showed decreases in hydraulic conductivity with elapsed time.   The decrease in hydraulic conductivity indicates that, in some cases, suffusion leads to clogging in the soil specimen.   Luo et al. (2012) described the evolution of suffusion in pore scale as: "fine particles migration $\rightarrow$ pores clogging $\rightarrow$ pushing out clogging pores $\rightarrow$ fine particles remigration."   These observations in the laboratory were made in a relatively short period, i.e., days.   However, the time scale for

initiation and continuation of suffusion in a real embankment or foundation is very slow, i.e. from months up to years (Fell *et al.*, 2003).

2.6. Analytical studies

Most of suffusion studies mentioned above focused on the phenomenon in a uniform one-dimensional seepage field, while the seepage flow in a real structure is more complex and so is the suffusion progress.   However, there is little study considering the geometry of a real structure on suffusion in the initiation and continuation phases.   The laboratory experiments of Lindow *et al.* (2009) suggested that the failure mechanism due to seepage is dependent on slope angle.   Sterpi (2003), Cividini and Gioda (2004) and Cividini *et al.* (2009) carried out finite-element analyses to examine the spatial and temporal distribution of fines under seepage with free surface by modifying the erosion model proposed by Sterpi (2003). Uzuoka *et al.* (2012), Zhang *et al.* (2013) and Zhang *et al.* (2014) demonstrated the temporal change of fines within the "geometry" of the embankment by numerical simulations.

2.7. Physical model tests

Experimental studies for internal erosion have been conducted on piping (Sellmeijer *et al.*, 2011, Koelewijn *et al.*, 2014) and contact erosion (Beguin *et al.*, 2012) in large-scales.   To the author' knowledge, current physical model tests for suffusion are limited in the small-scaled model tests (Yanagishi *et al.*, 1998; Maknoon and Mahdi, 2010; Saito *et al.*, 2012). Yanagishi *et al.* (1998) contedted an about 3 years seepage test on fines migration around the drainage material.   After seepage testing, the fines content was examined.   Then, spatial distribution of fines content as shown in Fig. 2-7 was obtained.   Maknoon and Mahdi (2010) focused on the initiation of external suffusion due to the water level increasing at the upstream.   The study modeled the embankment as three soil layers and was carried out in a series of physical model tests on a laboratory scale with various geometries and types of the materials.   Saito *et al.* (2012) provided eight hours of water supply, 16 hours of drainage, and 180 repetitions to a physical model, which was made of pit sand mimicking a levee. After seepage testing, the fines content was examined at four locations within the model levee.
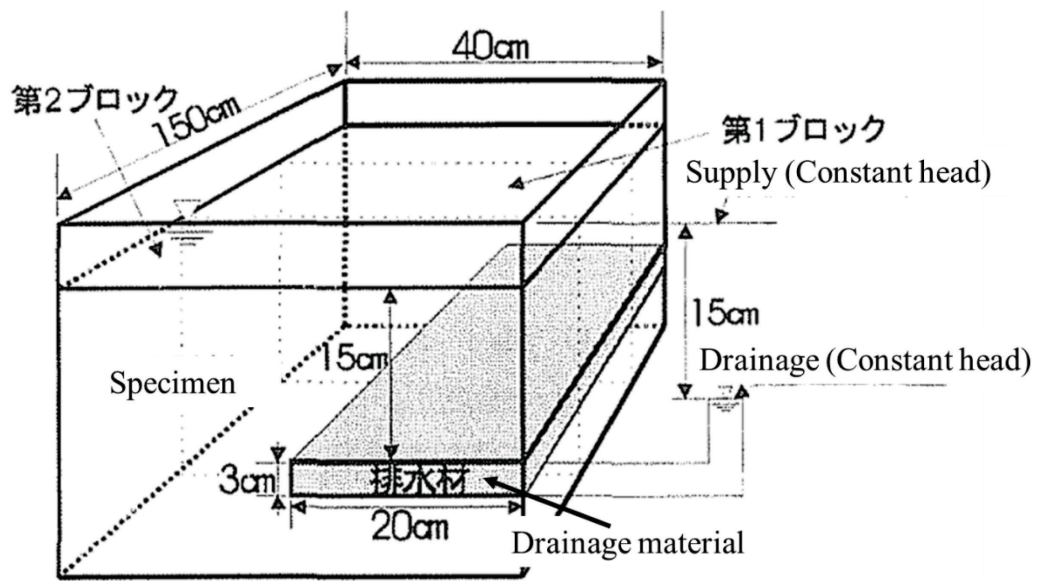
(a)   Experimental set up of Yamagishi *et al.* (1998)
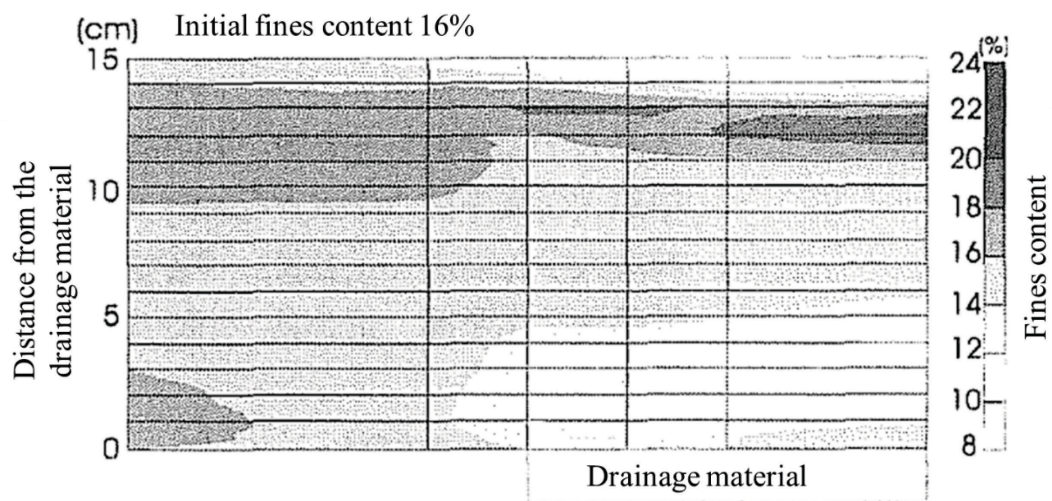
(b)   Spatial distribution around the drainage material after about 3years seepage

(Yamagishi *et al*.,1998)

Figure 2-7   Experiment of Yamagishi *et al*. 1998 (Yamagishi *et al*.,1998)

REFERENCES

Beguin, R., Fry, J. J., Picault, C., Courivaud, J. R., Faure, Y. H. & Philippe, P. Control of the risk of dike failure caused by contact erosion. *Proceedings of the 6th International Conference on Scour and Erosion*, 2012 Paris. pp. 1551-1558.

Bendahmane, F., Marot, D. & Alexis, A. 2008. Experimental parametric study of suffusion and backward erosion. *Journal of Geotechnical and Geoenvironmental Engineering,* 134(1)**,** pp. 57-67.

Bendahmane, F., Marot, D., Rosquoët, F. & Alexis, A. 2006. Characterization of internal erosion in sand kaolin soils. *European Journal of Environmental and Civil Engineering,* 10(4)**,** pp. 505-520.

Chang, D., Zhang, L. & Cheuk, J. 2014. Mechanical consequences of internal soil erosion. *HKIE Transactions,* 21(4)**,** pp. 198-208.

Chang, D. S. & Zhang, L. M. 2013. Critical Hydraulic Gradients of Internal Erosion under Complex Stress States. *Journal of Geotechnical and Geoenvironmental Engineering,* 139(9)**,** pp. 1454-1467.

Cividini, A., Bonomi, B., Vignati, G. C. & Gioda, G. 2009. Seepage-induced erosion in granular soil and consequent settlements. *International Journal of Geomechanics,* 9(4)**,** pp. 187-194.

Cividini, A. & Gioda, G. 2004. Finite-element approach to the erosion and transport of fine particles in granular soils. *International Journal of Geomechanics,* 4(3)**,** pp. 191-198.

Fell, R. & Fry, J. J. 2013. State of the art on the likelihood of internal erosion of dams and levees by means of testing. *In:* Bonelli, S. (ed.) *Erosion in Geomechanics Applied to Dams and Levees.* Londan, UK: ISTE-Wiley, pp. 1-99.

Fell, R., MacGregor, P., Stapledon, D., Bell, G. & Foster, M. 2014. *Geotechnical Engineering of Dams*, 2nd edn, Leieden, Netherlands: CRC Press/Balkema.

Fell, R., Wan, C. F., Cyganiewicz, J. & Foster, M. 2001. The time for development and detachability of internal erosion and piping in embankment dams and their foundation, Wales, UNICIV reports, 399, University of New South Wales, (Sidney).

Fell, R., Wan, C. F., Cyganiewicz, J. & Foster, M. 2003. Time for development of internal erosion and piping in embankment dams. *Journal of Geotechnical and Geoenvironmental Engineering,* 129(4)**,** pp. 307-314.

Foster, M. & Fell, R. 1999. A framework for estimating the probability of failure of embankment dams by internal erosion and piping using event tree methods, UNICIV reports, 377, University of New South Wales, (Sidney).

Fry, J. J. 2012. Introduction to the process of internal erosion in hydraulic structures: embankment dams and dikes. *In:* Bonelli, S. (ed.) *Erosion of Geomaterials.* London, UK: ISTE-Wiley, pp.1-36.

Honjo, Y., Haque, M. A. & Tsai, K. A. 1996. Self-filtration behavior of broadly and gap graded cohesionless soils. *Proceedings of the 2nd International Conference on Geofilters.* Montreal, pp. 227-236.

Ke, L. & Takahashi, A. 2012. Strength reduction of cohesionless soil due to internal erosion induced by one-dimensional upward seepage flow. *Soils and Foundations,* 52(4)**,** pp. 698-711.

Ke, L. & Takahashi, A. 2014a. Experimental investigations on suffusion characteristics and its mechanical consequences on saturated cohesionless soil. *Soils and Foundations,* 54(4)**,** pp. 713-730.

Ke, L. & Takahashi, A. 2014b. Triaxial erosion test for evaluation of mechanical consequences of internal erosion. *Geotechnical Testing Journal,* 37(2)**,** pp. 347-364.

Ke, L. & Takahashi, A. 2015. Drained monotonic responses of suffusional cohesionless soils. *Journal of Geotechnical and Geoenvironmental Engineering,* 141(8).

Kenney, T. C. & Lau, D. 1985. Internal stability of granular filters. *Canadian Geotechnical Journal,* 22(2)**,** pp. 215-225.

Kenney, T. C. & Lau, D. 1986. Internal stability of granular filters: Reply. *Canadian Geotechnical Journal,* 23(3)**,** pp 420-423.

Kezdi, A. 1979. *Soil Physics: Selected Topics (Developments in Geotechnical Engineering),* Amsterdam,New York: Elsevier Science.

Koelewijn, A. R., de Vries, G., van Lottu, H., Förster, U., van Beek, V. M. & Bezuijen, A. Full-scale testing of piping prevention measures: three tests at the Ijkdijk. *Proceedings of the 8th International Conference on Physical modelling in Geotechnics*, 2014, Perth. pp. 891-897.

Li, M. & Fannin, R. J. 2008. Comparison of two criteria for internal stability of granular soil. *Canadian Geotechnical Journal,* 45(9)**,** pp .1303-1309.

Li, M. & Fannin, R. J. 2012. A theoretical envelope for internal instability of cohesionless soil. *Géotechnique,* 62(1), pp. 77-80.

Lindow, N., Fox, G. & Evans, R. 2009. Seepage erosion in layered stream bank material. *Earth Surface Processes and Landforms,* 34, pp. 1693-1701.

Luo, Y., Qiao, L., Liu, X., Zhan, M. & Sheng, J. 2012. Hydro-mechanical experiments on suffusion under long-term large hydraulic heads. *Natural Hazards,* 65(3)**,** pp. 1361-1377.

Maknoon, M. & Mahdi, T. F. 2010. Experimental investigation into embankment external suffusion. *Natural Hazards,* 54(3)**,** pp. 749-763.

Marot, D., Bendahmane, F. & Konrad, J.-M. 2011. Multichannel optical sensor to quantify particle stability under seepage flow. *Canadian Geotechnical Journal,* 48(12)**,** pp. 1772-1787.

Marot, D., Bendahmane, F. & Nguyen, H. H. Influence of angularity of coarse fraction grains on internal erosion process. *Proceedings of the 6th International Conference on Scour and Erosion*, 2012, Paris. pp. 887-894.

Moffat, R. & Fannin, R. J. 2011. A hydromechanical relation governing internal stability of cohesionless soil. *Canadian Geotechnical Journal,* 48(3)**,** pp. 413-424.

Moffat, R., Fannin, R. J. & Garner, S. J. 2011. Spatial and temporal progression of internal erosion in cohesionless soil. *Canadian Geotechnical Journal,* 48(3)**,** pp. 399-412.

Moraci, N., Mandaglio, M. C. & Ielo, D. 2014. Analysis of the internal stability of granular soils using different methods. *Canadian Geotechnical Journal,* 51(9)**,** pp. 1063-1072.

Muir Wood, D., Maeda, K. & Nukudani, E. 2010. Modelling mechanical consequences of erosion. *Géotechnique,* 60(6)**,** pp. 447-457.

Perzlmaier, S., Muckenthaler, P. & Koelewijn, A. R. 2007. Hydraulic criteria for internal erosion in cohesionless soil. *In:* Fell, R. & Fry, J. J. (eds.) *Internal Erosion of Dams and Their Foundations.* London: Taylor & Francis Group.

Philippe, P., Beguin, R. & Faure, Y. 2013. Contact erosion. *In:* Bonelli, S. (ed.) *Erosion in Geomechanics Applied to Dams and Levees.* Wiley-ISTE, pp 179-190.

Richards, K. S. & Reddy, K. R. 2012. Experimental investigation of initiation of backward erosion piping in soils. *Géotechnique,* 62(10)**,** pp. 933-942.

Richards, K. S. & Reddy, K. R. 2014. Kinetic Energy Method for predicting initiation of backward erosion in earthen dams and levees *Environmental & Engineering Geoscience,* 20(1)**,** pp. 85-97.

Sail, Y., Marot, D., Sibille, L. & Alexis, A. 2011. Suffusion tests on cohesionless granular matter. *European Journal of Environmental and Civil Engineering,* 15(5)**,** pp. 799-817.

Saito, Y., Kuwano, R. & Sasaki, T. The model tests on a permeability of ground against repeated process of seepage. 47 th Japan National Conference on Geotechnical Engineering, 2012 Hachinohe. pp. 903-904. (In Japanese).

Sato, M. 2014. *Study on progress of internal erosion and its effects on mechanical properties.* Ph.D., The University of Tokyo, (In Japanese).

Sellmeijer, H., de la Cruz, J. L., Van Beek, V. M. & Knoeff, H. 2011. Fine-tuning of the backward erosion piping model through small-scale, medium-scale and IJkdijk experiments. *European Journal of Environmental and Civil Engineering,* 15(8), pp. 1139-1154.

Shire, T., O'sullivan, C., Hanley, K. J. & Fannin, R. J. 2014. Fabric and effective stress distribution in internally unstable soils. *Journal of Geotechnical and Geoenvironmental Engineering,* 140(12).

Skempton, A. W. & Brogan, J. M. 1994. Experiments on piping in sandy gravels. *Géotechnique,* 44(3)**,** pp. 449-460.

Sterpi, D. 2003. Effects of the erosion and transport of fine particles due to seepage flow. *International Journal of Geomechanics,* 3(1)**,** pp. 111-122.

Terzaghi, K. 1939. Soil mechanics: a new chapter in engineering science. *Journal of the Institution of Civil Engineers,* 12(7)**,** pp. 106-142.

Tomlinson, S. S. & Vaid, Y. P. 2000. Seepage forces and confining pressure effects on piping erosion. *Canadian Geotechnical Journal,* 37(1)**,** pp. 1-13.

Uzuoka, R., Ichiyama, T., Mori, T. & Kazama, M. Hydro-mechanical analysis of internal erosion with mass exchange between solid and water. *Proceedings of the 6th International Conference on Scour and Erosion*, 2012 ,Paris. pp. 655-662.

Wan, C. F. & Fell, R. 2008. Assessing the potential of internal instability and suffusion in embankment dams and their foundations. *Journal of Geotechnical and Geoenvironmental Engineering,* 134(3)**,** pp. 401-407.

Yamagishi, K., Takahashi, S., Nishibayashi, K., Nishida, T. & Shimizu, M. 1998. Characteristic of fine fraction movement around the drainage material in the permeability test. *32th Japan National Conference on Geotechnical Engineering.* Kumamoto, Japan. pp. 2033-2044. (In Japanese).

Zhang, X., Dong, J., Huang, Z., Nie, X., Wong, H. & Wang, J. X. 2014. Study of soil structures strength and stiffness loss based on thermodynamics and continuum mechanics. *Environmental Earth Sciences*, 73(8), pp. 4143-4149.

Zhang, X. S., Wong, H., Leo, C. J., Bui, T. A., Wang, J. X., Sun, W. H. & Huang, Z. Q. 2013. A Thermodynamics-Based Model on the Internal Erosion of Earth Structures. *Geotechnical and Geological Engineering,* 31(2)**,** pp .479-492.

Chapter 3 Scaling law

3.1. Introduction

Physical model tests are conducted systematically under carefully controlled conditions in order to find out partial or entire behavior of a physical object for the complexity engineering problem.   Moreover, to understand the phenomena which cannot be explained by theory, physical model tests may be performed.   It can also provide evidences that support the theory.

When we conduct physical model tests using a small model, idealization and/or simplification are introduced, which make the phenomena observed in the small-scaled model can differ from those in the full scale, i.e., in prototype.   In addition, the geometrically similar small model does not necessarily reproduce the same phenomena occur in the full scale.   To ensure the similarity between the small-scaled model and prototype, the scaling laws are required.   Yamaguchi (1980) defined the meaning of the scaling laws as follows:

   "*Scaling laws are that laws which prescribe how physical quantity obtained from model conducted under the similarity condition and that observed from prototype are related.*"

In the physical modelling, dimensionless products, composed of representative quantities and required to be equal for model and prototype, is denoted as π number. They are dimensionless products that play a key role on a phenomenon (Emori *et al.*, 2000).   There are three ways in deriving scaling laws by correlating physical quantities in the model and prototype (Emori *et al*., 2000; Yamaguchi, 1980).

(1) Scaling laws based on governing differential equation or its integrated form: It is a method to set up the π numbers as dimensionless numbers by obtaining the ratios of one term to the other term, utilizing the fact that each term has the same dimension in the differential equation.   This method is usually applied if there are governing equations that can describe the accurate behavior of the phenomenon.

(2) Parameter method: The method which lists relative parameters and set up the π numbers by combining several parameters into dimensionless groups according dimensional analysis.

(3) Principal π number method: To set up the scaling laws and the physical laws governing the phenomenon in the prototype are assessed and the π numbers, which are derived from that laws, are equalized.

3.2. Seepage action on movable particles

The fluid force related to the fluid drag can be classified as external force, fluid pressure force, inertial force, viscous force, gravitational force, elastic force, surface tension force and they can be expressed by the variables such as force F, dimension l, velocity v, density ρ, viscosity μ, bulk modulus B, gravity g, pressure change Δp, surface tension T. Each types of fluid force defines as external force: F, fluid pressure force: $\Delta p l^2$, internal force: $\rho v^2 l^2$, viscous force: $\mu v l$, gravitational force: $\rho g l^3$, elastic force: $B l^2$, surface tension force: $T l$, respectively (Muir Wood, 2003).

To apply the scaling laws, hydraulic actions on movable particles are summarized as follows from some existing researches.

3.2.1. Hydraulic shear stress based on bed-load transport

Piping erosion on clayey soil has been modeled based on empirical shear-induced interfacial erosion model on sediment transport, which is well-known in river engineering field as shown Fig. 3-1. The erosion rate $\dot{\varepsilon}_{er}$, which indicates the mass of soil eroded per unit area and time, are described with threshold laws as bellow (Wan and Fell, 2004; Bonelli and Brivois, 2008; Fujisawa $et\ al.$, 2010; Haghighi $et\ al.$, 2013);

$$\dot{\varepsilon}_{er} = k_{er}\left(\tau - \tau_c\right) \tag{3.1}$$

where k_{er}, τ and τ_c denote the erosion coefficient, the shear stress between the flowing liquid and the soil and critical shear stress, which, respectively. Erosion occurs when the shear stress is bigger than the critical shear stress. Haghighi $et\ al.$ (2013) deduced that the shear stress at the interface between the flowing liquid and soil in pipe as following:

$$\tau = -\nabla P \frac{r(t)}{2} \tag{3.2}$$

where $\nabla P = \Delta P / L$ is the applied pressure gradient projected along the axis and direction of flow (Fig. 3-1). $r(t)$ is the diameter of the pipe.
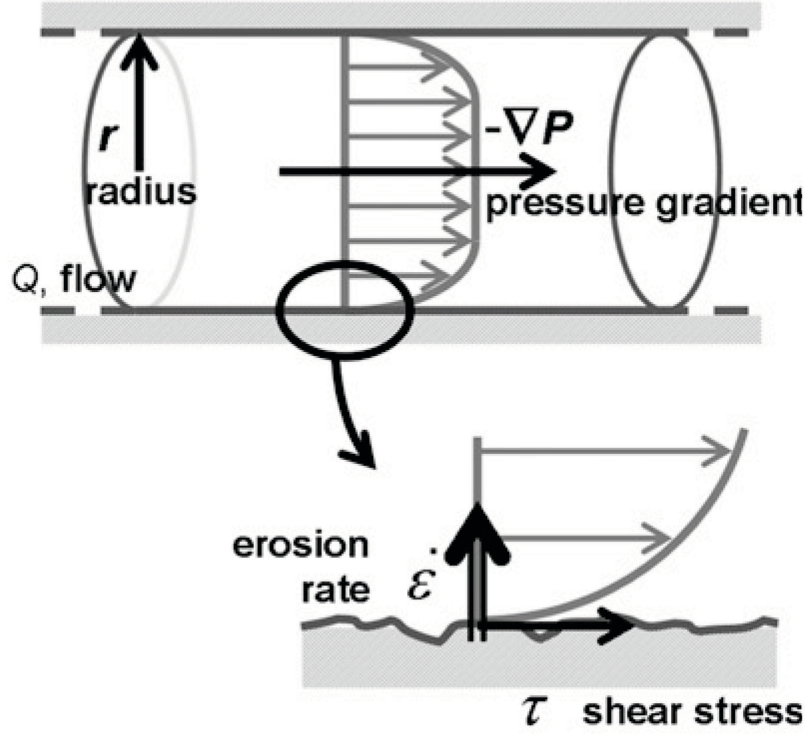
Figure 3-1   Schematic drawing of the interface (Haghighi *et al.* (2013))

Fujisawa *et al.* (2010) estimated that shear stress by the following equation based on Hagen-Poiseulle flow in the pore tube as:

$$\tau = \rho_w g i \sqrt{2Kn} \tag{3.3}$$

where i and K denote the hydraulic gradient and the intrinsic permeability.

Wan and Fell (2004) suggested that the hydraulic shear stress along the pre-formed hole are expressed as:

$$\tau = \rho_w g i \frac{r(t)}{4} \tag{3.4}$$

where, the diameter of the pipe $r(t)$ is given as following (Wan and Fell, 2004):

$$r(t) = \left(\frac{16Q^2 f_L}{\pi^2 \rho_w gi} \right)^{1/3} \quad \text{(laminar flow conditions)}$$

$$(3.5)$$

$$r(t) = \left(\frac{64Q^2 f_T}{\pi^2 \rho_w gi} \right)^{1/5} \quad \text{(Turbulent flow conditions)}$$

where Q (m³/s) is the flow rate f_L and f_T (kg/m³) are friction factors relating shear stress to the mean flow velocity.

Richards and Reddy (2014) proposed a methodology based on kinetic energy to assess suffusion and backward erosion initiation potential in existing earthen dams and levees constructed of cohesionless soil. That paper described the interparticle bond strength at initiation F as shown Fig. 3-2. Here, hydraulic shear stress at the soil-fluid contact is expressed as $\tau = \rho_f v^2$. Then interparticle bond strength can be given by following.

$$F = \beta \left(\frac{d^3}{8} \right) \rho_f \tau_c = \beta \left(\frac{d^3}{8} \right) \rho_f v_c^2 \qquad (3.6)$$

where v, v_c^2 d and β denote seepage shear velocity, critical seepage velocity, particle diameter, a unitless proportionality coefficient, respectively.
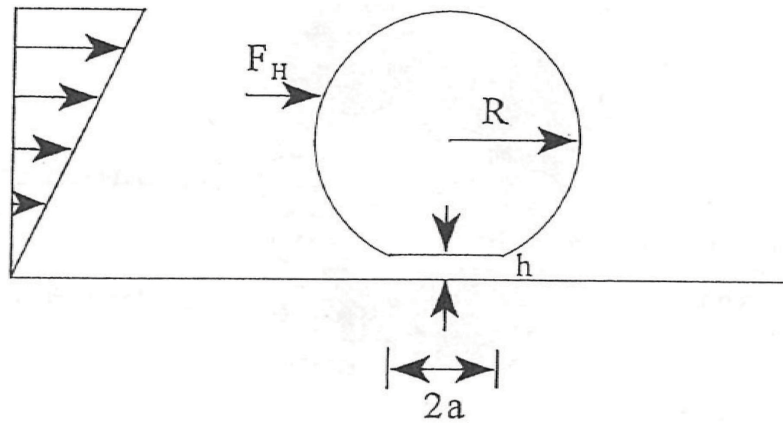
Figure 3-2   Schematic drawing of the torque balance of an individual spherical particle
(Reddi and Bonala (1997))

3.2.2. Slope angle effects on hydraulic gradient

The relationship between hydraulic gradient and slope angle was expressed by Hira *et al.* (1997) based on theoretical slope stability problem and seepage force acting on a single particle suggested by Akai (1956). If we consider equilibrium of forces based on the theory of the infinite slope stability, hydraulic gradient can be given as following on block ABCD in Fig 3-3:

$$i = (1-n)\frac{(\rho_s - \rho_w)}{\rho_w}\frac{\sin(\phi - \theta_{sl})}{\sin\phi} \qquad (3.7)$$

where ϕ, θ_{sl} and n denote the internal friction angle, slope angle and porosity, respectively.
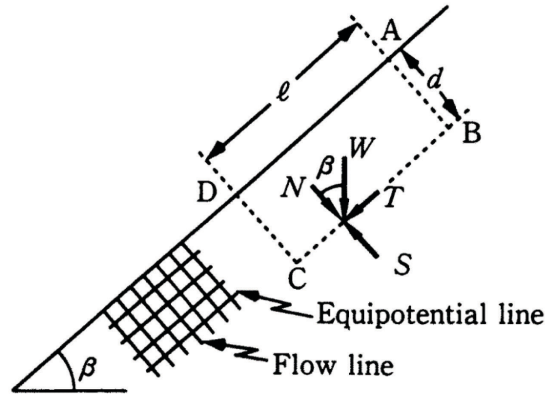
Figure 3-3   Equilibrium of forces normal to slope acting on plane BC (Hira *et al.* (1997))

On the other hand, if we consider equilibrium of forces on half particle, hydraulic gradient can be given as following in Fig. 3-4.

$$i = \frac{4}{3}\frac{(\rho_s - \rho_w)}{\rho_w}\frac{\sin(\phi - \theta_{sl})}{\sin\phi} \qquad (3.8)$$
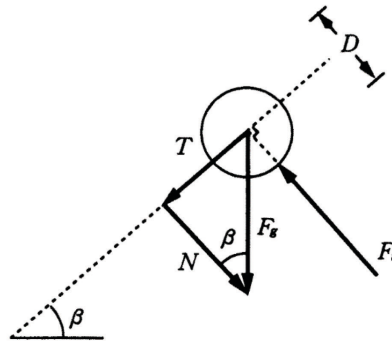
Figure 3-4   Equilibrium of forces normal to slope acting on half particles (Hira *et al.* (1997))

3.3. Scaling laws in model tests on seepage flow under gravitational field

Muir Wood (2004) summarized a series of dimensionless groups. Table 3-1 shows the dimensionless groups related to fluid drag obtained by Muir Wood (2004).

Table 3-1   Dimensionless groups on fluid drag (Muir Wood, 2004)

Name	Group	
Reynolds	Inertial / Viscous	$\dfrac{\rho \upsilon l}{\mu}$
Froude	Inertial / Gravitational	$\dfrac{\upsilon^2}{gl}$
Mach	Inertial / Elastic	$\dfrac{\rho \upsilon^2}{B}$
Euler	Inertial / Pressure	$\dfrac{\rho \upsilon^2}{\Delta p}$
Weber	Inertial / (Surface tension)	$\dfrac{\rho \upsilon^2 l}{T}$
Drag coefficient	(External force) / Inertial	$\dfrac{F}{\rho \upsilon^2 l^2}$

3.3.1. Scaling laws for steady laminar flow

(1) Scaling laws based on governing differential equation by Takada and Hosoyamada (1958)

The conditions to satisfy the similarity rule between the model and prototype in the seepage physical model tests are:

1) The form of macro boundary of flow is geometrically similar.

2) From the standpoint of kinematics, equation of motion and equation of continuity are satisfied at all times.

The equation of motion for fluid resistance and apparent viscosity in gravity filed can be expressed as:

$$\frac{1}{n}\frac{DV}{Dt} = -\mathrm{grad}\left(gz + \frac{P}{\rho}\right) - \frac{\mu}{\rho}\frac{V}{k"} + \frac{\mu}{n\rho}\nabla^2 V^3 \qquad (3.9)$$

The equation of continuity for fluid resistance and apparent viscosity can be also explained as:

$$\mathrm{div}\,V = 0 \qquad (3.10)$$

For each element, respective variables can be rearranged by use of dimensionless quantity l_0, V_0, t_0, P_0 and g_0 as: dimension $l = ll_0$, velocity $V = VV_0$, time $t = (l/U)t_0$, pressure $p = \rho U_2 P_0$, gravity $g = (U_2/l)g_0$. Because of this, operators in Eq. (3.9) and (3.10) can be non-dimensional as following:

$$\mathrm{grad} = \left(\frac{1}{l}\right)\mathrm{grad}_0, \ \ \mathrm{div} = \left(\frac{1}{l}\right)\mathrm{div}_0, \nabla^2 = \left(\frac{1}{l^2}\right)\nabla^2_0 \qquad (3.11)$$

These non-dimensional equational relations and the assumption that apparent viscosity is negligible small compared with the fluid resistance can be developed the equation for scaling laws under Darcy flow conditions as:

$$\frac{l_p}{l_m} = \left(\frac{k_p}{k_m}\right)^2 \qquad (3.12)$$

Therefore, this scaling law cannot be unsatisfied in the small-scale in gravity filed if the material used for the prototype and the model are the same.

(2) Parameter method

Muir Wood (2004) summarized a series of scale factor in the geotechnical engineering in gravity filed and centrifugal acceleration field. Table 3-2 shows the selective scale factors related to seepage problems with material and fluid for the prototype and the model in gravity filed obtained by Muir Wood (2004). Here, the fluid and soil used for the physical model test with small scale are same as prototype.

Table 3-2   Scale factor in gravity filed (Muir Wood, 2004)

Quantity	General	Scale factors
length	N_l	$1/N$
Mass density	N_ρ	1
Acceleration	N_g	1
Stiffness	N_G	$1/N$
Pore fluid viscosity	$N_{\rho f}$	1
Permeability (Darcy's Law)	$N_{\rho f} N_g / N_\mu$	1
Hydraulic gradient	$N_\rho / N_{\rho f}$	1
Time (diffusion)	$N_\mu N_l^2 / N_G$	$1/N$

(3) Principal π number method

Tohda (1999) discussed scaling laws for seepage tests by using principal π number method. The representative parameters were selected as force F, dimension (height) $l(h)$, velocity v, density ρ, surface tension T, gravity g. The index "m" and "p" indicate model and prototype, respectively. First, he derived scaling law on laminar flow in saturated zone related to steady seepage problems without deformation of ground from three governing equations; seepage, surface tension, and gravity. The π numbers which are ratio of seepage force to gravity, and ratio of surface force to gravity can give following scaling laws:

$$\frac{v_p (\gamma_w)_p}{k_p \rho_p G_p} = \frac{v_m (\gamma_w)_m}{k_m \rho_m G_m} \tag{3.13}$$

$$\frac{R_p T_p}{\rho_p G_p L_p^{\ 3}} = \frac{R_m T_m}{\rho_m G_m L_m^{\ 3}} \tag{3.14}$$

where R indicates the capillary radius.

Next, he discuss the scaling laws in the gravity filed.   Firstly, consider that fluid and soil used for the prototype and the model are same.   By focusing on saturated zone, scaling laws in this case can be expressed in Eq. (3.15).   (Eq. (3.14) is neglected.

$$\frac{t_p}{t_m} = \frac{L_p}{L_m} = N \qquad (3.15)$$

That is seepage time for model can be given as $t_m = \frac{1}{N} t_p$.

If we consider the the scaling law for seepage-induced deformation or particle migration problems, Reynolds and Froude numbers are not satisfied simultaneously.   Small-scale modelling is therefore not possible under such conditions.

3.3.2.   Scaling laws on erosion

Fox et al. (2006) explained the sediment transport rate of bank erosion at near-vertical stream banks based on empirical shear induced interfacial erosion model on sediment transport which are well-known in river engineering field.   They defined the function of transport rate of erosion per unit width as following:

$$q_s = f\left(\tau, \mu, h, \rho_w, \rho_{sg}, d, g\right) \qquad (3.19)$$

where, τ, μ, h, ρ_w, ρ_{sg}, d, and g denote the shear stress, viscosity, head, density of water, density of sediment grain, grain size, and gravitational acceleration, respectively. They were only concerned with transport of grains in water and flow depths greater than a few times the grain size.   Thus, dimensionless sediment flux q_s^* can be derived as Eq. (3.20) and (3.21) by dimensionless shear stress τ^*.

$$q_s^* = a\tau^{*b} \qquad (3.20)$$

$$q_s^* = \frac{q_s}{\sqrt{(s-1)gd^3}} \qquad (3.21)$$

Fox et al. (2006) assumed that the shear stress is dependent on the seepage force proposed by Howard and McLane (1988) as following:

$$\tau^* = \frac{C_2'' q}{(s-1)nK} \qquad (3.22)$$

where a and b are empirical regression parameters; C_2'' is empirical parameter that depends on the packing coefficient; q is Darcy's velocity or discharge per unit flow area (assumed

equal to the width of the lysimeter times the average flow depth at the lysimeter outlet); K is hydraulic conductivity; n is porosity of the seepage layer; and s is ratio of solid to fluid density; s is the ratio of solid to fluid density. Fox *et al.* (2007) devised the dimensionless shear stress from Eq. (3.22) on near-vertical stream banks by a factor equivalent to $\sin(\theta) = q_y/q$ (q_y is the seepage vector perpendicular to the bank slope) to deal with bank reduce the magnitude of the seepage force due to bank angle. In this case, the dimensionless shear stress becomes:

$$\tau^* = \frac{C_2'' q \sin(\theta)}{(s-1)nK}$$ (3.23)

Maknoon and Mahdi (2010) studied the initiation of external suffusion caused by rising the water level at upstream using a laboratory-scale model as shown Fig. 3-5. The solid discharge by unit surface area, E, was quantified by means of four non-dimensional groups (Hydraulic gradient i, Relative density D_r, Sand's dimensionless diameter d*, porosity, n) by using the method of Buckingham's π theorem. In that paper, dimensionless solid discharge E^* was derivable from theory of π as bellow.

$$E^* = \frac{E}{\sqrt{\gamma_w^2 d/g}} = f(d_*, p, i, D_r)$$ (3.24)

They assumed that d, P, D_r are almost constant. Therefore, Eq. (3.17) can be modified as following:

$$E^* = \frac{E}{\sqrt{\gamma_w^2 d/g}} = f(i)$$ (3.25)
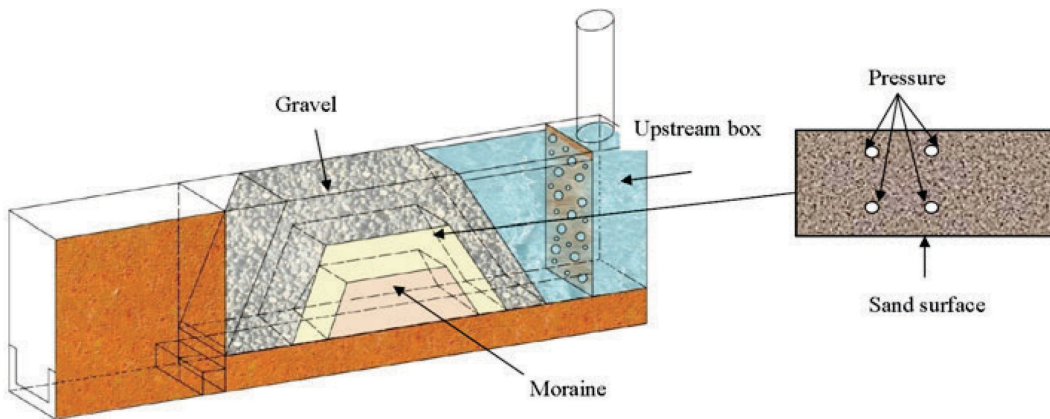
Figure 3-5   Schematic diagram of experiment on external suffusion

(Maknoon and Mahdi (2010))

3.3.3. Scaling laws on strength

In this thesis, the observation of seepage-induced fines transport in an embankment is focused and the stability problems are not considered.　However, in the extreme case, the suffusion may result in the collapse of the embankment.　In this case, the strength of the soil above the phreatic surface may play an important role as the strength due to suction in unsaturated zone by capillary rise affect the stability of the slope and the scaling laws for the unsaturated zone are not satisfied if the fluid and soil used in the model are same as those in prototype.

3.4.　Limitation of physical model test under gravitational field

As far as saturated seepage flow is concerned, the hydraulic gradient field in the model embankment is similar to a possible prototype, provided that geometry of the embankment and water head at the boundaries are consistent.　However, if the phreatic water surface exists and the internal erosion is involved, the following problems may arise and these are limitation of this experiment: (1) Relative position of the phreatic surface, i.e., the relative capillary rise, in the small-scale model becomes higher than that in the prototype because the water pressure is relatively small compared with the atmosphere pressure, and (2) erosion-induced contractive deformation in the small-scale model can be diminished, since a soil becomes more dilative under the small confining pressure.　In addition to these, the confining pressure dependency of fines loss is the other concern.　Ke and Takahashi (2014) carried out a series of one-dimensional downward seepage tests on a similar mixture with fines contents of 35 % under the several confining pressures and showed erosion potential decreases with an increasing in confining pressure.　Bendahmane *et al*. (2008) also showed a similar tendency on different internally instable soil.　Moffat *et al*. (2011) and, Moffat and Fannin (2011) demonstrated that an increase in effective confining pressure would cause an increase in the critical hydraulic gradient for erosion.　Tomlinson and Vaid (2000) investigated effect of the confining pressure on the initiation of piping experimentally. Their results indicate that the confining pressure has a certain influence on internal stability if the ratio between coarse particles and fines is not so large.　Having these under consideration, the stress level of embankment may have little effect on suffusion.　Therefore, useful data on the spatial change of fines content can be obtained by physical model tests in small-scale models.

As described above, scaling laws on some important parameters are not satisfied in the small-scaled model under the ordinary gravity filed.　As Kokusho (2014) noted in his book, small-scaled physical model test can only give the qualitative information on a phenomenon.　He also mentioned that the difficulty to evaluate the experimental results quantitatively.　Only the way to derive the quantitatively information from the small-scaled model test is as follow.

> *Numerical analysis approach can be verified by comparing experimental results. If the experiments are performed using the small-scaled model, we should accept the results as the facts without considering the scaling laws.　If inconsistencies in the scaling laws are attributed to the low confining pressure in the small-scaled model, mechanical properties of the materials should be examined under the low confining pressure.　If we can simulate the experiments using the specially obtained mechanical properties of the materials, it can be said that the numerical analysis approach is verified and we can use it for simulating the behavior of prototype ground.*

Therefore, physical model test described in Chapter 5 is numerically simulated using existing simple erosion model based on elemental erosion tests and it will be explained in Chapter 6.

REFFERENCES

Akai, K. 1956. On the local fillure of the downstream sope of embankments due to the percolating flow. *Transactions of the Japan Society of Civil Engineers,* 36, pp. 44-49. (In Japanese).

Bendahmane, F., Marot, D. & Alexis, A. 2008. Experimental parametric study of suffusion and backward erosion. *Journal of Geotechnical and Geoenvironmental Engineering,* 134(1)**,** pp. 57-67.

Bonelli, S. & Brivois, O. 2008. The scaling law in the hole erosion test with a constant pressure drop. *International Journal for Numerical and Analytical Methods in Geomechanics,* 32(13)**,** pp. 1573-1595.

Emori, I., Saito, K. & Sekimoto, K. 2000. *Scale Models in Engineerin,* 3edn, Tokyo, Japan: Gihodo. (In Japanese).

Fox, G. A., Chu-Agor, M. L. & Wilson, G. V. 2007. Erosion of Noncohesive Sediment by Ground Water Seepage: Lysimeter Experiments and Stability Modeling. *Soil Science Society of America Journal,* 71(6)**,** pp. 1822-1830.

Fox, G. A., Wilson, G. V. & Rerileti, R. K. 2006. Sediment transport model for seepage erosion of streambank sediment. *Journal of Hydrologic Engineering,* 11(6)**,** pp. 603-611.

Fujisawa, K., Murakami, A. & Nishimura, S. 2010. Numerical analysis of the erosion and the transport of fine particles within soils leading to the piping phenomenon. *Soils and Foundations,* 50(4)**,** pp. 471-482.

Haghighi, I., Chevalier, C., Duc, M., Guédon, S. & Reiffsteck, P. 2013. Improvement of Hole Erosion Test and Results on Reference Soils. *Journal of Geotechnical and Geoenvironmental Engineering,* 139(2)**,** pp. 330-339.

Hira, M., Miwa, K., Wakamatsu, C. & Mitsutake, Y. 1997. Failure condition of shirasu talus deposit subjected to seepage force normal to slope. *Transactions of the Japanese Society of Irrigation, Drainage and Reclamation Engineering,* 190, pp. 21-26.   (In Japanese).

Howard, A. & McLane, C. 1988. Erosion of cohesionless sediment by groundwater seepage. *Water Resources Research,* 24(10)**,** pp. 1659-1674.

Ke, L. & Takahashi, A. 2014. Experimental investigations on suffusion characteristics and its mechanical consequences on saturated cohesionless soil. *Soils and Foundations,* 54(4)**,** pp. 713-730.

Kimura, T. 1989. A new method of soil test - Scale models and similarity rule in soil mechanics. *Presentation materials on latest various problems on soil mechanics and foundation engineering.* Japanese Geotechnical Society.

Kokusho, T. 2014. *Fundamentals of earthquale Geo-Dynamics,* Tokyo, Japan: Kajima Institute Publishing Co., Ltd. (In Japanese).

Maknoon, M. & Mahdi, T. F. 2010. Experimental investigation into embankment external suffusion. *Natural Hazards,* 54(3)**,** pp. 749-763.

Moffat, R. & Fannin, R. J. 2011. A hydromechanical relation governing internal stability of cohesionless soil. *Canadian Geotechnical Journal,* 48(3)**,** pp. 413-424.

Moffat, R., Fannin, R. J. & Garner, S. J. 2011. Spatial and temporal progression of internal erosion in cohesionless soil. *Canadian Geotechnical Journal,* 48(3)**,** pp. 399-412.

Muir Wood, D. 2004. Phisical modelling. *Geotecnical modelling.* Oxfordshire, United Kingdom: Spon Press.

Reddi, L. N. & Bonala, M. 1997. Critical shear stress and its relationship with cohesion for sand-kaolinite mixtures. *Canadian Geotechnical Journal,* 34(1)**,** pp. 26-33.

Richards, K. S. & Reddy, K. R. 2014. Kinetic Energy Method for predicting initiation of backward erosion in earthen dams and levees *Environmental & Engineering Geoscience,* 20(1)**,** pp. 85-97.

Takata, Y. & Hosoyamada, K. 1957. On the preclation through the dike of mouded stone and earth (I) Model experiment. *Journal of the Agricultural Engineering Society, Japan,* 25(5)**,** pp. 448-450. (In Japanese).

Tohda, J. 1999. Similarity law in model tests on seepage problem coupled with graound failure and dinamic loading. *The 54th Japan Society of Civil Engineers annual meeting,* pp. 606-607. (In Japanese).

Tomlinson, S. S. & Vaid, Y. P. 2000. Seepage forces and confining pressure effects on piping erosion. *Canadian Geotechnical Journal,* 37(1)**,** pp. 1-13.

Wan, C. F. & Fell, R. 2004. Investigation of rate of erosion of soils in embankment dams. *Journal of Geotechnical and Geoenvironmental Engineering,* 130(4)**,** pp. 373-380.

Yamaguchi, H. 1980. Model tests in geomechanics: Their meaning and accuracy. *Soil mechanics and foundation engineering,* 28(5)**,** pp. 3-7. (In Japanese).

Chapter 4   Reproductive experiment of

suffusion phenomenon in embankment

4.1.   Introduction

The aim of this Chapter is to reproduce initiation of suffusion phenomenon and its continuation in an embankment, physical model tests in small-scaled model are conducted with controlling experimental parameters, such as hydraulic boundaries condition, fines content of the soil.   The eroded soil mass and flow rate are measured to confirm the incidence of suffusion, and to select the best experimental condition for further tests described later in Chapters 5 and 7.

4.2.   Soil materials

For reproduction of the suffusion phenomenon in the small-scaled model, an attempt is made to select material which is vulnerable to suffusion.   According to previous studies on suffusion initiation, gap-graded (see Line 3 in Fig. 4-1) or upwardly concaved (see Line 4 in Fig. 4-1) soils are known as vulnerable to suffusion.   Determination of the fines content and grain size is made by considering following three criteria described by Wan and Fell (2008);

1) *The size of the fine soil particles must be smaller than the size of the constrictions between the coarser particles, which form the basic skeleton of the soil;*

2) *The amount of fine soil particles must be less than enough to fill the voids of the basic skeleton formed by the coarser particles.   If there are more than enough fine soil particles for void filling, the coarser particles will be "floating" in the matrix of fine soil particles, instead of forming the basic soil skeleton; and*

3) *The velocity of flow through the soil matrix must be high enough to move the loose fine soil particles through the constrictions between the larger soil particles.*

For easy interpretation of the test results, mixtures of fines and coarse fractions are used for the models.   Such gap-graded soils exist in glacial tills in Canada and New Zealand, but

35

sometimes we use such a material for filling: To use a dredged soil as a fill material, workability improvement is made either by mixing cement or by mixing pit sand.   Typically, the latter is a gap-graded soil.   Although use of such a material can exaggerate the test results, it allows (a) easy distinction between the base and erodible materials and (b) easy observation of the fines migration in a short period.
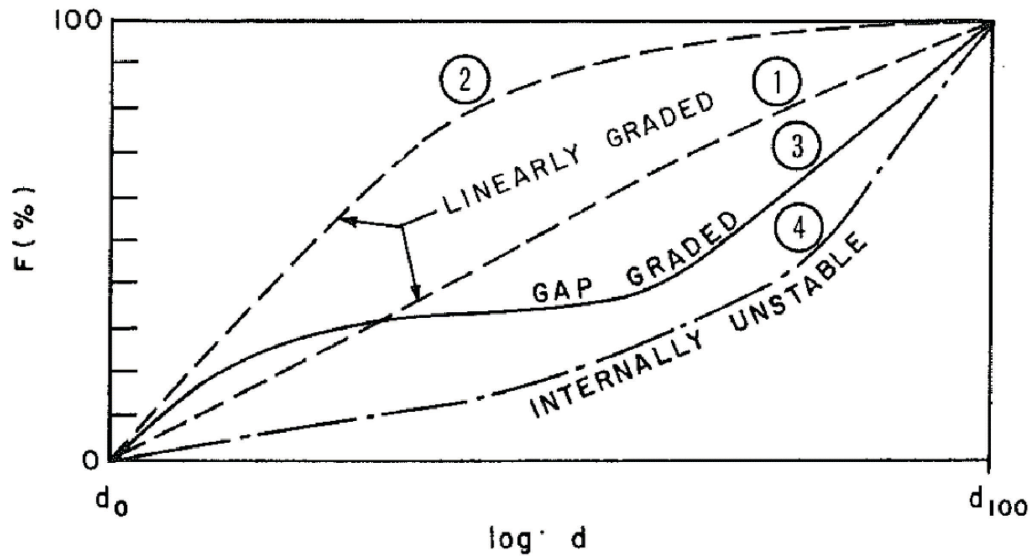
Figure 4-1   Classification of the grain size distribution of soils (after Lafleur *et al.*,1989)

Based on the works by Ke and Takahashi (2012, 2014) in Tokyo Institute of Technology, Silica sand No. 3 and Silica sand No.8 are used as the model materials.   Silica sand No. 3 models the soil skeleton, while Silica sand No.8 is used as the erodible fine particles in the voids of the coarse skeleton.   The grain size distribution curves of both Silica sands and basic properties of the materials are shown in Fig. 4-2 and Table 4-1, respectively.   Hereafter, the Silica sand No. 8 is referred to fines for simplicity even though the Silica sand No. 8 is not strictly classified as fines by the Japanese Industrial Standards (JIS).

The fraction of total mass is expressed as the sum of mass fraction of the coarse particles C_c and mass fraction of the fine particles FC;

$$C_c + FC = 1 \tag{4.1}$$

The mass fraction of the coarse particles C_c can be described by the relationship between the void ratio of coarse particles e_c and average porosity of fine particles n_f,

36

$$C_c \geq \frac{1}{1 + e_c(1 - n_f)} \qquad (4.2)$$

Internal stability of mixtures is influenced by fines content. The maximum value of mass fraction of the fine particles FC can be obtained when coarse particles are loosely packed, and the fine particles are compacted inside the voids of the coarse particles. In this study, as shown in Table 4-1, the maximum void ratio of Silica No.3 sand is 1.009 and minimum void ratio of Silica No.8 is 0.7. In instance, the value $C_c > 0.63$ is obtained from Eq. (4.2). Therefore, the estimated maximum mass ratio of erodible fine particles by seepage is 37% from Eq. (4.1). This value is called critical content of fines by Skempton and Brogan (1994). In the tests, the erodible fine particles should be smaller than 37% because the void ratio is lower than 1.009 due to compaction during mixtures preparation, and the fine particles are expected to be less densely packed with a larger n value.

The chosen fines contents of mixture are 10 %, 15 % and 25 %. The grain size distribution curves of mixtures and basic properties of each material are shown in Fig. 4-3 and Table 4-2, respectively. According to several criteria on the seepage-induced internal stability (Chang and Zhang, 2013; Wan and Fell, 2008; Li and Fannin, 2008), the mixtures of this study are categorized as "Internally instable material" and is vulnerable to suffusion if seepage takes place. The calculated critical hydraulic gradient for zero effective stress is 1.0 according to Terzaghi's equation. Ke and Takahashi (2012) performed a series of one-dimensional upward seepage tests on a similar mixture with fines contents of 14.3, 16.7, 20 and 25 %. Their critical gradient for suffusion i_{sc} was linearly correlated with the fines content ($i_{sc} = -0.0037FC + 0.302$, $R^2 = 0.997$). From this linear relationship, the expected critical gradient against suffusion for the mixtures used (10, 15 and 25% fines content) are 0.27, 0.25 and 0.21, respectively.
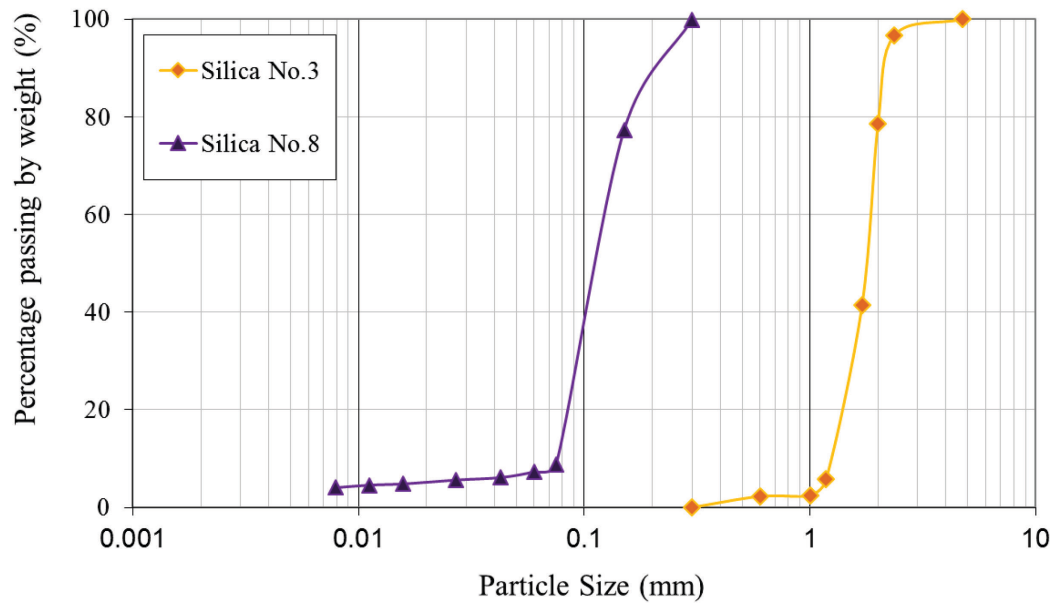
Figure 4-2   Grain size distribution curves of Silica No.3 and No.8

Table 4-1   Physical properties of Silica No.3 and No.8 sand (Ke and Takahashi, 2014)

Physical property		Silica No.3 (coarse fraction)	Silica No.8 (fines)
Specific gravity, Gs		2.645	2.645
Maximum void ratio, e_{max}		1.009	1.33
Minimum void ratio, e_{min}		0.697	0.703
Median particle size D_{50} (mm)		1.76	0.16
Effective particle size D_{10} (mm)		1.37	0.087
Uniformity coefficient, CU		1.5	1.7
Curvature coefficient, CC		1.1	0.96
Hydraulic conductivity	30%[1]	6.6×10^{-3}	3.4×10^{-5}
(m/s)	60%[1]	5.6×10^{-3}	2.6×10^{-5}
[refer Ke, 2014]	80%[1]	4.9×10^{-3}	2.1×10^{-5}
Grain Description		Sub-rounded ~ Sub-angular	

Note: (1) Relative density

38
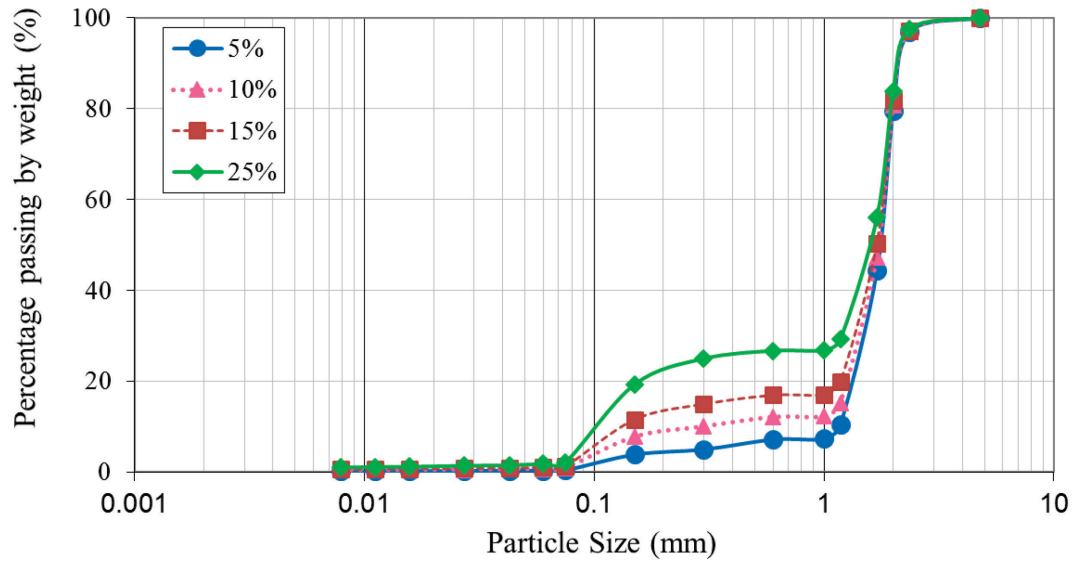
Figure 4-3　Grain size distribution curves of mixtures

Table 4-2　Physical properties of tested soil

Physical property	Specimen 5	Specimen 10	Specimen 15	Specimen 25
Specific gravity, Gs	2.645	2.645	2.645	2.645
Fines content (%), FC	5	10	15	25
Maximum void ratio, e_{max}	1.01	0.94	0.79	0.77
Minimum void ratio, e_{min}	0.70	0.65	0.53	0.37
Median particle size D_{50} (mm)	1.76	1.73	1.70	1.60
Effective particle size D_{10} (mm)	1.17	0.3	0.138	0.102
Uniformity coefficient, CU	1.5	6.1	13.4	17.1
Curvature coefficient, CC	1.1	3.8	7.9	8.02
(D_{15c}/d_{85f})gap	7.76	7.76	7.76	7.76
Hydraulic conductivity (m/s) [1]	3.9×10^{-3}	3.0×10^{-3}	1.7×10^{-3}	9.4×10^{-5}
Grain Description		Sub-rounded ~ Sub-angular		

Note: (1) Permeability tests are conducted on partially saturated soil with tap water under void ratio of the coarse skeleton $e_s = 0.885$, relative density of the coarse skeleton $Dr_s = 40\%$.

4.3. Experimental apparatus and procedure

Side view of the experimental system is schematically illustrated in Fig. 4-4. The embankment model is made in a steel box with 500mm in width, 150mm in breadth and 350mm in depth. The box has two tanks at both sides, named "water supply tank" and "drainage tank", respectively. Vertical sidewalls between the drainage tank and the embankment model provide a metal gauze so that only water and fines less than 0.25mm can flow through. By pouring the water in water supply tank, seepage flow in the model ground could be realized. Seepage water from the model embankment eventually passes through the drainage tank and finally discharges from the outlet. Eroded fines are collected by sieve of size 0.075mm located near outlet of the steel box. The discharge rate of water is measured by cylinder at the outlet. Here, the effect of particles smaller than 0.075mm were not considered due to the very small amount.
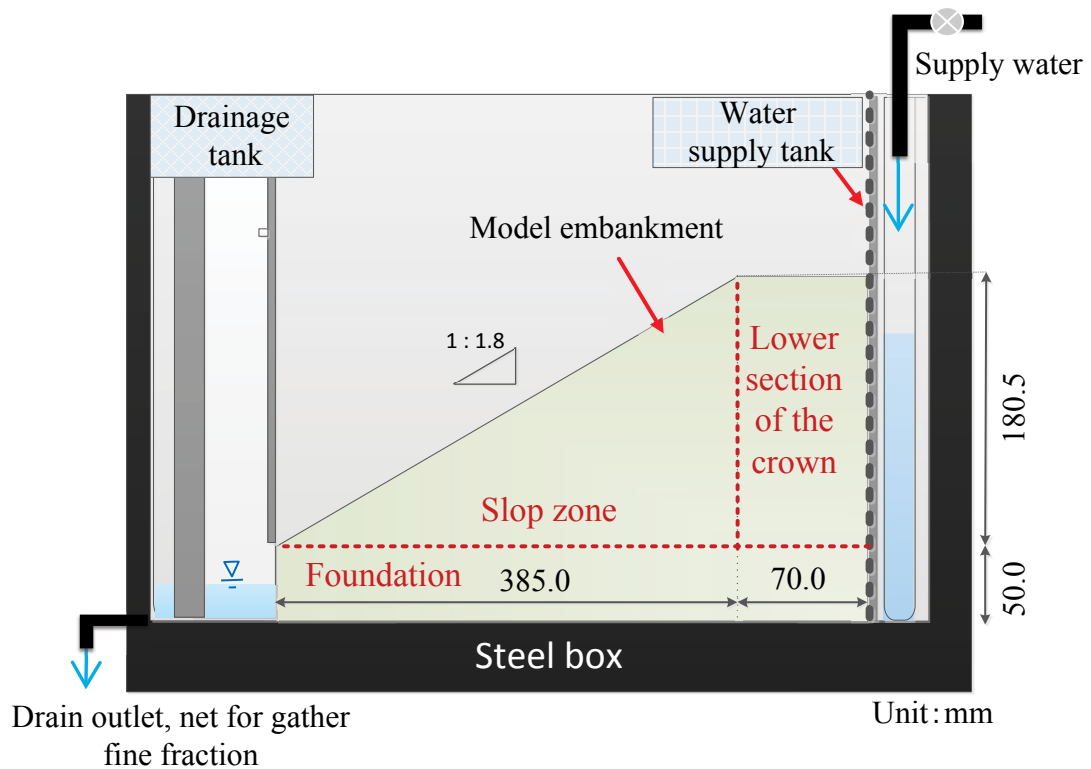
Figure 4-4   Side view of experimental system

To prevent material separation during preparation of the model embankment, the moist tamping method (Ladd, 1978) is employed. Water contents of model ground with fines content of 10%, 15% and 25% area are 2%, 3%, and 5%, respectively. The sand is

compacted layer by layers with thickness of 20mm. Then, the model ground is scraped off with a shaped frame (Photo. 4-1) and formed to be a 230.5mm high model embankment (Fig. 4-4). The model embankment is composed of two areas, the "foundation zone" and the "slope zone" (includes the "slope zone" and the "lower section of the crown") as shown in Fig. 4-4. The foundation zone is a 50 mm-thick horizontal layer and the slope zone is embankment with a slope of 1: 1.8. The target density is the minimum density of each mixture. Boundary condition at the upstream side has two patterns; one is constant flow rate (*Cases* 15%Q is 4533mm³/min, 25%Q is 1267mm³/min) and the other is constant head (172mm). Boundary condition at the downstream side has also two patterns: In Type A, the water level is set at a height of 35mm from the bottom, while it is empty at the bottom in Type B. Since the size of the outlet for Type A is small, the water level can change (initial height is 0mm, maximum height, approximately, 35mm) if flow rate exceeds threshold value (approx. 3000 ml/min). Boundary condition at the downstream site of each type is schematically illustrated in Fig. 4-5.
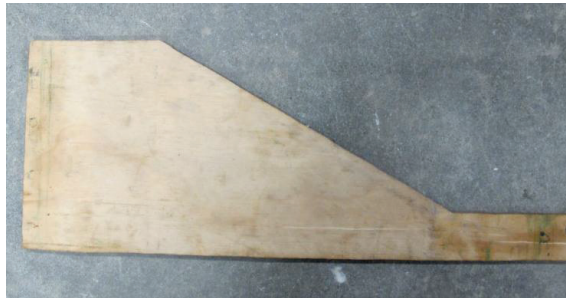
(a) Shaped frame (b) Framing an embankment
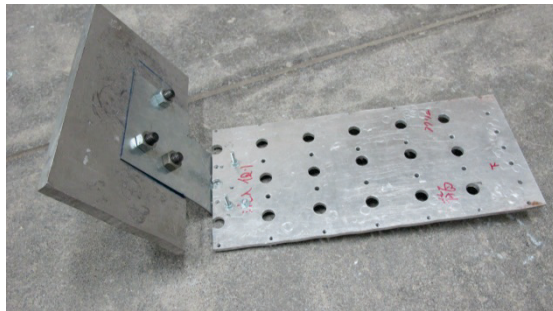
(c) Framing aid for slope zone (d) Framing aid for top of slope zone

Photograph 4-1   Side view of experimental system

(a) Type A (Case15%H-A)　　　　　　　(b) Type B (Case15%H-B)
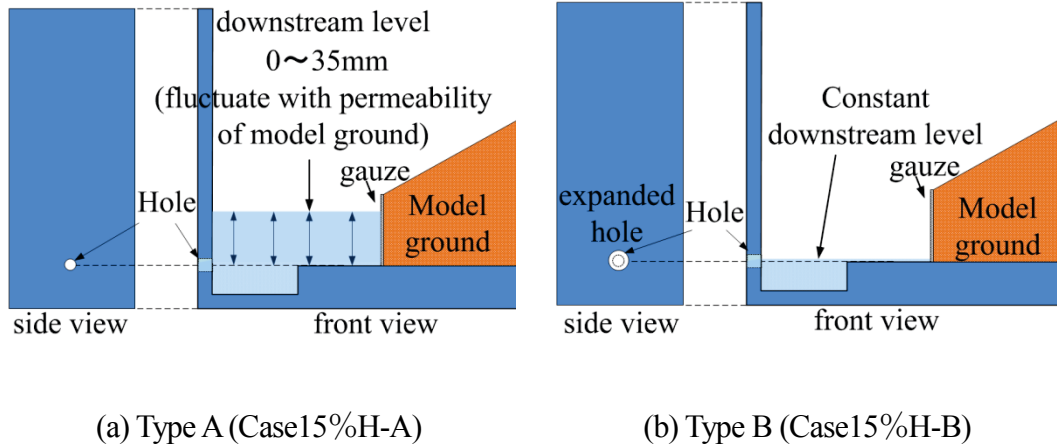
Figure 4-5　　Boundary condition at the downstream side

4.4. Experiment procedures and conditions

In this study, six test cases are conducted as shown in Table 4-3. During the seepage test, mass of eroded fines and change in position of the phreatic surface against elapse time are measured. Here, the hydraulic conductivity is calculated using Dupuit assumption with the visually observed phreatic surface and measured discharge rate. Within the scope of this study, at the beginning of the seepage test, position of the phreatic surface and unsaturated zone does not change much depending on the material used. Temporal change of position of phreatic surface is estimated based on the visual observation using photographic images.

4.5. Results and discussion

4.5.1. Mass of eroded soil against elapse times

Figure 4-6 shows evolutions of normalized eroded soil mass with time. The amount of eroded fines is normalized by the total amount of Silica sand No.8 under the phreatic surface before the seepage test. By comparing *Cases 15%Q* and *25%Q, 10%H-A* and *15%H-A*, it can be noted that the larger the fines content, the less the suffusion in the early stage of seepage tests (Figure 4-6 (a)). This result indicates that the larger the fines content makes the larger the ratio of fines stored in the coarse particles void formed, leading to the narrower the flow channel that is used to transport separated fines.

Table 4-3   Test cases of seepage test

Case	Content of Silica sand No.8 (%)	Boundary condition of levee crown	Boundary condition of levee toe	Minimum density (g/cm³)	Dry density (g/cm³)	Seepage time (min)	Hydraulic conductivity of initial state (mm/sec)	Hydraulic conductivity of end of seepage test (mm/sec)
15%Q	15	Constant Flow	A	1.567	1.582	720	7.91	9.04
25%Q	25	Constant Flow	A	1.497	1.583	5760	3.10	2.65
10%H-A	10	Constant Head	A	1.543	1.535	10140	11.65	7.87
10%H-B	10	Constant Head	B	1.543	1.544	22850	8.08	3.96
15%H-A	15	Constant Head	A	1.567	1.603	11710	4.23	13.80
15%H-B	15	Constant Head	B	1.567	1.558	20670	6.37	2.62

In *Cases 15%H-A*, and, *10%H-A*, amount of eroded soil significantly increases after a certain elapsed time, compared with the other cases (Figure 4-6 (b)).   The exact causes are unclear, but it is inferred that the decrease of the fines by suffusion expands along the flow channel and makes the erosion easier.   Other possible reason is that the occurrence of a relatively strong flow between the sidewall and soil in this cases.

Evolutions of discharge rate of water at the toe with time are shown in Fig. 4-7.   For the cases with Type A boundary condition at the downstream (*Cases 10%H-A* and, *15%H-A*), if the flow rate exceeds the threshold value (approx. 3000 ml/min), the water level of hydraulic boundary at the toe rises (maximum 35 mm).   In this case, cross-sectional area of the downstream boundary becomes large.   Cumulative eroded soil mass ratio with time in Figs. 4-6(a) and 4-7 suggest that flow rate and hydraulic boundaries condition have strong effects on initiation

and progress of suffusion.　By comparing *Cases 15%Q* and *15%H-A*, the amount of eroded fines of *Case 15%Q* is larger than that of *Case 15%H-A*.　In *Case 15%H-A*, where the boundary condition at the upstream is constant head, position of the phreatic surface does not change with time.　In this case, the fines at the center of the embankment can move toward downstream. On the other hand, *Case 15%Q*, where the boundary condition at the upstream is constant flow rate, the hydraulic conductivity increases due to the lowering of phreatic surface by suffusion.　In this case, the supply of the fines from the central part of the embankment to the bottom part is limited.　This may have made erosion of the fines at the bottom part faster, leading to the expanding of the flow channel and making the erosion easier in the bottom part.

(a)　　Short period　　　　　　　　(b)Long period
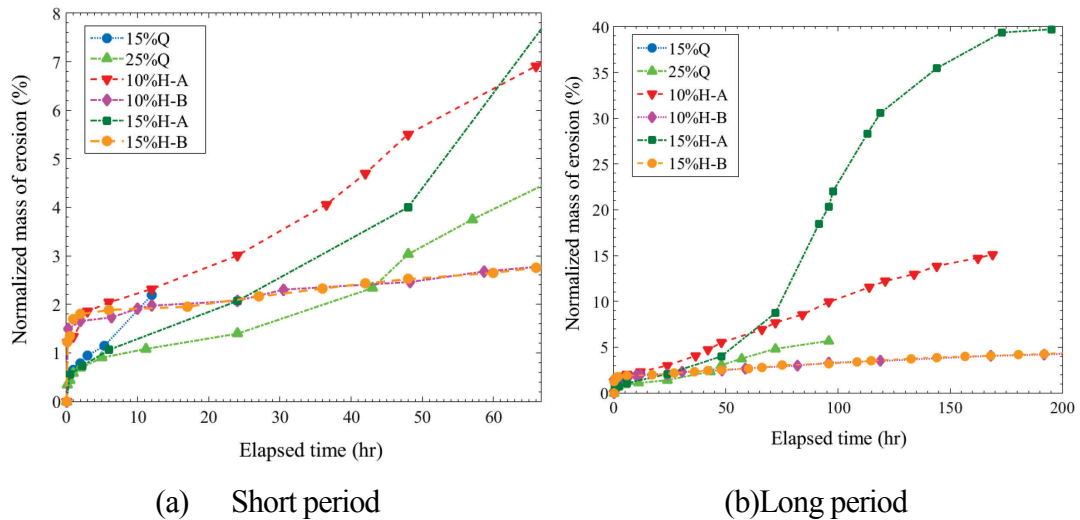
Figure 4-6　　Evolution of normalized eroded soil mass
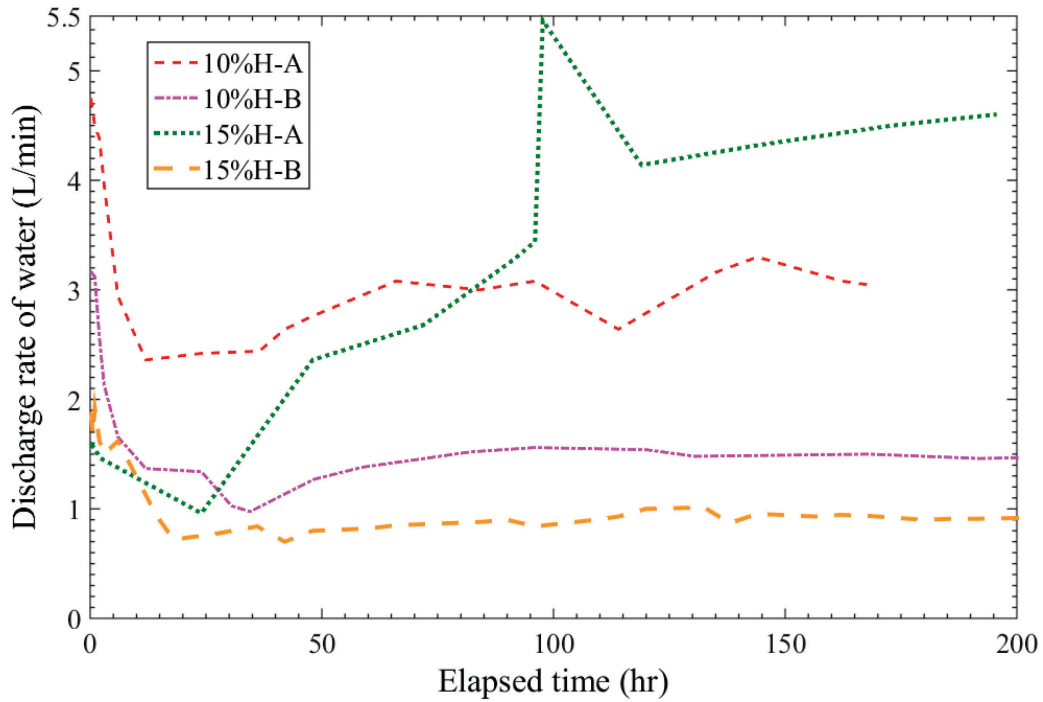
Figure 4-7   Evolution of discharge rate of water

4.5.2.   Mean flow velocity of model ground

Mean flow velocity distributions in *Cases 15%H-A*, and, *15%H-B* are shown in Fig. 4-8. This mean flow velocity is calculated by the continuity equation for the steady flow.   In *Case 15%H-A*, the mean flow velocity increases with time.   Similar trends are observed in the other same hydraulic boundary condition at downstream cases, except *Case 10%H-A*. In *Case 10%H-A*, at first the mean flow velocity decreases with time, while it starts increasing after the elapsed time of 24hours.   The change in flow velocity may also support that expansion of active channel and increase of void occurs due to progress of suffusion. The increase of velocity leads to tractive force that transports sediment larger.   Suffusion is progressively developed from middle of the foundation near downstream boundary.   This can also be explained by the grain size analysis for each part after the experiments as shown in Table 4-4.   The value of fines content is relatively small in the upstream side (distance from the toe: 289-385 mm) due to no supply of fine particles from the upper stream side. On one hand, in *Case 15%H-B*, the mean flow velocity decreases with time.   Similar trends are observed in the other same hydraulic boundary condition at downstream *Case 10%H-B*. The direct cause of decrease in flow velocity may be concentration of water flow at the

45

downstream hydraulic boundary.　　The local clogging makes decrease hydraulic conductivity of whole of model ground.　　Herewith, the decrease of velocity makes additional clogging by fines in the central part of slope.　　This can also be explained by the grain size analysis of *Case 15%H*-B for subdivided areas of the model embankment after the seepage testing as shown in Fig. 4-9.　　*Case 10%H-B* exhibits the same tendency as in *Case 15%H-B*.

(a) Case15%H-A　　　　　　　　　　　　(b) Case15%H-B
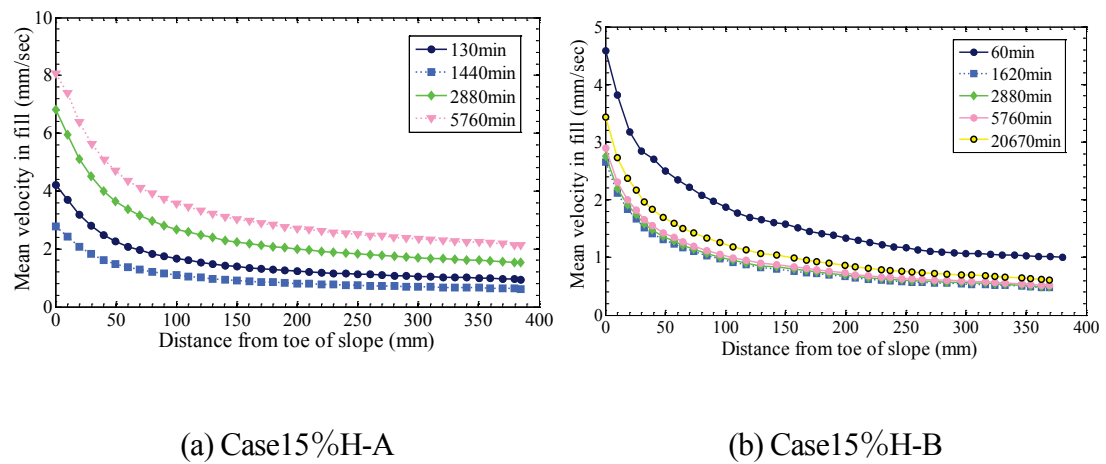
Figure 4-8　　Change of mean flow velocity distribution
in Cases 15%H-A and 15%H-B

Table 4-4　　Horizontal distribution of fines content

Case	Initial state	Distance from the slope toe			
		0-96 mm	96-193 mm	193-289 mm	289-385 mm
15%Q	14.54	12.8	14.12	14.21	12.03
25%Q	25.55	23.82	24.64	25.61	24.71
10%H-A	9.94	7.69	10.82	10.46	5.22
15%H-A	15.34	8.44	10.22	6.98	5.94

Unit (%)

46
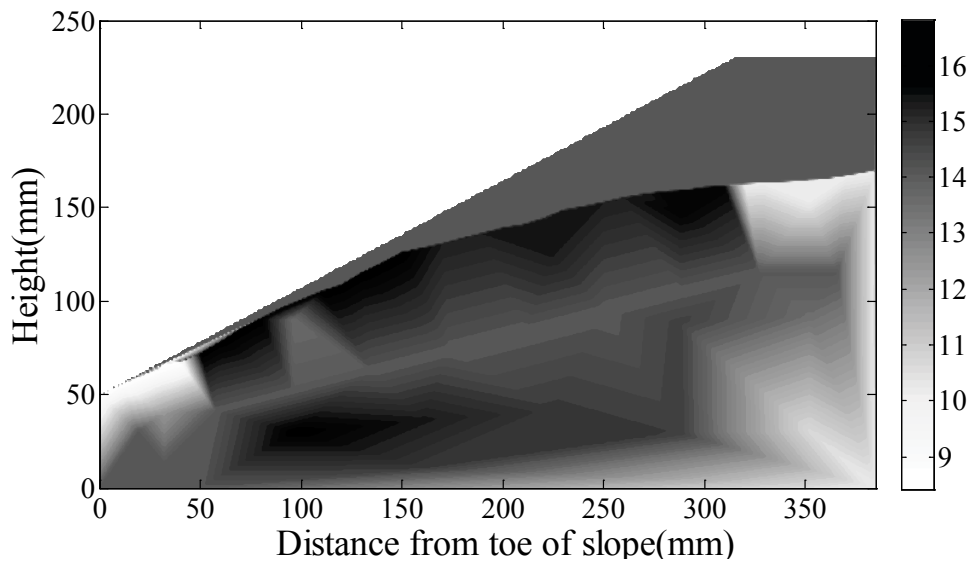
Figure 4-9　　Spatial distribution of fines content
after the seepage test (Case 15%-H, after 20670min)

4.6.　Summary

In this Chapter, a series of physical model tests on seepage-induced suffusion in embankments is conducted.　By considering effects of amount of fines and hydraulic boundaries condition on soil erodibility, the suffusion-induced destabilization of the embankment is examined and the following conclusions are drawn:

1.　Seepage-induced suffusion in embankments can be reproduced with the small-scaled loosely compacted embankment models in the laboratory.

2.　The larger the fines content, the less the suffusion in the early stage of seepage tests. After a certain elapsed time, the decrease in the fines due to suffusion can widen the flow channel and the internal erosion rate can increase.

3.　The increase of flow velocity by suffusion makes tractive force larger.　In addition, suffusion is progressively broadened from the toe to center of the embankment.

4.　Hydraulic boundary condition at the downstream has a significant effect on amount of eroded fines.

Based on the finding in this Chapter, the test conditions in the following Chapters are determined.

47

REFERENCES

Chang, D. S. & Zhang, L. M. 2013. Extended internal stability criteria for soils under seepage. *Soils and Foundations,* 53(4)**,** pp. 569-583.

Ke, L. 2014. *Investigation on internal erosion characteristics and its mechanical consequences for saturated non-cohesive soil (phD thisis).* Doctor of Philosophy, Tokyo Institute of Technology.

Ke, L. & Takahashi, A. 2012. Strength reduction of cohesionless soil due to internal erosion induced by one-dimensional upward seepage flow. *Soils and Foundations,* 52(4)**,** pp. 698-711.

Ke, L. & Takahashi, A. 2014. Experimental investigations on suffusion characteristics and its mechanical consequences on saturated cohesionless soil. *Soils and Foundations,* 54(4)**,** pp. 713-730.

Ladd, R. S. 1978. Preparing test specimens using undercompaction. *Geotechnical Testing Journal,* 1(1)**,** pp. 16-23.

Lafleur, J., Mlynarek, J. & Rollin, A. 1989. Filtration of broadly graded cohesionless soils. *Journal of Geotechnical Engineering,* 115(12)**,** pp. 1747-1768.

Li, M. & Fannin, R. J. 2008. Comparison of two criteria for internal stability of granular soil. *Canadian Geotechnical Journal,* 45(9)**,** pp. 1303-1309.

Skempton, A. W. & Brogan, J. M. 1994. Experiments on piping in sandy gravels. *Géotechnique,* 44(3)**,** pp. 449-460.

Wan, C. F. & Fell, R. 2008. Assessing the potential of internal instability and suffusion in embankment dams and their foundations. *Journal of Geotechnical and Geoenvironmental Engineering,* 134(3)**,** pp. 401-407.

Chapter 5   Physical model tests on suffusion process in homogenous embankment

5.1.   Introduction

In this chapter, the suffusion process under the unsteady and steady seepage conditions in embankments are presented.   A series of physical model tests on seepage-induced suffusion are performed in small-scaled models by using the developed seepage apparatus capable of reproduction of suffusion in the physical model described in a previous chapter to examine the seepage-induced suffusion process in an embankment with foundations during the phases of initiation and continuation of erosion.   Cumulative eroded soil mass and discharged rate of water are measured during the seepage tests and the erosion mechanism for gap-graded cohesionless soil under the unsteady seepage, steady seepage, and repeated permeation is elaborated.   The spatial extent of erosion-induced fines content variation is discussed through sieve analyses on subdivided areas of the model embankment after seepage testing. The representative erosion-induced variation of hydraulic conductivity of the whole embankment is also presented.   Then the influence of the effective first permeation, time under the steady seepage flow, and repeated permeation is discussed by the comparison of the testing data with the representative data.

5.2.   Soil specimens

To simplify the phenomenon, a mixture of fine and course fractions, a gap-graded soil, is used for the models.   Such a gap-graded soil exist in glacial tills in Canada and New Zealand, but sometimes we use such a material for filling: To use a dredged soil as a fill material, workability improvement is made either by mixing cement or by mixing pit sand. Typically, the latter is a gap-graded soil.   Although use of such a material can exaggerate the test results, it allows (a) easy distinction between the base and erodible materials and (b) easy observation of the fines migration in a short period.

Based on the works by Ke and Takahashi (2012, 2014), Silica sand No. 3 and Silica sand No.8 are also used as the model materials in this series of tests.   Again, Silica sand No. 3

49

models the soil skeleton, while Silica sand No.8 is used as the erodible fine particles in the voids of the coarse skeleton.   Hereafter, the Silica sand No. 8 is referred to fines for simplicity even though the Silica sand No. 8 is not strictly classified as fines by the Japanese Industrial Standards (JIS).   Based on the results in chapter 4, the chosen fines content of the mixture is 15 %.   The particle size distribution curves of each sand and the mixture and basic properties of the mixture material were shown in Chapter 4 in Fig. 4-1 and Table 4-1, respectively.

As described in Chapter 4, the mixture is categorized as "Internally instable material" and is vulnerable to suffusion if seepage takes place (Chang and Zhang, 2013; Wan and Fell, 2008; Li and Fannin, 2008).   The calculated critical hydraulic gradient for zero effective stress is 1.0 according to Terzaghi's equation.   From linear relationship in previous one-dimensional seepage tests on a similar mixture by Ke and Takahashi (2012) described in Chapter 4.2, the expected critical gradient against suffusion for the mixture used (15 % fines content) is 0.25.

5.3. Test system

The embankment models are made in a steel box with inner dimensions of 500 mm×150 mm×350 mm as shown in Fig. 5-1(a).   The box has two tanks on both sides, namely the "water supply tank" and the "drainage tank."   The vertical sidewalls between the tank and embankment model contain a metal mesh so that only water and fines less than 0.25 mm can flow through.   By pouring water into the water supply tank, seepage flow in the ground can be modeled.   The boundary heads reach 190 mm and 40 mm at the upstream and downstream sides, respectively, in around 30-40 minutes for all the cases.   Seepage water from the model embankment eventually passes through the drainage tank and finally discharges from the outlet.   The drainage tank has two holes, one is to discharge the eroded soil and some quantity of water (small hole located at a level of 0 mm) and the other is to maintain a constant head (large hole located at a level of 40 mm).

As shown Fig. 5-1(b), discharged soil and water flow into a small container via an aluminum angle.   The small container is filled with water to a constant level and is located near the steel box.   Eroded fines are collected by a suspended bowl on wires underwater in the small container.   To prevent the outflow of fines to the outside of the bowl and to help the sedimentation of fines, it is covered with filter paper on the side surface.   The cumulative

eroded mass is recorded automatically by a load cell (Kyowa Electronic Instruments Co., Ltd., LVS-2KA (Photo. 5-1), measureable range: 0 - 20 N) connected with the wires.   The calibration of a load cell is carried out before the each seepage tests and the mass balance is also checked by amount of collected eroded soil after the tests.
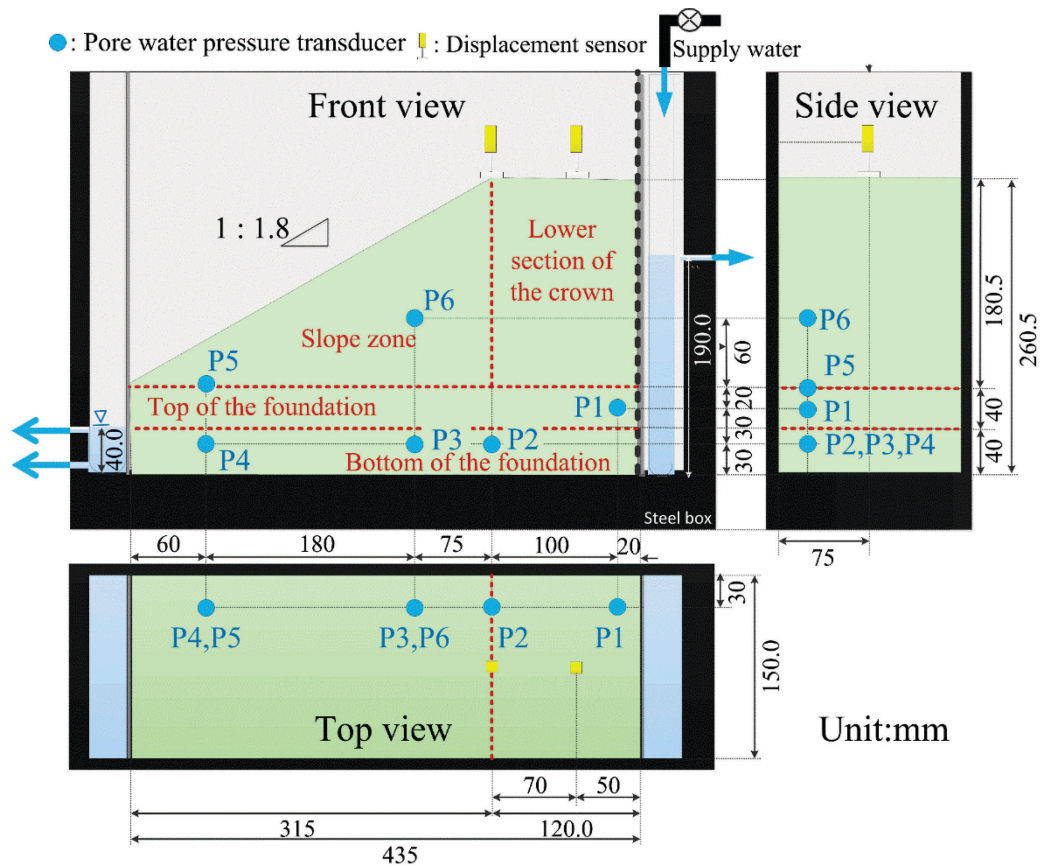
(a) Physical model
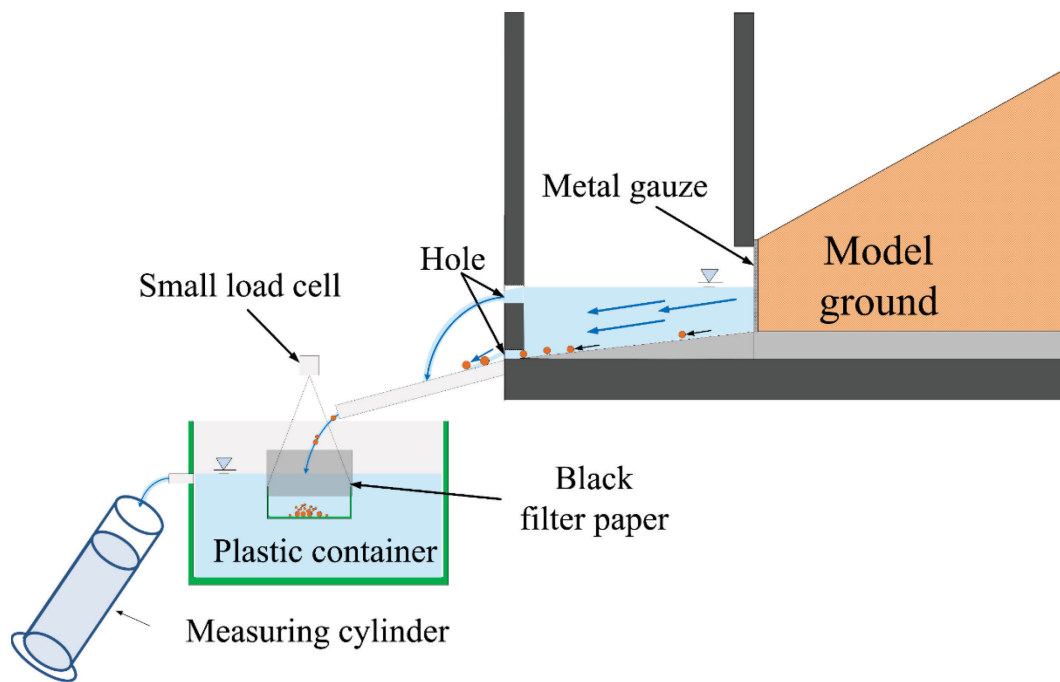
(b) Sampling on eroded fines

Figure 5-1   Schematic diagram of experimental system

To prevent material separation during preparation of the model embankment, the moist tamping method (Ladd, 1978) is employed.   The soil is compacted by layers with the thickness of 20mm where sensors are not located.   The pore pressure transducers used are SSK Micro Pressure Transducer P306V-01 (Photo. 5-2, measurable range: 0 - 10kPa).   The automated seepage system used, which is capable of investigating either the seepage conditions or erosion ratio, could conduct measurements and controls by PC.   All the measuring devices are connected to amplifiers and then to a universal recorder (Kyowa Electronic Instruments Co., Ltd., EDX-100A) connected PC.   All of the controls of the seepage test and data recording are through a software (Dynamic data acquisition software) with the interactive visual interface, developed by Kyowa Electronic Instruments Co., Ltd. To avoid formation of concentrated water path along the wiring of the sensors, the pore pressure transducers are put near the back side of the steel box.   An effort is made to measure the pore water pressure properly.   However, response of the sensor output is not so sharp, i.e., the full saturation of the sensors may not have been achieved, since the tests started from the state where the model embankment was under partially saturated condition with small water content.   Even so, the sensor readings can be used to detect water arrival and to

measure pore water pressure change.　The target dry density is 1.560 g/cm^3 (void ratio e = 0.695, relative density Dr = 35 %).　The initial moisture content is 3.0 %.　After making the level ground, the model ground is scraped off with a shaped frame and formed to be a 260.5 mm high embankment.　To prevent the occurrence of a strong flow between the side wall and model and to eliminate the boundary restriction form side wall, a mixture of grease (Silicone oil compound, Shin-Etsu Silicone Co., Ltd., KS-63W) and silicon oil (Silicone fluid, Shin-Etsu Silicone Co., Ltd., KF-96-1000CS) are put on the inside surface of the wall. Therefore, particles migration at the boundary surface are eliminated almost entirely.　In other words, the process of suffusion unfortunately cannot be observed from transparent glass on one side of a steel box.

Photograph 5-1　　Miniature lord cell (Kyowa Electronic Instruments Co., Ltd., LVS-2KA) (*Reference* Kyowa Electronic Instruments Web site)
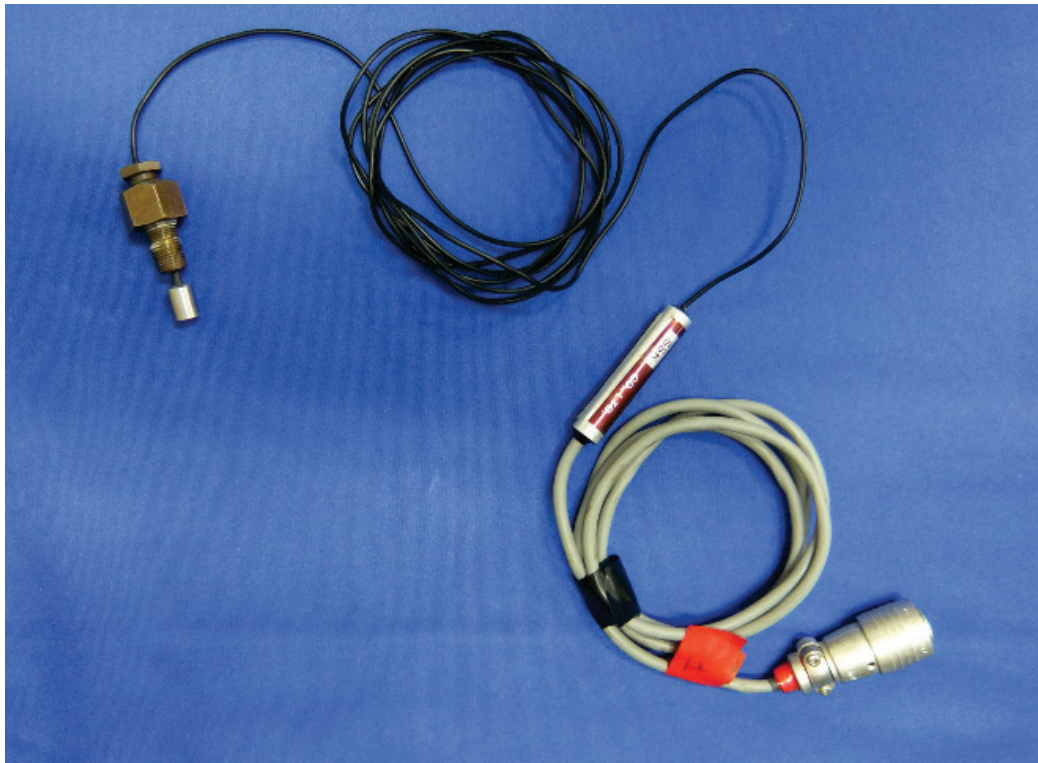
Photograph 5-2   Pore pressure transducer (SSK Micro Pressure Transducer P306V-01)

The model embankment is composed of two areas, the "foundation zone" (includes the "top of the foundation" and the "bottom of the foundation") and the "slope zone" (includes the "slope zone" and the "lower section of the crown") as shown in Fig. 5-1 (a). The foundation zone is an 80 mm-thick horizontal layer and the slope zone is an embankment with a slope of 1: 1.8. According to statistical survey of dam failures, this type of zoning, which have no zoning of materials or no downstream filter, is most vulnerable to the internal erosion (Foster and Fell, 2001; Fry *et al.*, 2012).

5.4. Experiment procedures and conditions

In this study, seepage flow stages of an unsteady seepage condition (first permeation to partially saturated model) and a steady seepage condition are reproduced by use of the above experimental system. First, the transport of fines in the above-mentioned stages is examined. By controlling the water level at the upstream boundary, the influence of repeated permeation on spatial change of fines in the embankment is also examined. Detailed test conditions and a conceptual diagram on controlled water level at the upstream

boundary are summarized in Table 5-1 and Fig. 5-2.   Elapsed time is measured from the pouring of water into the water supply tank.   Seepage flow in the embankment reaches a near steady condition in 30-40 minutes.

In total eight tests are conducted.   *Case St1* was conducted to investigate the erosion during the first permeation stage (unsteady seepage condition) and the test is terminated as soon as steady seepage condition was reached (Fig. 5-2).   In the other cases (*Cases St20, St24, St48* and *St280*), the seepage is continued for a prescribed time with keeping the water heads at the boundaries constant.

Table5-1　　Test cases of seepage testing

Case	Dry density (Mg/m³)	Seepage time (hr)	Repeat count of supply and drainage	Fines content at bottom layer	Number of sampling areas	Cumulative eroded soil mass (g)	Eroded soil ratio (%)
St1	1.559	0.55	1	15	48	22.77	0.764
St20	1.562	20	1	15	48	32.37	1.085
St24	1.560	24	1	15	48×3	34.88	1.169
St48	1.567	48	1	15	66	28.03	0.913
St280	1.560	280	1	15	45	154.67	5.190
St96RS4	1.560	96	4	15	48	44.55	1.495
St96RS8	1.560	96	8	15	95	43.11	1.447
St280RS40	1.559	280	40	15	47	234.82	7.885
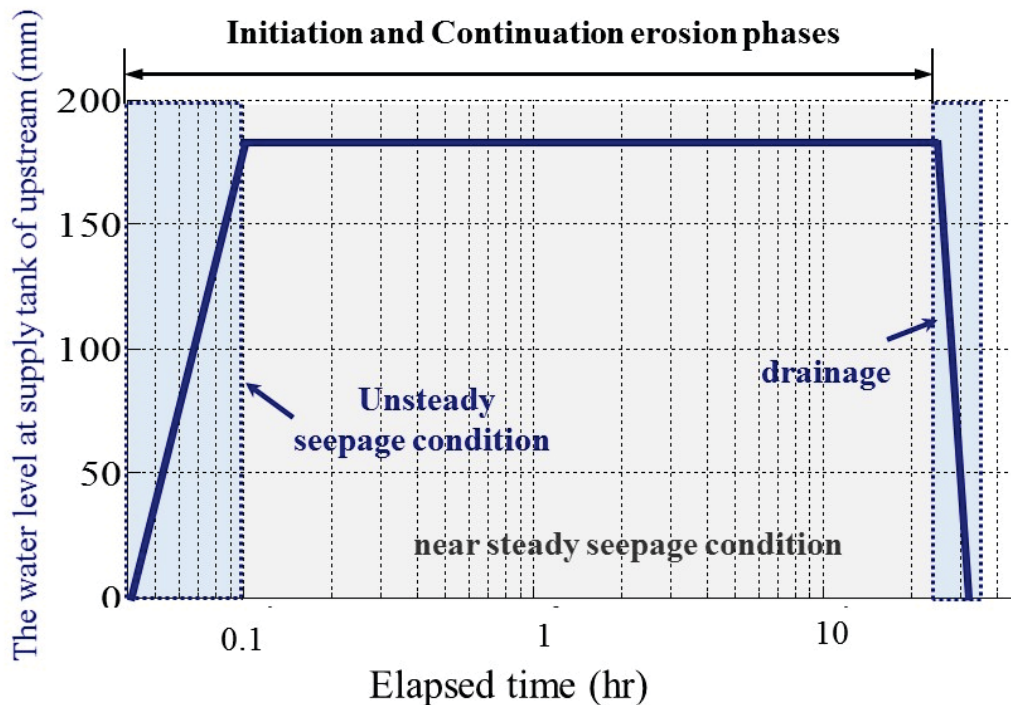
Figure 5-2　　Conceptual diagram on controlled water level at water supply tank

Cases St96RS4, *St96RS8* and *St280RS40* are carried out to assess the influence of rising and lowering phreatic surface on spatial change of fines in the embankment. *Case St96RS4* consists of 1440 minutes of water supply, 1440 minutes of drainage, and four repetitions to the physical model. In *Case St96RS8* repeated water penetrations are provided in eight cycles of 720 minutes duration. In this case, the value of the pore water pressure transducer at P1 in Fig. 5-1 showed a maximum head fluctuation of plus or minus 50 mm due to complications in the experimental system. In *Case St280RS40*, the repeated permeation times are random. The objective of *Case* St280RS40 is to understand how spatial distribution of fines in embankment is affected by rising and lowering phreatic surface. To exaggerate the spatial change of fines, the rising and lowering of the water level at the upstream are randomly made as many as we could.

During the seepage test, the crown settlement is measured by displacement sensors. However, even in *Cases St280* and *StRS40*, which showed relatively large settlements, the maximum values are 0.16 mm and 0.21 mm at the top of the slope and 0.06 mm and 0.24 mm at the center of the crown during the seepage tests. Compared with the initial model height of 260.5 mm, it can be said that overall volume change of the model embankment was negligible. Therefore, the volume change of the embankments is not considered in this study.

After the seepage test, sieve analyses in each area of the embankment are carried out to estimate the extent of erosion-induced fines content variation. The number of sampling areas for sieve analyses is given in Table 1. Since no previous study has reported the detailed distribution of the fine fraction in the physical model, this is one of the features of this study.

5.5. Results and discussion

5.5.1. First permeation-induced change in spatial distribution of fines (*Case St1*)

Figure 5-3 shows evolutions of the cumulative eroded soil mass and variations of pore water pressure with time for *Case St1*. The left vertical axis is for the evolutions of the cumulative eroded soil mass while the right one is for the variation of pore water pressure. The variation of pore water pressure is not directly indicated water level. It depends on not only hydrostatic pressure, but also influence of immediate fines distribution. From this figure, it

57

can be seen that pore water pressure increases with raising of water level at all the measurement points until around 0.2 hour. After that, they show a peak value around an elapsed time of 0.2 hour. Finally, they reach near steady seepage condition.
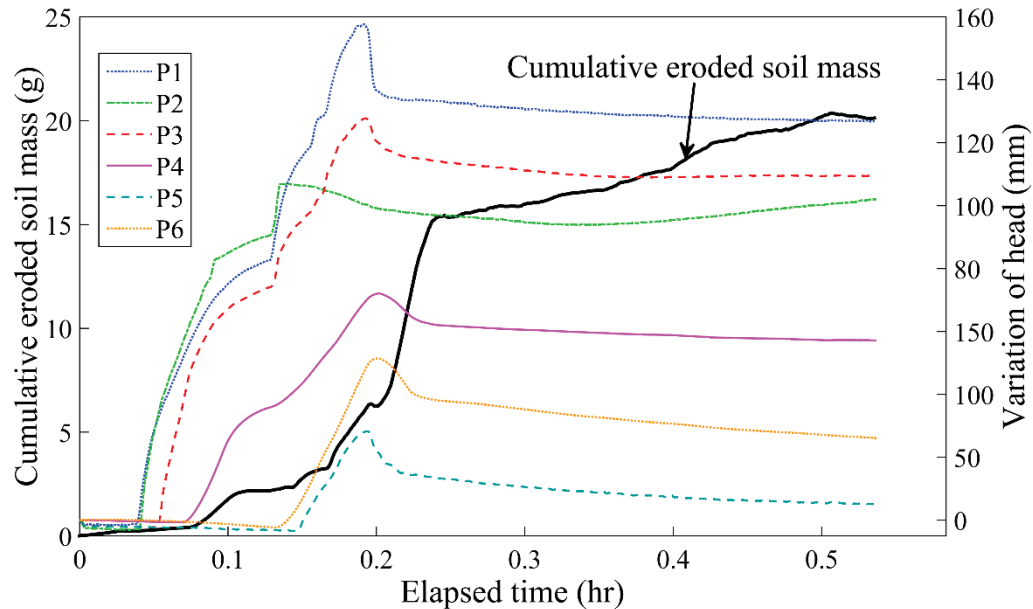
Figure 5-3   Evolutions of cumulative eroded soil mass and variation of a pore water pressure from initial value for *Case St1*

Initiation of fines eroded out is observed almost as soon as the pore water pressure located at bottom of the toe (P4 in Fig. 5-1) starts rising. Major fines erosion takes place over a period of around 0.15 hours (540 seconds) after the detection of the eroded soil from the model. After that, increment of eroded soil mass with time becomes small. These suggests that a relatively large amount of soil is eroded under the unsteady seepage condition, i.e., during the first permeation of water to the embankment.

The distribution of change in the fines content normalized by the initial value is plotted in Fig. 5-4 for *Case St1*. Change in spatial distribution of fines is calculated by assuming that the initial fines content is uniform in all parts of model embankment before the seepage tests.

Decrease in fines is observed throughout the model, especially at the bottom of the foundation near the downstream boundary (Fig. 5-4).   The majority of this change in spatial distribution of fines may have occurred before reaching the near steady state.   A lot of fines washing out during the first permeation may be attributed to the disappearance of suction due to saturation and reposition of fines by hydraulic force.   First arrival of seepage water may cause an effective stress change, resulting in a small change in structure of the soil.   A particle held in a stable position before wetting suffers a hydraulic force, such as a seepage force and a buoyancy force, when seepage water reaches the particle.   Then, a movable particle initiates the migration or transportation.   The initiation might depend on the particle size and/or initial position in the void of the coarse skeleton.   This particle migration or transportation leads to change in the immediate local flow conditions and an infinitesimal collapse of initial structure of the soil.   As a result, fines reposition takes place.   Fell *et al.* (2003) described that vulnerability to dam failure is greater on first water filling or at historic high reservoir water level.   Namely, marked change in hydraulic stability against seepage of embankment occurs during the wetting.
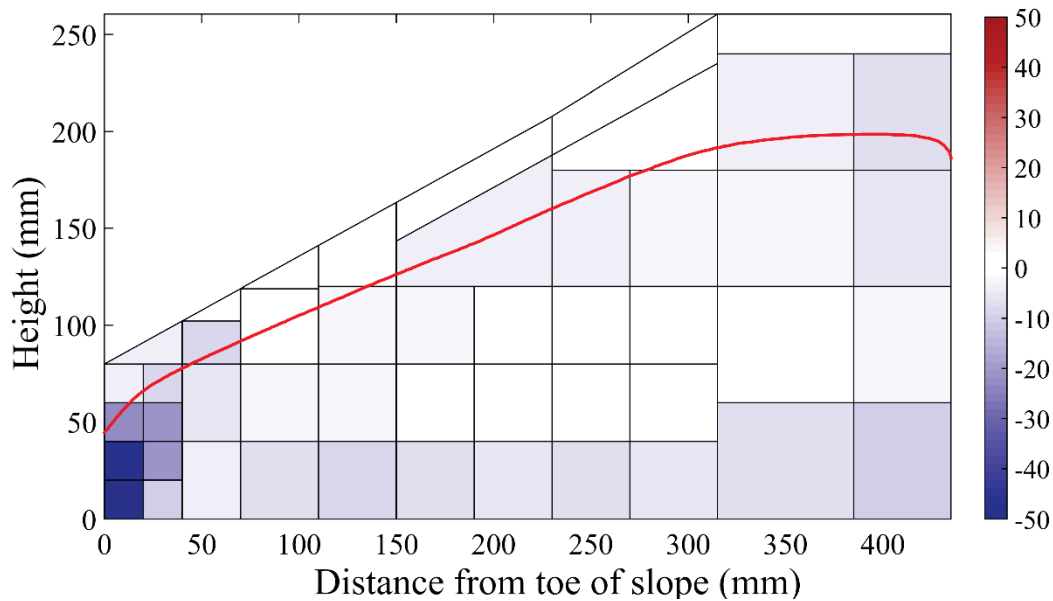
Figure 5-4   Change of spatial distribution of fines in embankment for *Case St1*

5.5.2. Characteristics of erosion under the steady seepage flow

Figure 5-5 shows evolutions of the cumulative eroded soil mass for *Cases St20, St24* and *St48*, erosion rates derived from the cumulative eroded soil mass and discharge rate of water at the toe with the exception of *Cases St1*.   The right vertical axis is for the normalized mass of erosion.   The amount of discharged fines is normalized by the total amount of Silica sand No.8 in the model before the seepage test.   In *Case St48*, the data are not collected continuously.   The total eroded soil masses are as summarized in Table 5-1.   As shown in Fig. 5-5, major fines erosion takes place in the early stage of the seepage tests (until around 1-4 hour).   In this period, the discharge rate is relatively large.   After that, the erosion rates get smaller and the discharge rate also gradually decreases with time to 0.4-0.6 *L/min.*

Some discrepancies in the cumulative eroded soil mass exists, i.e., the eroded soil mass are relatively large in *Case St280* (see Table 5-1) and the discharged rate is also large in this case, compared with the other cases.   The exact causes are unclear, but the author infer the occurrence of a relatively strong flow between the sidewall and soil in this case.   However, as the spatial distributions of fine fraction at the middle cross section in this case show a coherent trend compared with the other cases, this test result is also used to discuss about the progress of suffusion in the following subsections.

The main cause of the fines erosion in the early stage of the seepage tests (until around 1-4 hour) is attributed to disappearance of suction due to water permeation and reposition of fines by hydraulic force as described above.   After the early stage of the seepage tests, the evolution of suffusion slowly continues under the near steady seepage condition in the embankment, as described by Luo *et al.* (2012) for the one-dimensional seepage test, i.e., fine particles migration $\rightarrow$ pores clogging $\rightarrow$ pushing out clogging pores $\rightarrow$ fine particles remigration (Fig. 5-6).

The variation of pore water pressure with time for *Case St48* is shown in Fig. 5-7.   The head at all the measurement points was applied slowly over a period of nearly 0.2 hour.   After that, they show a peak value around an elapsed time of 0.2 hour.   The values of pore water pressure got stable at an elapsed time of approximately 2 hour.   A sharp increase in the pore water pressure detected at 2.85 hour at P1.   The values of pore water pressure, except at P1, gradually decreased with time until an elapsed time of around 4.5 hour.   The pore water

pressure at P3, P4, and P5 exhibited no significant change with time after the peak value at 0.2 hour elapsed time.   They shows only slightly increases in pore water pressure.   Ke and Takahashi (2014) explained this kind of variation of hydraulic condition as; *the soil grains gradually change their position for self-balance at this stage and correspondingly, the specimen deforms. After a certain period, the packing of soil grains reaches a new equilibrium without the further erosion of fines.   As a result, the hydraulic gradient becomes constant.*

On the other hand, the pore water pressures at P1, P2, and P6 exhibited increase in pore wore pressure with fluctuation.   The behavior might be explained by the local change in hydraulic conductivity, which is attributed to fines migration or clogging, as described by Luo *et al.* (2012).

Distributions of change in the fines content normalized by the initial value are plotted in Fig. 5-8 for all the cases.   After a certain elapsed time, it became difficult to observe the accurate phreatic surface for wetting of soil.   Then, phreatic surface could not be observed the phreatic surface exception of *Cases St1*.   Therefore, in the figure, the observed phreatic surface before the end of *Case St1* is indicated by a solid line again to indicate brief position of phreatic surface for each cases.   All results show that fines content is decreased as a whole, especially for elements contacted by the water surfaces of the drainage tank at the downstream boundary.   A decrease in fines in the elements near the upstream boundary is also seen because of the absence of supply of fines from upstream.   The followings can be observed from the figure:
- In Cases *St24*, *St 48* and *St280* (Fig. 5-8 (b-d)), a regressive decrease of fines along the phreatic surface is observed from middle of the foundation near downstream boundary.
- In *Case St20*, an increase in the fines content is observed in some elements.
- In *Case St48*, although the seepage time of *Case St48* is longer than that of *Cases St20* and *St24* the cumulative eroded soil mass of *Case St48* is relatively small.
- In *Case St280*, the magnitude of change of spatial distribution of fines is large compared with the other cases.   It also shows an increase in fines in the foundation round horizontally 30 mm and 280 mm distant from the toe of the slope.
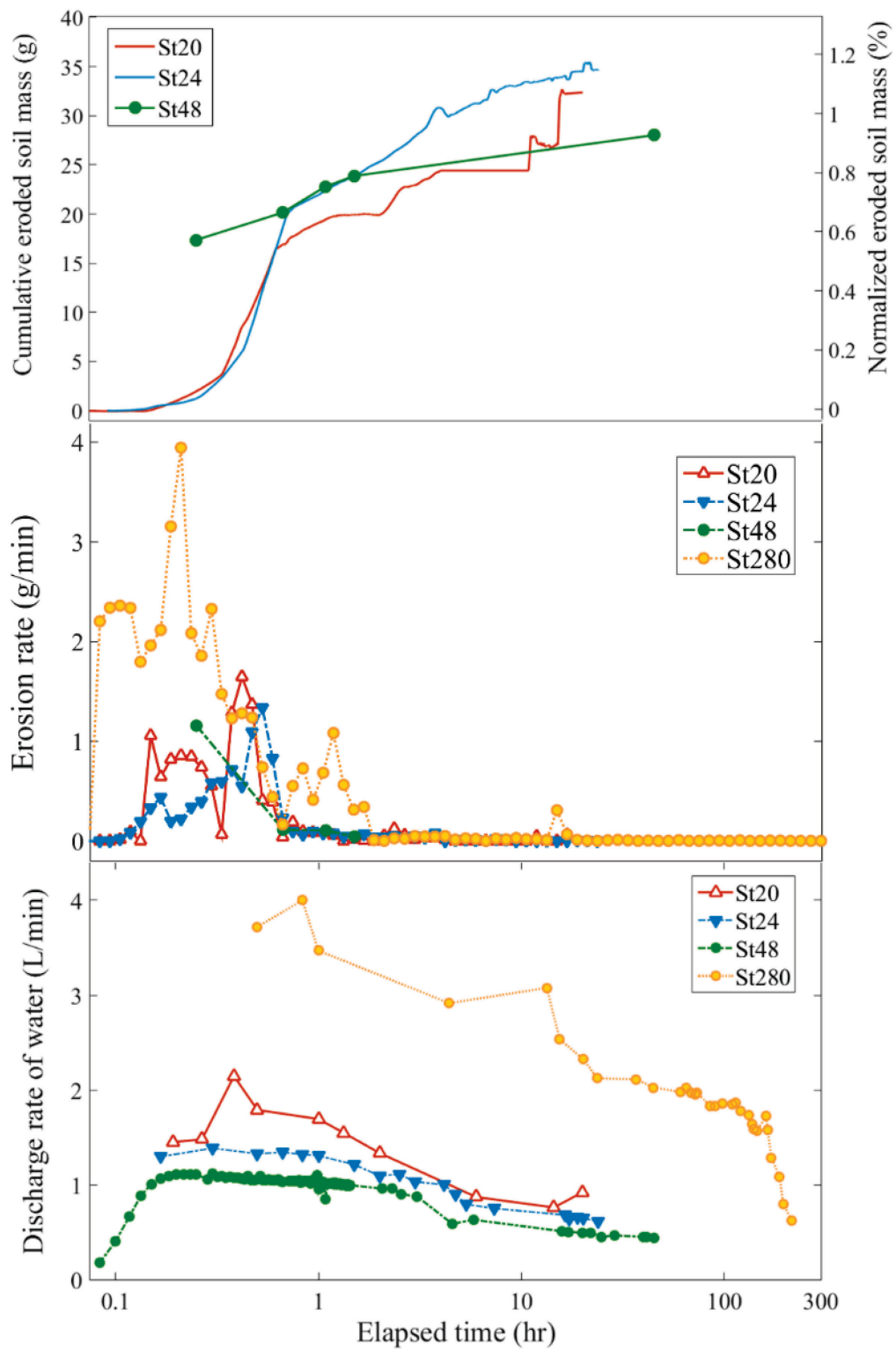
Figure 5-5   Evolutions of cumulative eroded soil mass for *Cases St20*, *St24* and *St48* and
evolutions of discharge rate of water for *Cases St20*, *St24*, *St48* and *St280*
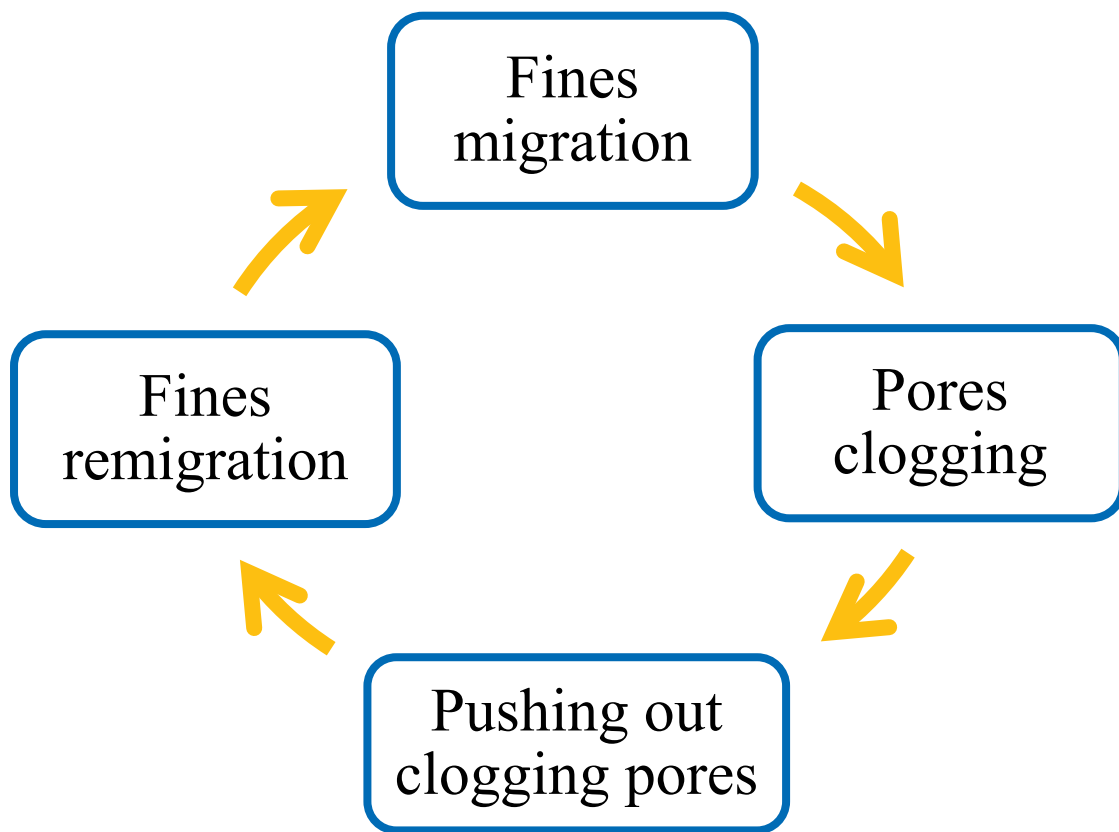
Figure 5-6   The evolution of iterative suffusion process (Luo *et al.* 2012)
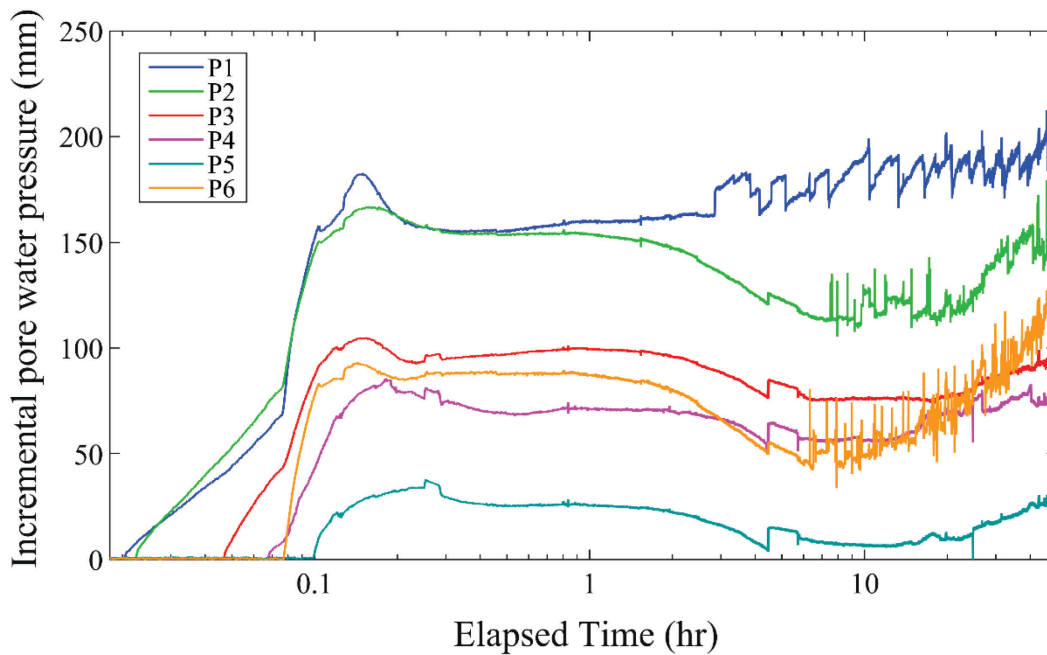
Figure 5-7   Variation of a pore water pressure from initial value for *Case St48*

As seen in Figs. 5-5, the erosion rate correlates with flow rate.   In other words, the transportation of particles correlates with the hydraulic conductivity of the entire embankment.   During the steady seepage, the erosion rates get smaller and the discharge rate also gradually decreases with time.   Previous one-directional seepage tests showed a similar trend, i.e., a decrease in hydraulic conductivity with elapsed time (*e.g.* Lafleur, 1999; Bendahmane *et al.,* 2008; Marot *et al.,* 2012) as observed in Fig. 5-5.   The decrease in hydraulic conductivity may be result of the suffusion-induced clogging in the soil specimen. Lafleur (1999) showed that the variations in general hydraulic conductivity of a specimen depends on the spatial distribution of fines in specimens in their interpretation of downward filtration tests on geotextiles and cohesionless soils (see Fig. 5-9).   If this interpretation is applied to this study, it can be said that the general hydraulic conductivity of the embankment depends on the spatial distribution of the fine fraction in the embankment.

Marot *et al.* (2012) showed that higher angularity of coarse fraction grains is conducive to increasing the suffusion resistance and also decreases the hydraulic conductivity.   Silica sand is a categorized as sub-rounded to sub-angular material.   This contributes to the decrease in the flow rate in the model embankment.
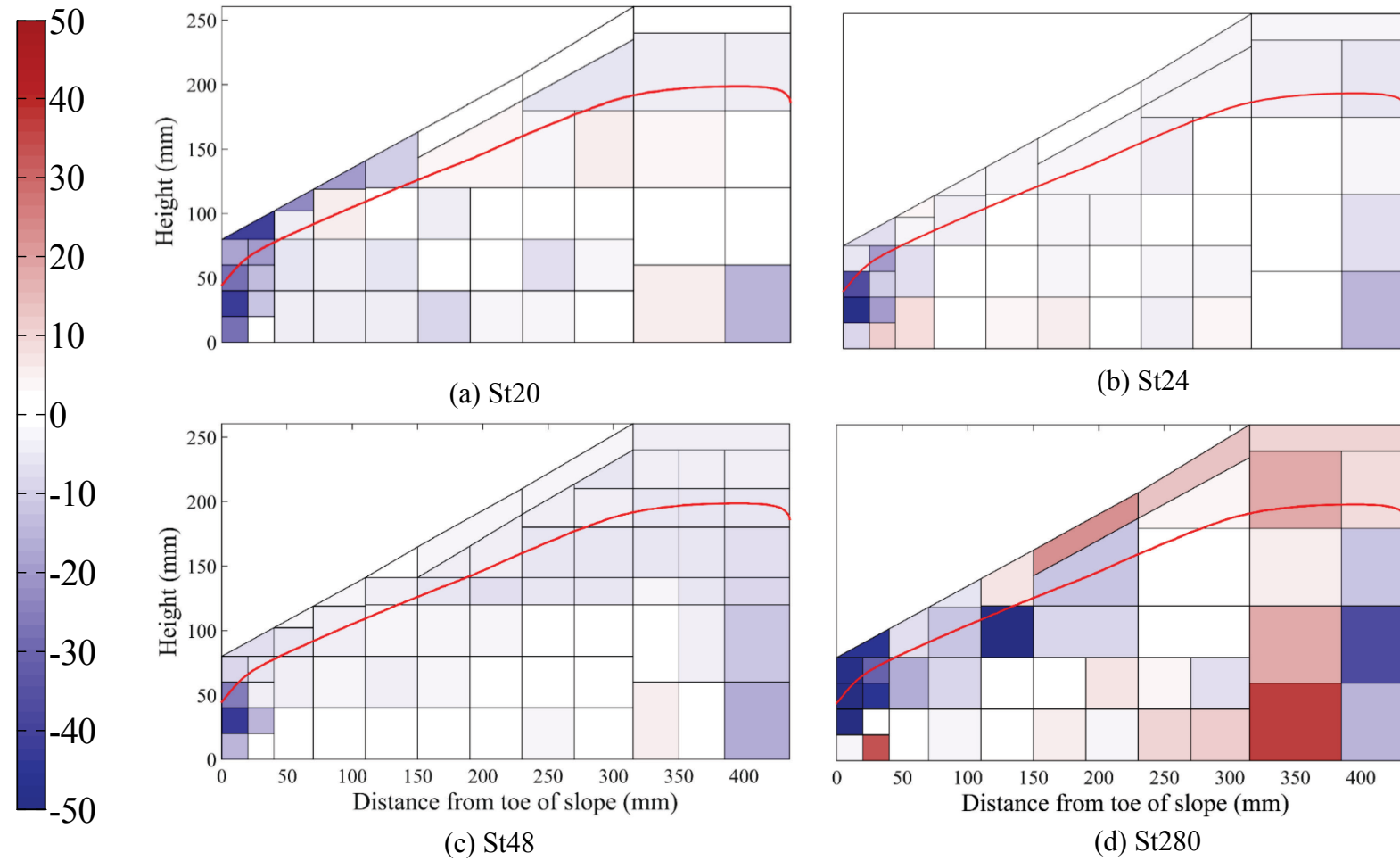
Figure 5-8   Change of spatial distribution of fines in embankment for *Cases St20, St24, St48* and *St280*
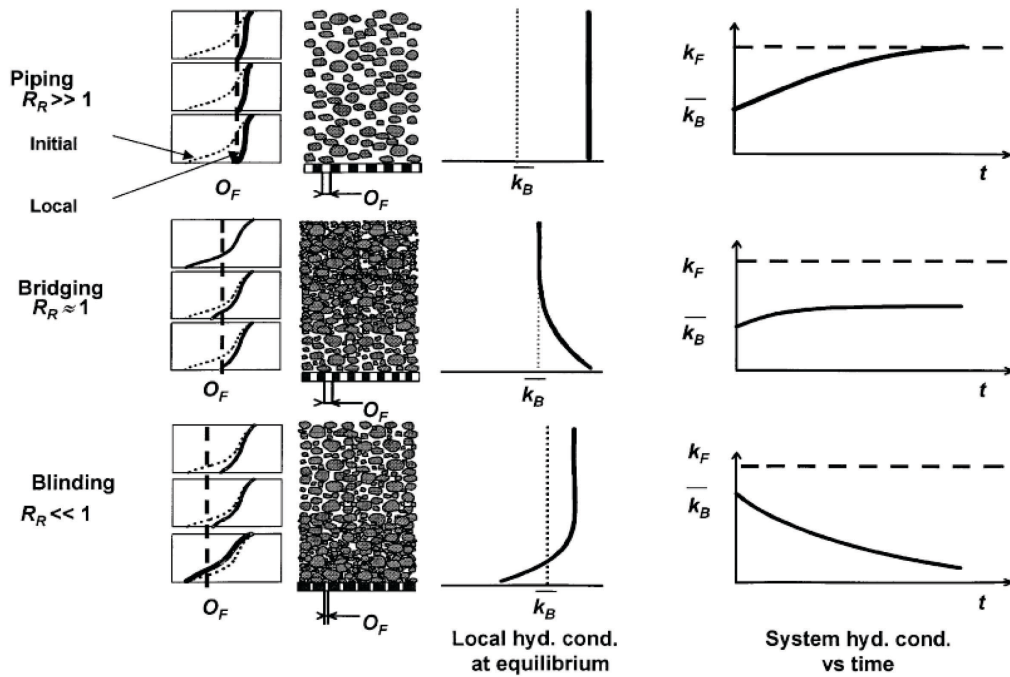
Figure 5-9   Pore structure changes during the filtration of broadly graded soil (Reference by Lafleur (1999))

To understand the progress of suffusion in the embankment under steady seepage flow, an attempt is made to visualize the change of the fines content distribution using the tests having different seepage time.   Assuming all initial test conditions and erosion processes are the same, the tests are arranged by ascending order of the seepage time or cumulative eroded mass.   To eliminate the fines content change during the transient stage, i.e., before the seepage flow becomes stable, the incremental change of the normalized fines content with time is calculated and plotted in Fig. 5-10 by making *Case St1* as a reference.

It is not very clear, but a decrease in fines is observed in the slope zone and in the upper half of the foundation while an increase in fines can be seen in the bottom half of the foundation over one or two days of steady seepage (Fig. 5-10 (a)-(c)).   The contrast becomes clearer with the elapse time.   In *Case 280,* a lot of fines are eroded out (it should be noted that the discharge rate in this case is larger than the other cases though) and a large reduction of fines occurred at Area B near the toe and Area C near the phreatic surface in the slope zone (Fig. 5-10 (d)).
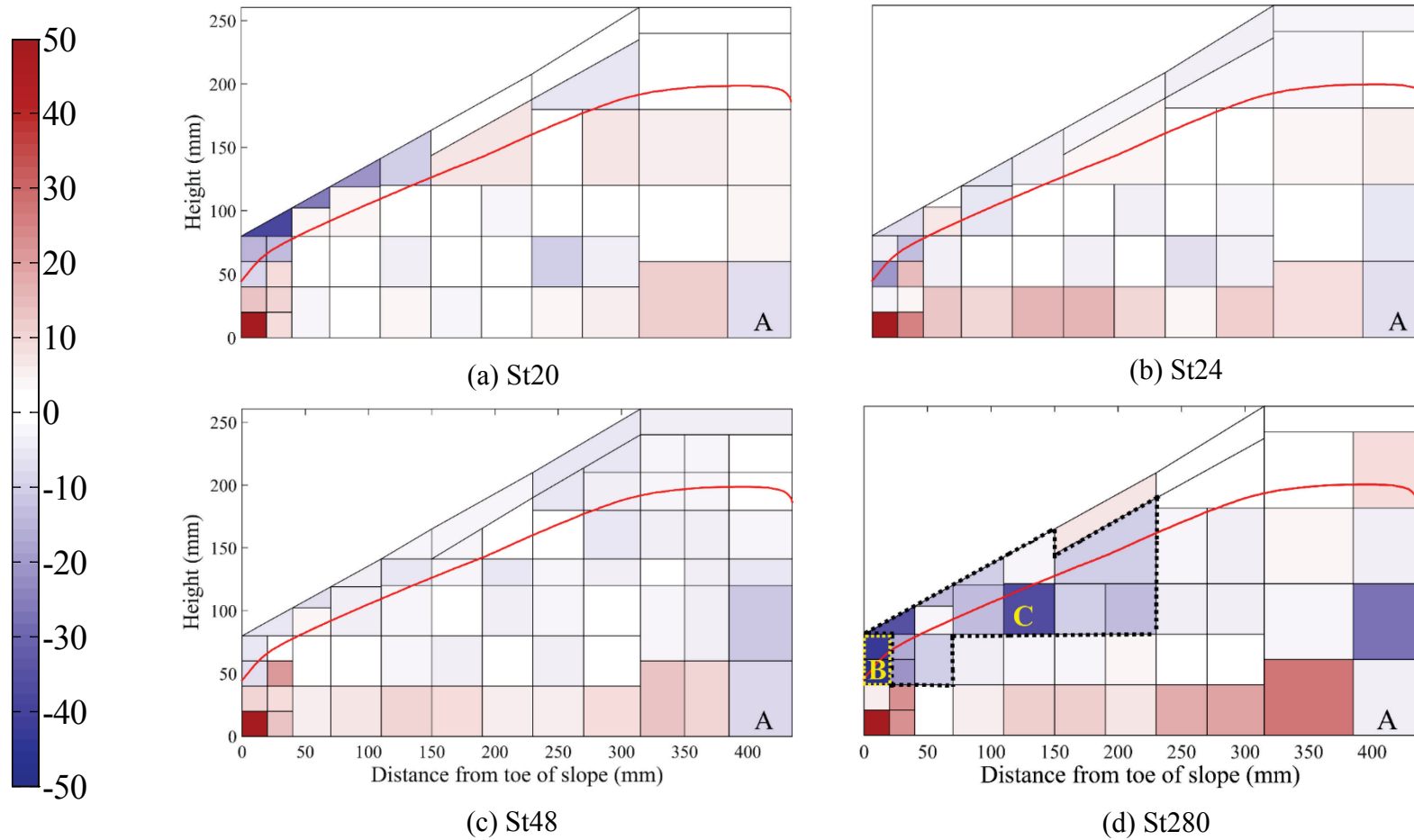
Figure 5-10   Incremental change of normalized fines content with time by making *Case St1* as a reference, (a) *Case St20* (20 hours), (b) *Case St24* (24 hours), (c) *Case St48* (48 hours), (d) *Case St 280* (280 hours)

An increase in fines can be observed in the bottom of the foundation at around 0-70 mm horizontally and 315-385 mm distant from the toe of the slope under steady seepage flow. These fines increased areas develop in the horizontal direction with time and amount of eroded soil mass. As the seepage flow is mostly horizontal at the foundation, leftward horizontal migration of the fines is expected. However, the decreasing rate at element A is relatively small, compared with an increasing rate at the further downstream locations in the bottom of the foundation. A possible explanation for this is the migration of fines in the other directions. Namely, the eroded fines move not only by seepage flow but also by gravitational vertical force and deposit in the foundation. This local concentration of fines in the embankment may have caused a decrease in the hydraulic conductivity of the whole embankment as shown in Fig. 5-5, which is consistent with the interpretation of the elemental test by Lafleur (1999).

In *Case St24*, the embankment model was divided in the depth direction into three parts; the front, middle and back parts after the seepage test. Sieve analyses in each area of the embankment were carried out to evaluate the boundary restriction form side wall and sensors. The number of sampling areas for sieve analyses is 48×3 (see Table 5-1). Figure 5-11 shows spatial distribution of fines in embankment after seepage test in *Case St24*. The results indicate they have few effects on the boundary restriction form side walls (see Fig. 5-11 (b), (d)). In physical model tests, the pore pressure transducers were put near the back side of the steel box to avoid formation of concentrated water path along the sensors and its wiring. The spatial distribution of fines content in embankment at the back side section (Fig. 5-11 (d)) denotes the almost same tendency of other cross-section and their average (Fig. 5-11 (a), (b) and (c)). It would suggest that they have few effects on existing sensors in modelling fines migration in embankment.
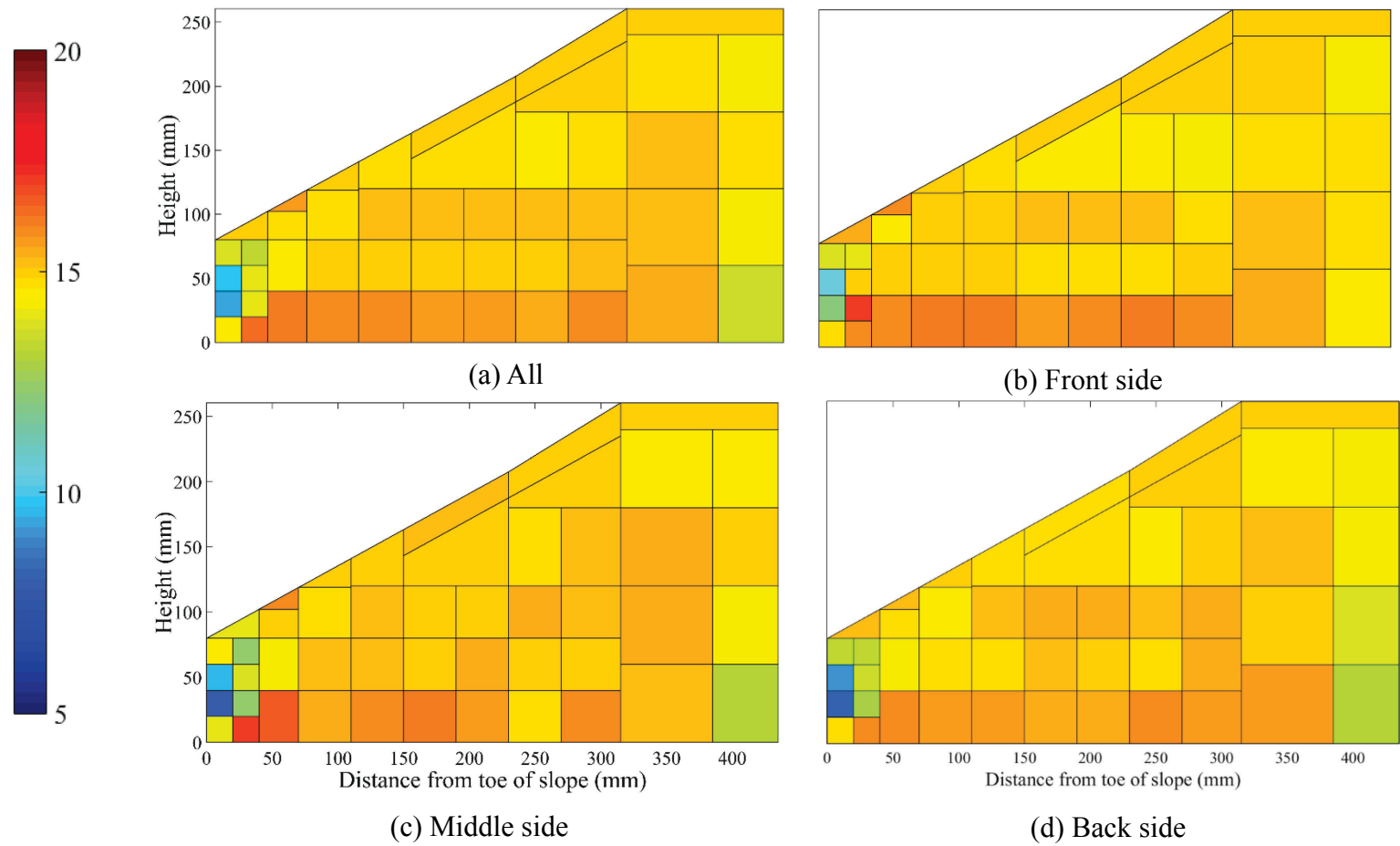
Figure 5-11   Cross-section on spatial distribution of fines content in embankment after seepage test in Case St24, (a) All, (b) Front, (c) Middle, (d) Back

5.5.3. Effect of repeated permeation

To investigate the characteristics of erosion in a regular pattern of rising and lowering phreatic surface, the result of *Case St96RS4*, which has well-controlled boundary water level and regular repeated permeation, is focused upon.   Figure 5-12 shows evolutions of the cumulative eroded soil mass at each of the seepage periods for *Case St96RS4*.   This result shows that erosion of fines occurred mostly during the first seepage period.   From the second period, the eroded mass is decreased.   In all seepage periods, major fines erosion takes place until around 5 hours.

Changes in the discharge rate of water at the toe for each seepage period of *Case St96RS4* are shown in Fig. 5-13.   In this figure, it is observed that the discharge rate of water increases slightly from third seepage period.   This means that the general hydraulic conductivity of the embankment increases with increasing times of repeated permeation. The erosion apparently becomes negative at some points in Fig. 5-12.   The exact causes are unclear, but the author infer the disturbance of the water in the plastic container in Fig. 5-1 (b) by some trouble leaded to variation of the measurement value.

The variations of pore water pressure with time for each seepage period of *Case St98RS4* are shown in Fig. 5-14.   This result shows that pore water pressure increases with increasing times of repeated permeation.   This is probably because rising of phreatic surface and increasing in the general hydraulic conductivity of the embankment due to suffusion.   This means that seepage flow activated by increasing times of repeated permeation.   The variations of pore water pressure at P5 and P6 dramatically drops to negative value after the "peak" (Fig. 5-14 (e), (f)).   It indicates that the measurement points were unsaturated at the corresponding seepage period.   From the second period, the variations of pore water pressure at P5 and P6 show positive value.   This is attributed to rising of phreatic surface due to increasing times of repeated permeation, i.e. development of suffusion.

Figure 5-15 shows evolutions of the cumulative eroded soil mass for *Cases St280* and *St280RS40*.   In *Case St280RS40*, discharge rate of water is not measured.   However, according the evolutions of the cumulative eroded soil mass at the first seepage period for

Cases St280 and *St280RS40*, the discharge rate of water of *Case St280RS40* might be expected to be the same level.
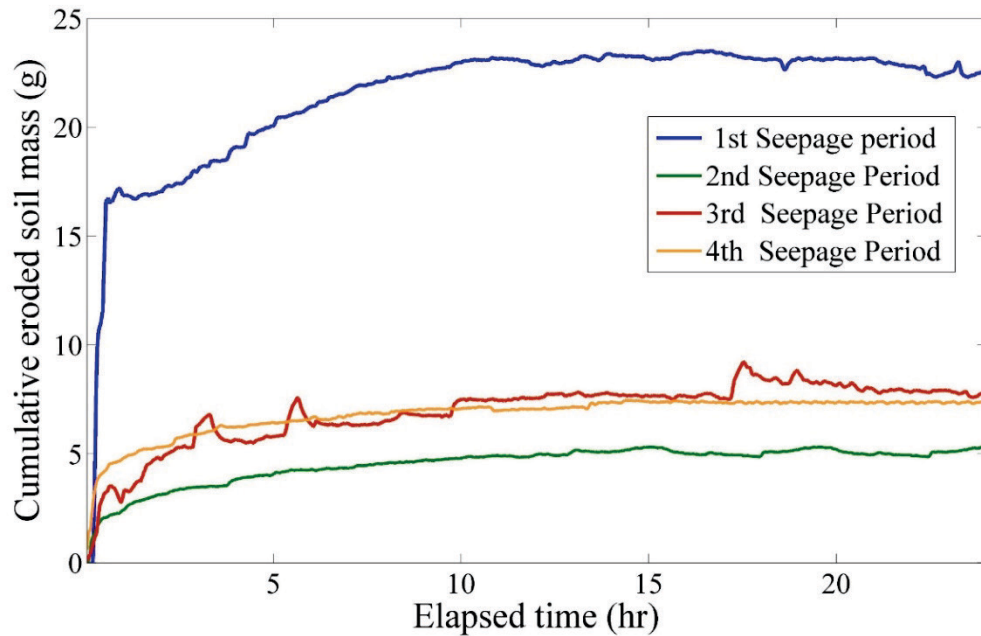
Figure 5-12   Evolutions of cumulative eroded soil mass at each seepage period for *Case St96RS4*
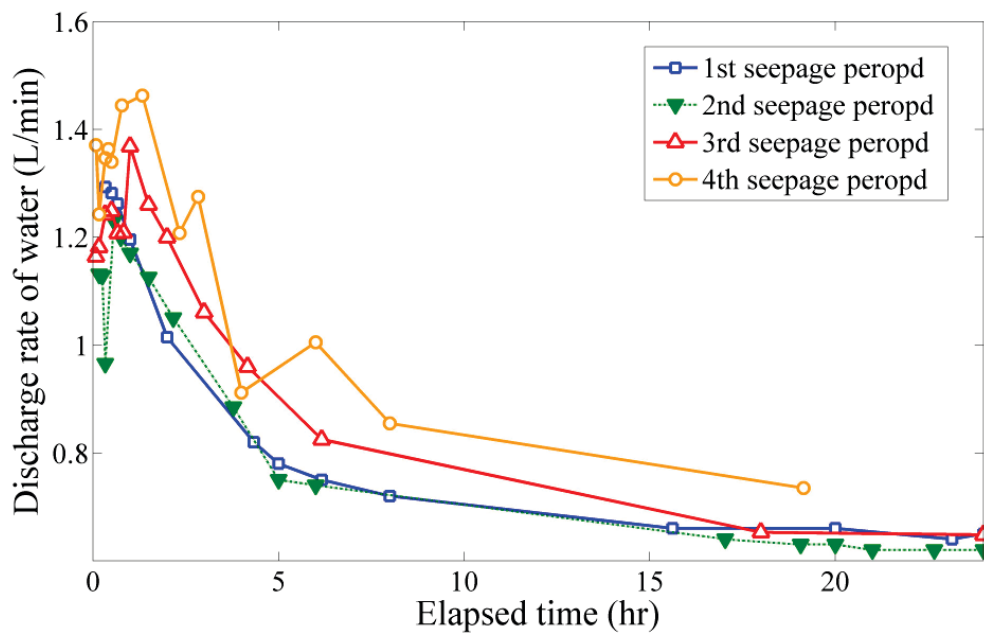
Figure 5-13   Evolutions of discharge rate of water for *Case St96RS4*

(a) P1

(b) P2

(c) P3

72
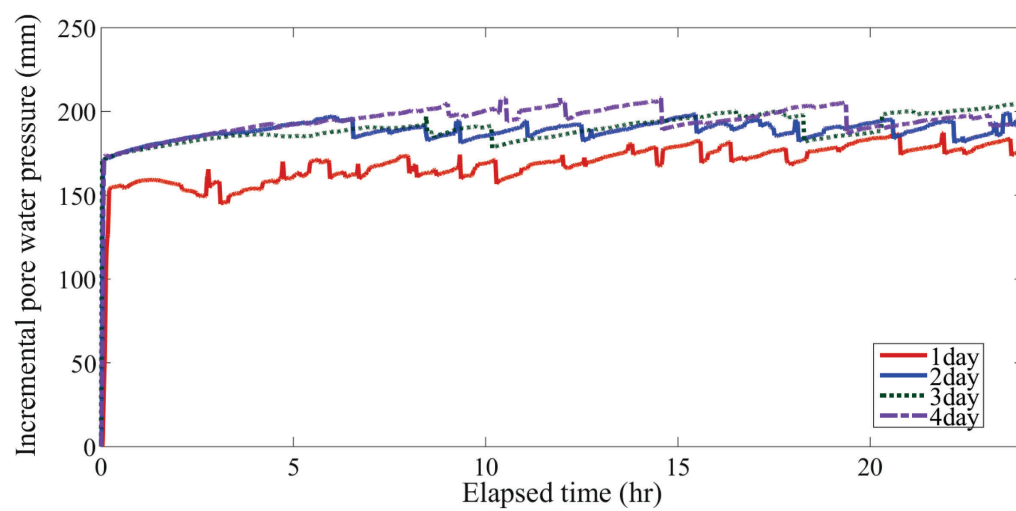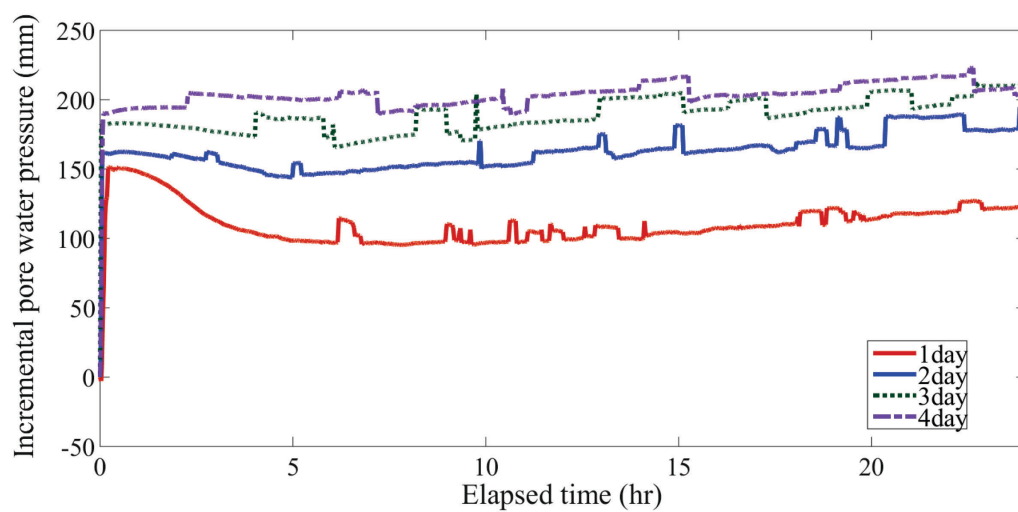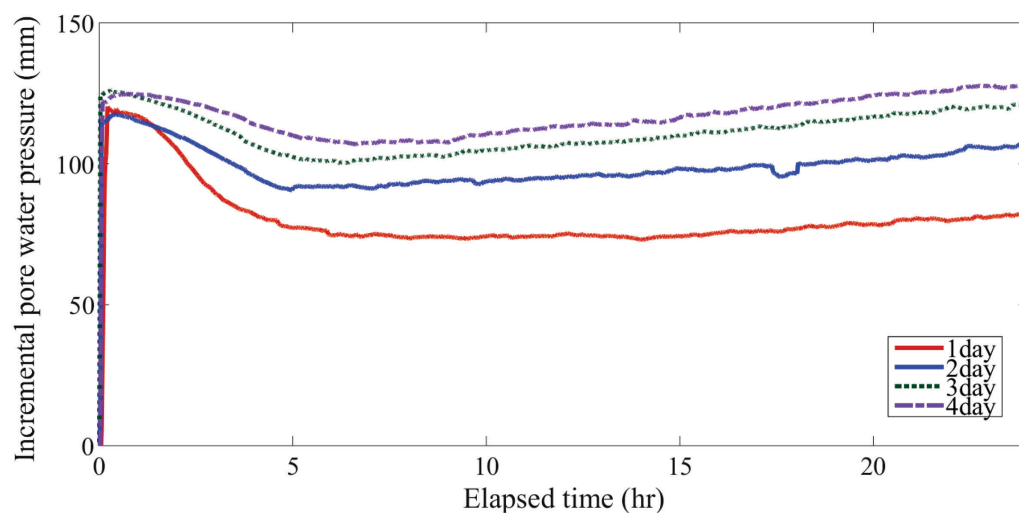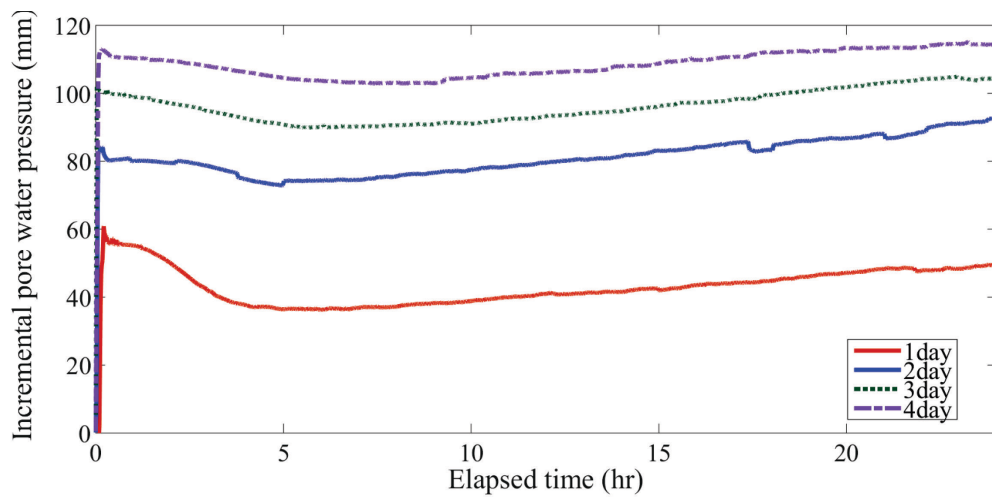
(d) P4
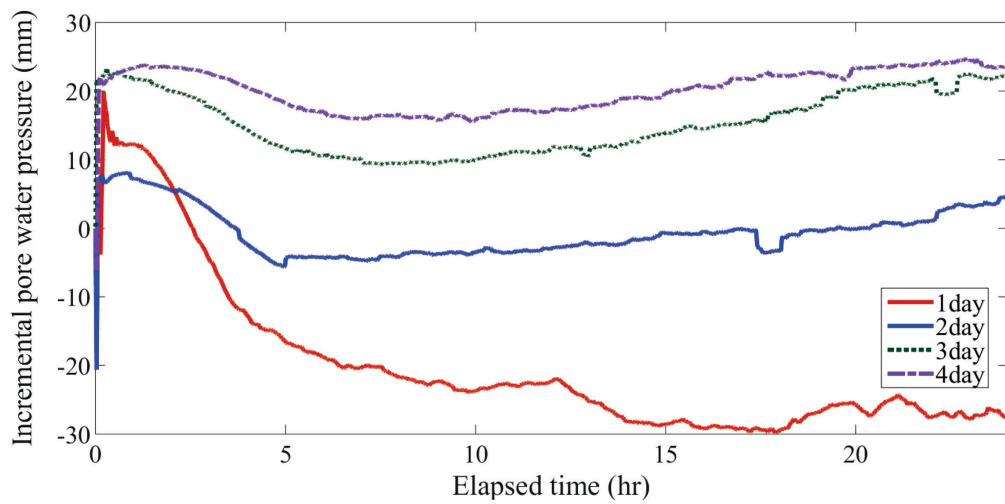
(e) P5
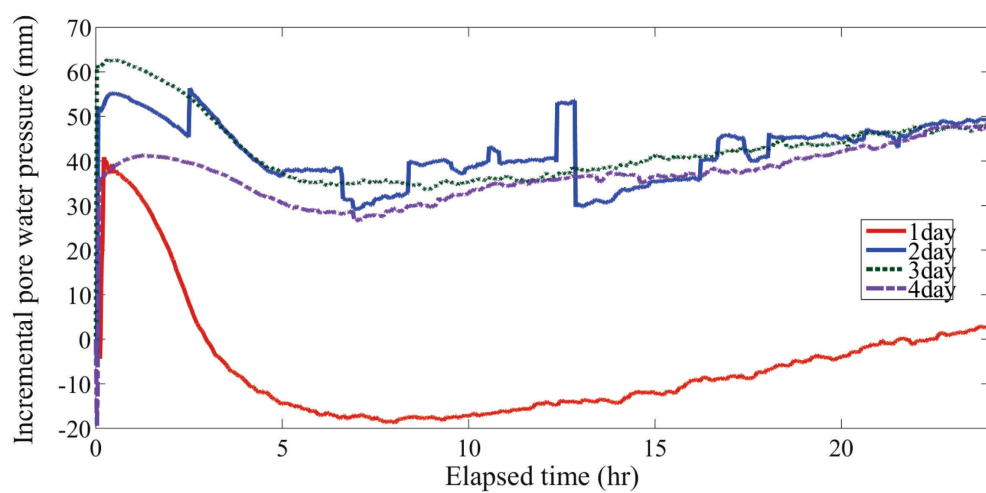
(f) P6

Figure 5-14   Variation of a pore water pressure from initial value at each seepage period

for *Case St96RS4*

73
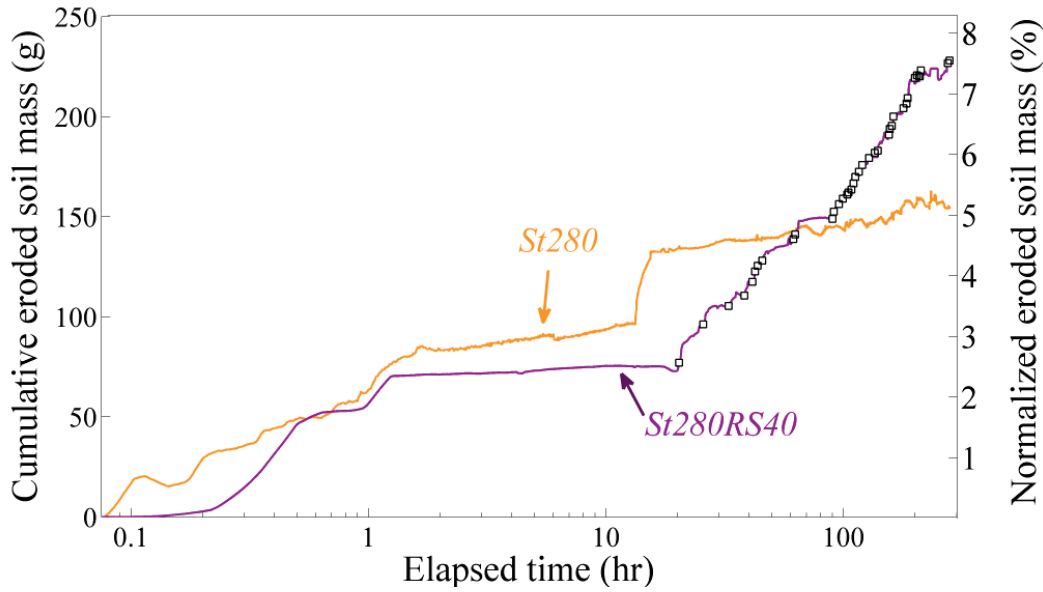
Figure 5-15   Evolutions of cumulative eroded soil mass for *Cases St280* and *St280RS40*

Distributions of changes in the fines content normalized by the initial value are plotted in Fig. 5-16 for *Cases St96RS4, St96RS8*, and *St280RS40*.   The following trend of changes in spatial distribution of fines can be understood from each figure:

·   In *Case St96RS4*, a decrease of fines can be seen from the middle of the foundation near the downstream boundary (Fig. 5-16 (a)).

·   In *Case St96RS8*, as shown in Fig. 5-16 (b), a decrease of fines can be confirmed from the middle of the foundation near the downstream boundary and the upper part of the slope zone.   A high concentration of fines is observed around the middle of the slope zone below the phreatic surface.

·   In *Case St280RS40*, a decrease in fines can be observed from the middle of the foundation near downstream boundary to the lower section of the crown.   The increase of fines at the foundation zone is larger and more extensive than the other cases (Fig. 5-16 (c)).

Major fines erosion in the early stage of each seepage period, as shown Fig. 5-10, are attributed to disappearance of suction due to saturation and reposition of fines by hydraulic force as described in the previous subsections.

74

To understand the effect of repeated permeation on the spatial distribution of fines, results of sieve analysis in *Cases St280* and *St280RS40* are compared at the same cumulative water supplying time.   The difference in the normalized fines content between *Cases St280* and *St280RS40* is plotted in Fig. 5-17.   From the figure, the clear boundary D-D' that separates the area of increase and decrease of fines is seen.   This indicates that a lot of fines are transported from decreased elements to elements located just below or obliquely downward due to repeated permeation.   Namely, repeated permeation leads to the prominent vertical transportation of fines at the boundary between the slope zone and the foundation zone. The cause of this formation of the clear boundary at D-D' remains unknown, but it can be said that drawdown between cycles allowed the transported fines to settle and this is one of the reasons for the marked increase in fines in the foundation zone.

5.5.4. Mass balance of eroded soil mass

Base on measurement of total eroded soil mass at the end of the physical model test and eroded soil mass calculated using results of spatial distribution of fines content in embankment after seepage test, mass balance of the eroded soil mass is examined to confirm the accuracies of the physical model tests and sieve analyses.   Figure 5-18 shows the relationship between sampled eroded soil ratio shown in Table 5-1 and calculated eroded soil ratio by using the results of spatial distribution of fines content in embankment after seepage test.   In general, they are linearly correlated, but the eroded soil mass measured at the outlet is smaller than that calculated from the sieve analyses.   This is probably due to not all the eroded soil could not be captured at the outlet during the seepage test.   However, as the sampled one is more or less linearly correlated with the calculated one, the discussions made in this chapter are effective, at least, qualitatively.

(a) St96RS4

(b) St96RS8
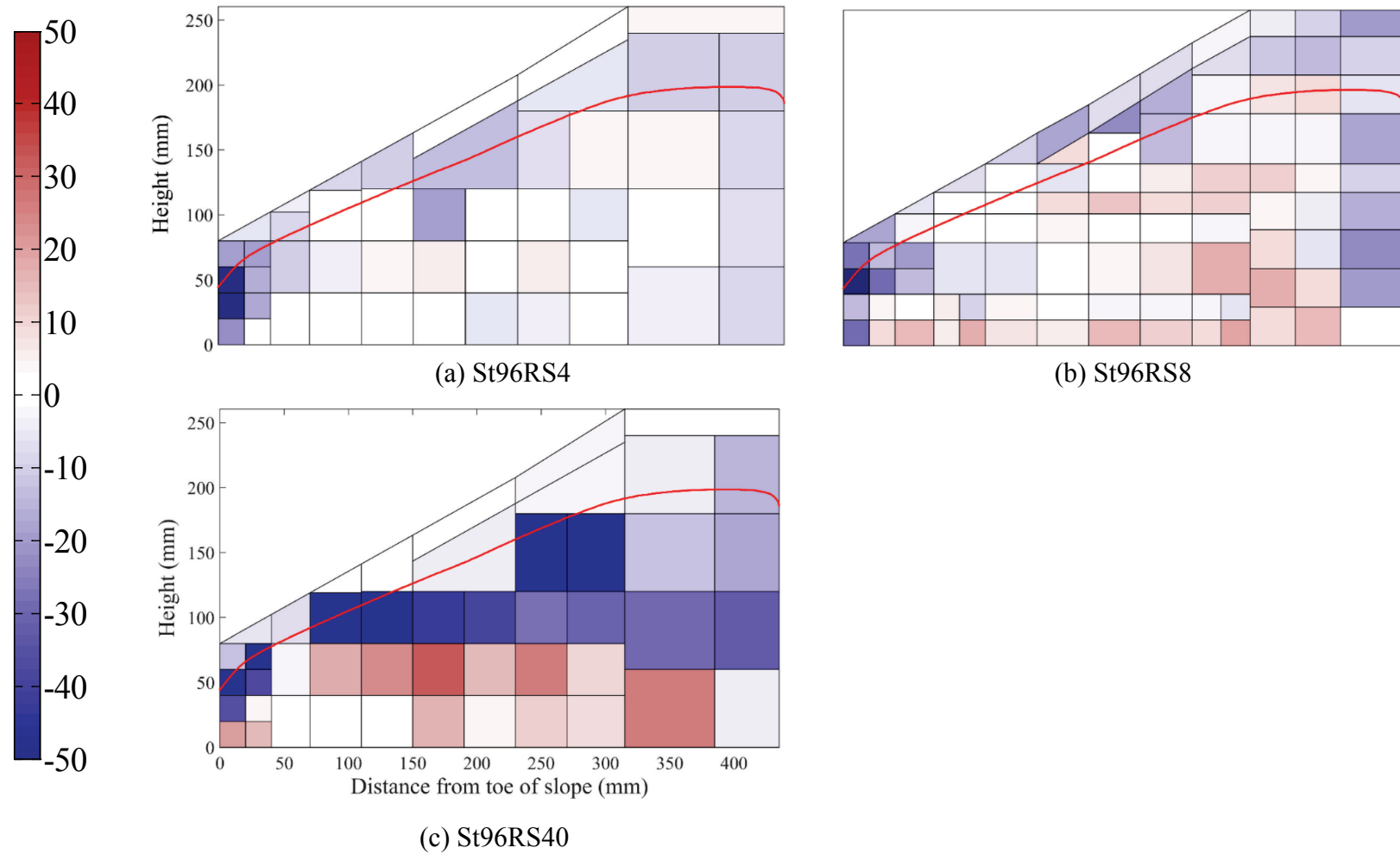
(c) St96RS40

Figure 5-16   Percentage change in spatial distribution of fines in embankment for *Cases St96RS4*, *St96RS8* and *St280RS40*
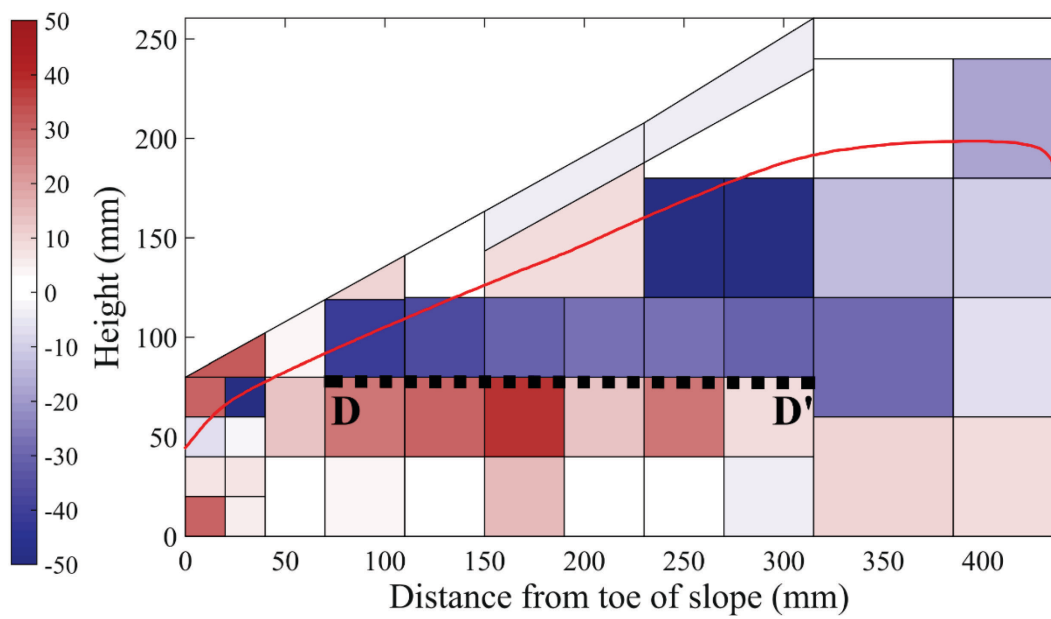
Figure 5-17　　　Spatial distribution of fines content in *Case St280RS40* normalized by that in *Case St280*
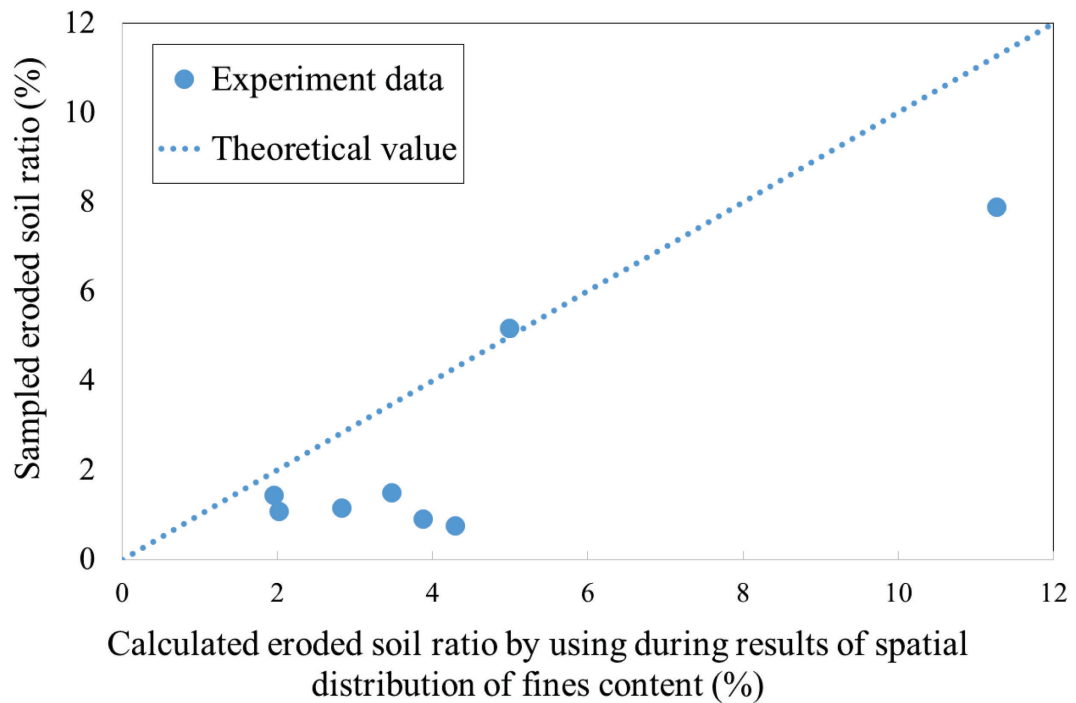
Figure 5-18　　　Relationship between sampled and calculated eroded soil ratios

5.6. Summary

In this chapter, a series of physical model tests on seepage-induced suffusion in a homogeneous embankment are conducted. Binary mixtures consisting of two Silica sands (Silica No.3 and No.8), having different dominant particle sizes, are used for the model embankment. The seepage-induced temporal and spatial variation of the fines content in embankments is examined through sieve analyses on subdivided areas of the model embankment after seepage testing and the following conclusions are drawn:

1. Seepage-induced suffusion in embankment can be reproduced with the small-scaled loosely compacted levee models in the laboratory.

2. Sieve analyses in each area of the embankment could help to successfully observe the spatial distribution of fines with in the model embankment.

3. Under the unsteady seepage condition, in the first permeation, major fines erosion takes place due to rising phreatic surface. Disappearance of suction and the transportation of fines with the seepage flow change the fines content distribution in the embankment.

4. After a certain elapsed time, suffusion develops backward along the phreatic surface from downstream in the embankments. Below the phreatic surface, the erodible fines not only move laterally by seepage flow but also move vertically due to the gravitational force and are deposited in the foundation. This deposition of the fines results in the expansion of the fine-rich region in the foundation and causes decrease in the permeability of the whole embankment. In addition, it is confirmed that the repeated permeation leads to the prominent vertical transportation of fines from the slope zone to the foundation zone.

REFERENCES

Bendahmane, F., Marot, D. & Alexis, A. 2008. Experimental parametric study of suffusion and backward erosion. *Journal of Geotechnical and Geoenvironmental Engineering,* 134(1)**,** pp. 57-67.

Chang, D. S. & Zhang, L. M. 2013. Extended internal stability criteria for soils under seepage. *Soils and Foundations,* 53(4)**,** pp. 569-583.

Fell, R., Wan, C. F., Cyganiewicz, J. & Foster, M. 2003. Time for development of internal erosion and piping in embankment dams. *Journal of Geotechnical and Geoenvironmental Engineering,* 129(4)**,** pp. 307-314.

Foster, M. & Fell, R. 2001. Assessing embankment dam filters that do not satisfy design criteria. *Journal of Geotechnical and Geoenvironmental Engineering,* 127(5)**,** pp. 398–407.

Fry, J. J., Vogel, A., Royet, P. & Courivaud, J. R. Dam failures by erosion: lessons from ERINOH data bases. *Proceedings of the 6th International Conference on Scour and Erosion.* Paris, 2012, pp. 273-280.

Ke, L. & Takahashi, A. 2012. Strength reduction of cohesionless soil due to internal erosion induced by one-dimensional upward seepage flow. *Soils and Foundations,* 52(4)**,** pp. 698-711.

Ke, L. & Takahashi, A. 2014. Triaxial erosion test for evaluation of mechanical consequences of internal erosion. *Geotechnical Testing Journal,* 37(2)**,** pp. 347-364.

Ladd, R. S. 1978. Preparing test specimens using undercompaction. *Geotechnical Testing Journal,* 1(1)**,** pp. 16-23.

Lafleur, J. 1999. Selection of geotextiles to filter broadly graded cohesionless soils. *Geotextiles and Geomembranes,* 17((5–6))**,** pp. 299-312.

Li, M. & Fannin, R. J. 2008. Comparison of two criteria for internal stability of granular soil. *Canadian Geotechnical Journal,* 45(9)**,** pp. 1303-1309.

Luo, Y., Qiao, L., Liu, X., Zhan, M. & Sheng, J. 2012. Hydro-mechanical experiments on suffusion under long-term large hydraulic heads. *Natural Hazards,* 65(3)**,** pp. 1361-1377.

Marot, D., Bendahmane, F. & Nguyen, H. H. Influence of angularity of coarse fraction grains on internal erosion process. *Proceedings of the 6th International Conference on Scour and Erosion*, 2012 Paris. pp. 887-894.

Wan, C. F. & Fell, R. 2008. Assessing the potential of internal instability and suffusion in embankment dams and their foundations. *Journal of Geotechnical and Geoenvironmental Engineering,* 134(3)**,** pp. 401-407.

Chapter 6   Numerical analyses on suffusion process in homogenous embankment

6.1. Introduction

In this chapter, the computational simulations are presented for a series of physical model tests to examine the seepage-induced suffusion process in an embankment on foundation ground.   In order to numerically simulate the physical model tests on the seepage-induced suffusion on a small-scaled homogeneous model embankment described in Chapter 5, a finite element analysis code, with existing simple erosion model, developed by Professor Akihiro Takahashi (Horikoshi *et al.*, 2015; Kokaki *et al.*, 2015) is used.   The existing simple erosion model is used and is calibrated by elemental erosion tests.

This chapter is organized as follows.   Firstly, the derivation of the governing equation and its discretization by the finite element method are made, followed by the derivation of the internal erosion model developed by Sterpi (2003), Cividini *et al.* (2009) and Uzuoka (2012). Secondly, the laboratory test with reference to Sterpi (2003) and Cividini *et al.* (2009) on reconstituted soil is presented.   The result is used to calibrate the erosion model used. Thirdly, the numerical simulation of the physical model tests described in Chapter 5 is presented.

A comparison results of the physical model tests and numerical simulation is beneficial to the estimation of erosion progress and is helpful for the retrofit of numerical internal erosion model.   It also demonstrates the applicability and limitations of the numerical model used. Therefore, in this chapter, results of physical model test mentioned in Chapter5 and numerical results mentioned in this Chapter are finally compared.

6.2. Governing equation and erosion model

6.2.1. Erosion model selection

Several internal erosion models have been developed. The basic concept of all internal erosion models is to have a mass balance equation describing the porosity increase during the erosion process. The mass balance equations on fluid, solid, and additional phase are formulated, complemented by an expression for the rate of soil erosion, namely, "erosion law" or "constitutive law of erosion". The Darcy velocity or the hydraulic gradient is regarded as the driving force.

The approach by Vardoulakis *et al*. (1996, 2001, 2004) and Papamichos and Vardoilakis (2005) have been applied to solve the sand production processes in the petroleum industry. The model is based on the three phase mixture model (solid, fluid, fluidized particles), porosity diffusion, and filtration law.

The approach described above is different from the concept of "critical shear stress", which is commonly used in river bed erosion, which has been adopted by some researchers as the erosion law (Bonelli *et al.*, 2006, 2008; Fujisawa *et al.*, 2010). The model deals with the progression of piping erosion process in which a continuous pipe is developed by a tangential flow of water. Those studies potentially postulate that the constrictions among coarse grains form an array of parallel capillary tubes along the direction of seepage flow and soil aggregate with unit mass will be dislodged from the internal surface of the tubes if the hydraulic shear stress is large enough. The hydraulic shear stress is obtained by Reddi's expression (Reddi *et al*., 2000). As long as the hydraulic shear stress reaches the critical shear stress, internal erosion initiates. This erosion law is commonly applicable to clay mixtures.

Sterpi (2003) performed upward seepage induced erosion tests to investigate the development of fines erosion by hydraulic gradient and time, and established an empirical law governing the phenomenon of particle erosion. The material parameters in this erosion law could be obtained by curve-fitting of results of the seepage tests. This method has already considered the phenomena of clogging and fines redeposition since the experimental results are affected by erosion, clogging and deposition of fines. Afterwards, Cividini and Gioda (2004), and Cividini *et al.* (2009) established a new erosion law expressing the

evolution of the eroded particles on the basis of the Sterpi model and analyzed the ground settlement in Milan City induced by underground erosion. Uzuoka *et al.* (2012) modified this hydraulic gradient based model so that the model can be applied to the problem with free surface by assuming that erosion depended on the absolute value of Darcy's flow velocity. In my studied, this Darcy's flow velocity based internal erosion model was used.

6.2.2. Variables related to internal erosion modeling and assumption

Here, the basic variables related to erosion in unsaturated soil are defined as follow. The void ratio e is expressed as the ratio of the volume of voids V_v to the volume of solids V_s.

$$e = \frac{V_v}{V_s} = \frac{V_a + V_w}{V_s} \tag{6.1}$$

Here, the volume of voids V_v consists of the volume of air and the volume of water in voids. Porosity is the ratio of volume of void V_v relative to the total volume V of soil and is defined as following expression.

$$n = \frac{V_v}{V} = \frac{V_a + V_w}{V} = \frac{e}{1+e} \tag{6.2}$$

Here, V_a denotes the volume of air. The volume water content θ is expressed as

$$\theta = \frac{V_w}{V} \tag{6.3}$$

Water content w is the mass of water in the soil and is expressed as

$$w = \frac{m_w}{m_s} \tag{6.4}$$

where, m_w and m_s denote the mass of water and soil particles, respectively. The expression for degree of saturation S_r is given by the following equation:

$$S_r = \frac{V_w}{V_v} = \frac{V_w}{V_a + V_w} \tag{6.5}$$

Expressing θ in term of S_r and n using Eq. (6.2) and (6.5), the Eq. (6.3) can be rewritten in the form:

$$\theta = S_r n \tag{6.6}$$

By using the relationships of Eq. (6.1), (6.3), and (6.5) and expressing the eS_r in term of the density of soil ρ_s, the density of water ρ_w and w, the equation becomes:

$$eS_r = \frac{\rho_s}{\rho_w} w \qquad (6.7)$$

The wet density of soil ρ_t therefore can be expressed by the following equation.

$$\rho_t = \frac{(1+w)\rho_s}{1+e} = \frac{\rho_s + eS_r\rho_w}{1+e} = (1-n)\rho_s + nS_r\rho_w = (1-n)\rho_s + \theta\rho_w \qquad (6.8)$$

Assuming that soil is composed of fines and coarse particles, which form the soil skeleton, the fines content by mass ratio Fc is defined by form of the mass of soil, $m = m_c + m_f$, as:

$$F_C = \frac{m_f}{m} = \frac{m_f}{m_c + m_f} \qquad (6.9)$$

where, m_f and m_c denote the mass of fines fraction and coarse fraction, respectively. The fines contents represented by volume ration f_c becomes $f_c = F_C$ if fines and coarse particles have the same density of soil particles.

If the velocity head can be neglected (i.e. $v^2 \fallingdotseq 0$) in a soil, the total head of water h is in the upward vertical direction of z axis defined by Bernoulli's principles as follows:

$$h = h_p + z = \frac{p}{\rho_w g} + z \qquad (6.10)$$

where, h_p is the pressure head (p: pressure, ρ_w: density of water, g: acceleration), z is the position head.

Eroded fines are assumed the fluidized particles in suspension, i.e., the eroded fines move with the fluid. Expressing the volume of the solid in the soil skeleton V_{sk} in term of the volume of the coarse soil V_{sc} and fines V_{sf} in the soil skeleton, the volume of the fluid mixture V_l of trapped fines and pore water in term of the volume of water V_w and trapped fines into fluid V_{ef}, and total volume V, those equations respectively become

$$V_{sk} = V_{sc} + V_{sf}$$
$$V_l = V_w + V_{ef} \qquad (6.11)$$
$$V = V_s + V_l + V_a$$

where, V_a denotes the volume of air in a pore. Then, volume water content θ defined in Eq. (6.3) and porosity defined in Ep. (6.2) can be rewritten as follows:

$$\theta = \frac{V_l}{V}$$

$$n = \frac{V_a + V_l}{V} = 1 - \frac{V_s}{V}$$

(6.12)

The fines concentration in fluid pore, C_{ef}, is defined as:

$$C_{ef} = \frac{V_{ef}}{V_l}$$

(6.13)

By using the above definition for fines concentration in the pore fluid, the mass of trapped fines in pore fluid per unit volume ρ_e is given as:

$$\rho_e = \frac{\rho_s V_{ef}}{V} = \frac{\rho_s C_{ef} V_l}{V} = \rho_s C_{ef} \theta$$

(6.14)

The mass of pore fluid per unit volume ρ_l also is expressed by using relations $V_{ef} = C_{ef} V_l$ and $V_w = V_l - V_{ef} = (1 - C_{ef}) V_l$ as:

$$\rho_l = \frac{\rho_s V_{ef} + \rho_w V_w}{V} = \rho_e + \left(\theta - \frac{\rho_e}{\rho_s} \right) \rho_w = \left\{ C_{ef} \rho_s + (1 - C_{ef}) \rho_w \right\} \theta$$

(6.15)

The fines content represented by volume ration f_c is defined as:

$$f_c = \frac{V_{sf}}{V_s} = \frac{V_{sf}}{(1-n)V}$$

(6.16)

According the Eq. (6.16), current the density of fines transported by the seepage flow in the soil element ρ_f can be obtained as follows:

$$\rho_f = \frac{\rho_s V_{sf}}{V} = (1-n)\rho_s f_c$$

(6.17)

The fines content contained both trapped fines in pore fluid and fines remaining in the soil skeleton by volume ration f_c' is also defined as:

$$f_c' = \frac{V_{sf} + V_{ef}}{V_s + V_{ef}} = \frac{(1-n)Vf_c + \dfrac{\rho_e}{\rho_s}V}{(1-n)V + \dfrac{\rho_e}{\rho_s}V} = \frac{(1-n)\rho_s f_c + \rho_e}{(1-n)\rho_s + \rho_e}$$

(6.18)

We sometimes carried out seepage tests and check the fines content after those tests. The fines content obtained by experiment corresponds to f_c'.

6.2.3. Derivation of the governing equations

The governing equation is derived in this subsection by reference to Sterpi (2003) and Cividini and Gioda (2004). They assumed that fines detached from soil skeleton by seepage flow and those detached fines move as suspended particles with the pore fluid. Here, the mass conservation equations on eroded/ transported fines will be explained. Practically, the equation on pore fluid flow is also needed to solve the problem. The equation used is the same as normal steady seepage flow analysis if seepage flow without volume change of a soil skeleton is simply considered. Therefore, it is omitted the part of about derivation of the steady seepage flow analysis in this dissertation.

Consider a two-dimensional infinitesimal control volume on $dA = dxdy$ on Fig. 6.1 filled with the transported fines of mass density. The rate of increase of the fines moving within a unit volume of the pore $\dot{m}_{ef}$ is derived with the assumption of incompressibility of soil particle by defining mass change of trapped fines into pore fluid in the soil element due to erosion per unit volume (i.e. erosion rate), Q_e, as :

$$
\begin{aligned}
\dot{m}_{ef} &= \left\{ \rho_e v_y - \left(\rho_e v_y + \frac{\partial (\rho_e v_y)}{\partial y} dy \right) \right\} dx \\
&\quad + \left\{ \rho_e v_x - \left(\rho_e v_x + \frac{\partial (\rho_e v_x)}{\partial x} dx \right) \right\} dy + Q_e dxdy \\
&= \left\{ -\left(\frac{\partial (\rho_e v_x)}{\partial x} + \frac{\partial (\rho_e v_y)}{\partial y} \right) + Q_e \right\} dxdy
\end{aligned}
\tag{6.19}
$$

In fact, detached and transported fines in pore fluid are redeposited in a soil skeleton at somewhere in the ground after moment. The redeposition of fines is not considered in this model and also in this numerical analysis described later for simplicity and due to the lack of experimental data. The erosion test described later in Section 6.3 has already accounted the phenomena of clogging and fines redeposition in the experimental results as the observable discharged fines from specimen attributes to the results of detachment and deposition in the soil element. However, this erosion law cannot express increase in fines anywhere in the soil because the erosion test gives only positive erosion rate expressed as the sum of detachment and deposition of fines. The detailed erosion test will explain in Section 6.3.

The mass change of eroded fines per unit time $\dot{m}_{ef}$ is also defined as:

$$\dot{m}_{ef} = \frac{\partial \rho_e}{\partial t} dxdy \tag{6.20}$$

By substituting Eq. (6.19) into Eq. (6.20), the continuity equation of transported fines can be yielded as follows:

$$\frac{\partial \rho_e}{\partial t} = -\left\{ \frac{\partial (\rho_e v_x)}{\partial x} + \frac{\partial (\rho_e v_y)}{\partial y} \right\} + Q_e \tag{6.21}$$

Then, we can get so-called the advection equation. Rewrite the equation by tensor representation, it becomes:

$$\frac{\partial \rho_e}{\partial t} + \frac{\partial (\rho_e v_i)}{\partial x_i} - Q_e = 0 \tag{6.22}$$
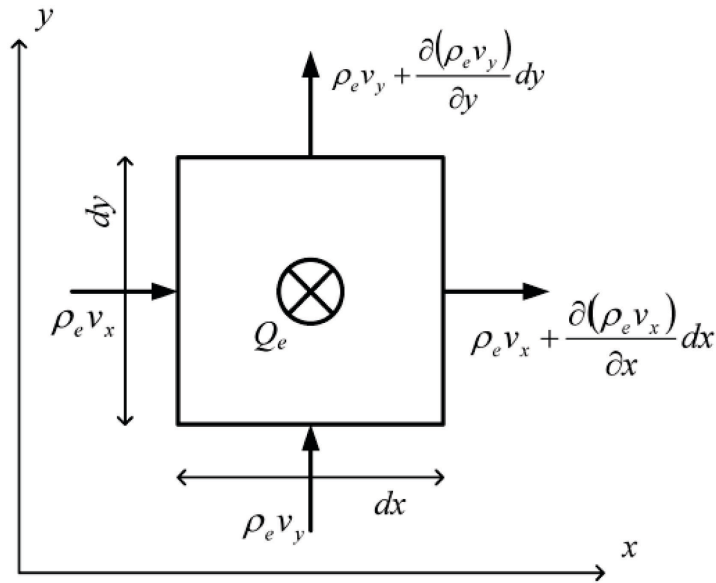
Figure 6.1   Two-dimensional infinitesimal control volume on transported fines

6.2.4. Space-time finite element formulation

The numerical method for solving governing Eq. (6.22) is explained here. The equation can often become unstable for the advection problem if the standard Galerkin method with one-order time derivatve is used. It is well known that standard Galerkin finite element method for convection dominated flows is equivalent to a central difference method. In order to stabilize the calculation, the Taylor-Galerkin method proposed by Donea (1984) is

used to solve the advection equation in Eq. (6.22). This method with third-order accuracy is that finite element equivalent of the Lax-Wenroff method with second-order accuracy developed in the deference method. In this method, the Taylor expansion in time precedes the Galerkin space discretion (Zienkiewicz *et al.*, 2013). $\rho_e\big|_{n+1}$ is expanded by the Taylor series in time (Donea, 1984; Zienkiewicx *et al.*, 2013):

$$\rho_e\big|_{n+1} = \rho_e\big|_n + \Delta t \frac{\partial \rho_e\big|_n}{\partial t} + \frac{\Delta t^2}{2}\frac{\partial^2 \rho_e\big|_n}{\partial^2 t} + o(\Delta t^3) \tag{6.23}$$

Form Eq. (6.22) we have

$$\frac{\partial \rho_e\big|_n}{\partial t} = -\frac{\partial\left(\rho_e\big|_n v_i\big|_n\right)}{\partial x_i} + Q_e\big|_n \tag{6.24}$$

and

$$
\begin{aligned}
\frac{\partial^2 \rho_e\big|_n}{\partial^2 t} &= \frac{\partial}{\partial t}\left(-\frac{\partial\left(\rho_e\big|_n v_i\big|_n\right)}{\partial x_i} + Q_e\big|_n \right) \\
&= -\frac{\partial}{\partial x_i}\left(\frac{\partial\left(\rho_e\big|_n v_i\big|_n\right)}{\partial t} \right) + \frac{\partial Q_e\big|_n}{\partial t} \\
&\approx -\frac{\partial}{\partial x_i}\left(\frac{\partial \rho_e\big|_n}{\partial t}v_i\big|_n + \rho_e\big|_n \frac{\partial v_i\big|_n}{\partial t} \right) \\
&\approx -\frac{\partial}{\partial x_i}\left\{ \left(\frac{\partial\left(\rho_e\big|_n v_j\big|_n\right)}{\partial x_j} + Q_e\big|_n \right)v_i\big|_n \right\}
\end{aligned}
\tag{6.25}
$$

Here, terms of acceleration of erosion $\partial Q_e/\partial t$ and pore water $\partial v_i/\partial t$ described as color of blue are neglected due to small value for simplicity. Substitution Eqs. (6.24) and (6.25) into Eq. (6.23) we have

$$\rho_e|_{n+1} = \rho_e|_n + \Delta t\left(-\frac{\partial\left(\rho_e|_n v_i|_n\right)}{\partial x_i} + Q_e|_n\right)$$

$$-\frac{\Delta t^2}{2}\frac{\partial}{\partial x_i}\left\{\left(-\frac{\partial\left(\rho_e|_n v_j|_n\right)}{\partial x_j} + Q_e|_n\right)v_i|_n\right\}$$

$$\Delta\rho_e|_n = \Delta t\left(-\frac{\partial\left(\rho_e|_n v_i|_n\right)}{\partial x_i} + Q_e|_n\right) \tag{6.26}$$

$$-\frac{\Delta t^2}{2}\frac{\partial}{\partial x_i}\left\{\left(-\frac{\partial\left(\rho_e|_n v_j|_n\right)}{\partial x_j} + Q_e|_n\right)v_i|_n\right\}$$

$$\Delta\rho_e + \Delta t\left(\frac{\partial\left(\rho_e v_i\right)}{\partial x_i} - Q_e\right) - \frac{\Delta t^2}{2}\frac{\partial}{\partial x_i}\left\{\left(-\frac{\partial\left(\rho_e v_j\right)}{\partial x_j} + Q_e\right)v_i\right\} = 0$$

Weak forms of Eq. (6.26) are obtained by principle of virtual work if we assume virtual fines density $\delta\rho_e$ is zero on boundary $\Gamma_{\rho e}$ in domain Ω.

$$\int_\Omega\left[\rho_e + \Delta t\left(\frac{\partial\left(\rho_e v_i\right)}{\partial x_i} - Q_e\right) - \frac{\Delta t^2}{2}\frac{\partial}{\partial x_i}\left\{\left(-\frac{\partial\left(\rho_e v_j\right)}{\partial x_j} + Q_e\right)v_i\right\}\right]\delta\rho_e d\Omega = 0$$

$$\Delta t\int_\Omega\left(\frac{1}{\Delta t}\Delta\rho_e + \frac{\partial\left(\rho_e v_i\right)}{\partial x_i} - Q_e\right)\delta\rho_e d\Omega \tag{6.27}$$

$$-\frac{\Delta t^2}{2}\int_\Omega\delta\rho_e\frac{\partial}{\partial x_i}\left\{\left(-\frac{\partial\left(\rho_e v_j\right)}{\partial x_j} + Q_e\right)v_i\right\}d\Omega = 0$$

$$\Delta t A - \frac{\Delta t^2}{2}B = 0 \tag{6.28}$$

A in Eq. (6.28) becomes:

$$A = \int_\Omega \left(\frac{1}{\Delta t} \Delta \rho_e + \frac{\partial(\rho_e v_i)}{\partial x_i} - Q_e \right) \delta \rho_e d\Omega$$

$$= \frac{1}{\Delta t} \int_\Omega (\delta \rho_e) \Delta \rho_e d\Omega - \int_\Omega \frac{\partial(\delta \rho_{ei})}{\partial x_i} \rho_e v_i d\Omega$$

$$- \int_\Omega (\delta \rho_e) Q_e d\Omega + \int_{\Gamma_q} (\delta \rho_{ei}) \bar{q}_e d\Gamma \qquad (6.29)$$

$$= \frac{1}{\Delta t} \int_\Omega (\delta \rho_e) \Delta \rho_e d\Omega + \int_\Omega \frac{\partial(\delta \rho_{ei})}{\partial x_i} \rho_e k \frac{\partial h}{\partial x_i} d\Omega$$

$$- \int_\Omega (\delta \rho_e) Q_e d\Omega + + \int_{\Gamma_q} (\delta \rho_{ei}) \bar{q}_e d\Gamma$$

Here, $\bar{q}_e$ denotes the mass of eroded fines per unit volume and time on boundary $\Gamma_{\rho e}$.

B in Eq. (6.28) becomes:

$$B = \int_\Omega \delta \rho_e \frac{\partial}{\partial x_i} \left\{ \left(\frac{\partial(\rho_e v_j)}{\partial x_i} - Q_e \right) v_i \right\} d\Omega$$

$$= \int_\Omega \frac{\partial}{\partial x_i} \left\{ \left(\frac{\partial(\rho_e v_j)}{\partial x_i} - Q_e \right) \delta \rho_e v_i \right\} d\Omega$$

$$- \int_\Omega \frac{\partial(\delta \rho_e)}{\partial x_i} \left(\frac{\partial(\rho_e v_j)}{\partial x_j} - Q_e \right) v_i d\Omega$$

$$= \int_\Omega \delta \rho_e \left(\frac{\partial(\rho_e v_j)}{\partial x_i} - Q_e \right) v_i n_i d\Gamma \qquad (6.30)$$

$$- \int_\Omega \frac{\partial(\delta \rho_e)}{\partial x_i} v_i \left(\frac{\partial(\rho_e v_j)}{\partial x_j} - Q_e \right) d\Omega$$

$$\approx - \int_\Omega \frac{\partial(\delta \rho_{ei})}{\partial x_i} v_i \left(\frac{\partial \rho_e}{\partial x_j} v_j + \rho_e \frac{\partial v_j}{\partial x_j} - Q_e \right) d\Omega$$

$$\approx - \int_\Omega \frac{\partial(\delta \rho_{ei})}{\partial x_i} k \frac{\partial h}{\partial x_i} \left(\frac{\partial \rho_e}{\partial x_j} k \frac{\partial h}{\partial x_j} + Q_e \right) d\Omega$$

Here, terms correspond to flax of time variation of trapped fines density in pore fluid on boundary and correspond to adventive by seepage velocity $\partial v_i / \partial x_i$ described as color of blue are neglected due to small value for simplicity. Therefore, weak form of the governing equation can be written as:

$$\frac{1}{\Delta t}\int_{\Omega}(\delta\rho_e)\Delta\rho d\Omega - \int_{\Omega}\frac{\partial(\delta\rho_e)}{\partial x_i}\rho_e v_i d\Omega + \frac{\Delta t}{2}\int_{\Omega}\frac{\partial(\delta\rho_e)}{\partial x_i}\rho_e v_i\left(\frac{\partial\left(\rho_e v_j\right)}{\partial x_j} - Q_e\right)d\Omega$$

$$= \int_{\Omega}(\delta\rho_e)Q_e d\Omega - \int_{\Gamma_q}(\delta\rho_e)\overline{q}_e d\Gamma$$

$$\frac{1}{\Delta t}\int_{\Omega}(\delta\rho_e)\Delta\rho d\Omega - \int_{\Omega}\frac{\partial(\delta\rho_e)}{\partial x_i}\rho_e k\frac{\partial h}{\partial x_i}d\Omega + \frac{\Delta t}{2}\int_{\Omega}\frac{\partial(\delta\rho_e)}{\partial x_i}\rho_e k\frac{\partial h}{\partial x_i}\left(\frac{\partial\rho_e}{\partial x_j}k\frac{\partial h}{\partial x_j} + Q_e\right)$$
$$\tag{6.31}$$

$$= \int_{\Omega}(\delta\rho_e)Q_e d\Omega - \int_{\Gamma_q}(\delta\rho_e)\overline{q}_e d\Gamma$$

Taylor-Galerkin method gives identical stabilizing terms written by color of red.

6.2.5. Derivation of the erosion model

Here, the internal erosion model is derived by reference to Cividini *et al.* (2009) and Uzuoka *et al.* (2012). It is assumed that eroded fines act as part of pore fluid with pore water. The current density of the fines in the soil skeleton ρ_f is described as:

$$\rho_f = (1-n)\rho_s f_c \tag{6.32}$$

Assuming that the mass change of trapped fines per unit volume Q_e (increase rate) depends on time derivative of fines content f_c, it is expressed by using Eq. (6.32) as following equation:

$$Q_e = -\frac{\partial\rho_f}{\partial t} = -(1-n)\rho_s\frac{\partial f_c}{\partial t} \tag{6.33}$$

In this equation, for simplicity, function is considered only time derivative of fines content f_c based on the assumption that change of porosity n is negligibly small.

From results of one dimensional erosion tests, Cividini *et al.* (2009) assumed that the erosion rate increases with increasing the square root of the hydraulic gradient and it decreases monotonously with time under constant hydraulic gradient. Based on these assumptions, time derivative of fines content f_c is formulated as flows:

$$\frac{\partial f_c}{\partial t} = -d_1\left(f_c - f_{c\infty}\right)i^{d_2} \tag{6.34}$$

where, i and $f_{c\infty}$ denote the hydraulic gradient and the ultimate fines content after long seepage period, respectively. d_1 is the a dimensional experimental parameter and $d_2 = 0.5$. The ultimate fines content $f_{c\infty}$ can be expressed to assume that erosion rate decreases with

91

decrease in the hydraulic gradient and this ultimate fines content decreases with increase in the hydraulic gradient. It can be written as:

$$f_{c\infty} = f_{c0} \left\{ (1-c)\exp(-a \cdot i^b) + c \right\} \tag{6.35}$$

where, f_{c0}, is the initial fines content. a, b and c denote the nondimensional material parameters controlling internal erosion, respectively. The parameters a, b and c in Eq. (6.35) can be obtained by back analysis of the experiment result described later in Fig. 6-2. To determine the parameter d_1 on the basis of these experimental result, Eq. (6.34) have to be numerically integrated with time. The model based on the hydraulic gradient aimed at the saturated soil. The erosion is overestimated at the unsaturated zone if this model are used for seepage problems with free surface. To avoid that problem, Eqs. (6.34) and (6.35) are rewritten based on the Darcy's velocity by reference to Uzuoka *et al.* (2012). It is assumed that the erosion rate depends on ratio Darcy's velocity v and reference velocity v_r (material parameter), Eq. (6.34) is modified as:

$$\frac{\partial f_c}{\partial t} = -d_1'\left(f_c - f_{c\infty}\right)\left(\frac{v}{v_r}\right)^{d2} \tag{6.36}$$

From Darcy's law, $v = ki$, above equation becomes

$$\frac{\partial f_c}{\partial t} = -d_1'\left(f_c - f_{c\infty}\right)\left(\frac{ki}{v_r}\right)^{d2} = -d_1'\left(\frac{k}{v_r}\right)^{d2}\left(f_c - f_{c\infty}\right)i^{d2} \tag{6.37}$$

where, k is the hydraulic conductivity of soil. d_2 denotes the material parameter. Cividini *et al.* (2009) set value corresponding to d_2 to 0.5 as shown in Eq. (6.34). However, Uzuoka *et al.* (2012) treat the value as a fitting parameter in the process of modification of model, therefore, the value are similarly treated as a fitting parameter in this dissertation. The parameter d_1 in Eq. (6.34) can be expressed by parameter in Eq. (6.37) as:

$$d_1 = d_1'\left(\frac{k}{v_r}\right)^{d2} \tag{6.38}$$

The ultimate fines content $f_{c\infty}$ is similarly obtained as:

$$f_{c\infty} = f_{c0}\left\{(1-c)\exp\left(-a'\left(\frac{v}{v_r}\right)^b\right)+c\right\} \qquad (6.39)$$

From Darcy's law, $v = ki$, above equation becomes

$$f_{c\infty} = f_{c0}\left\{(1-c)\exp\left(-a'\left(\frac{k}{v_r}\right)^b \cdot i^b\right)+c\right\} \qquad (6.40)$$

The parameter a in Eq. (6.35) can be expressed by parameter in Eq. (6.40) as:

$$a = a'\left(\frac{k}{v_r}\right)^b \qquad (6.41)$$

6.3. Parameter determination

To determine fitting parameters which is necessary in the internal erosion model described section 6.2, constant head seepage test with upward water flow is performed on mixture of silica No. 3 & No.8 by reference referenced by Sterpi (2003) and Cividini *et al*. (2009).

6.3.1. Soil specimens

Binary mixtures consist of two Silica sands (Silica No.3 and No.8), which are categorized as "internally instable material" by previous several criteria for the seepage-induced internal stability, are used for this upward seepage erosion test, in the same material described in Chapter 4 and 5. The chosen fines content of the mixture is 15 %. The particle size distribution curves of each sand and the mixture and basic properties of the mixture material are shown in Fig. 4-1 and Table 4-1, respectively. The vulnerability of this mixture soil to suffusion is assessed by several criteria methods (Chang and Zhang, 2013, Wan and Fell, 2008, Li and Fannin, 2008). As a result, the mixture of this study is categorized as "Internal instability".

The calculated critical hydraulic gradient for zero effective stress is 1.03 according to Terzaghi's equation. According to previous studies, suffusion occurs at a hydraulic gradient of about one-third to one-fifth of Terzaghi's critical gradient method for

homogeneous granular soil (*e.g.,* Skempton and Brogan, 1994). Several studies presented the relate initiation of suffusion to the critical hydraulic gradient. Skempton and Brogan (1994) proposed that the critical gradient i_{sc}, for internal unstable in the sand by:

$$i_{sc} = \alpha i_{Tc} \tag{6.42}$$

where i_{Tc} is the Terzaghi's critical gradient, α is a reduction factor, can be described by:

$$\alpha = \frac{\sigma'_f}{\sigma'_v} \tag{6.43}$$

where σ'_f portion of the effective stress on the fine particles, σ'_v is the vertical effective stress. Ke and Takahashi (2012) performed a series of one-dimensional upward seepage tests on a similar mixture with fines contents of 14.3, 16.7, 20 and 25%. The results of the critical gradient i_{sc}, for these internal unstable soil show that fines content was linearly correlated with the fines content (i_{sc} = -0.0037FC+0.302, R^2 = 0.997). From this linear relationship, the expected critical gradient against suffusion for the mixture used (15 % fines content) is 0.25. Therefore, the reduction factor α becomes 0.24.

Li (2008) evaluated the stress reduction factor by relationship between representative diameter of the fines fraction d_{85f}, diameter of the 85% mass passing in the fines fraction, and the average capillary tube diameter of the coarser fraction O_{50} as follows.

$$\alpha = 3.85 \left(\frac{d'_{85f}}{O_{50}} \right) - 0.616 \tag{6.44}$$

Here, O_{50} is defined as (Kovacs, 1981):

$$O_{50} = 4 \frac{n_c}{1 - n_c} \frac{D_h^c}{\alpha_D} \tag{6.45}$$

where n_c is porosity of skeleton and can be defined by $n_c = n + fc(1-n)$, α_D is the shape coefficient (6 for rounded particles, 7 to 9 for angular particles), and D_h^c is Kozeny effective diameter of coarse fraction and it is given as:

$$D_h^c = \frac{1}{\sum \frac{\Delta F_i^c}{D_i^c}} \tag{6.46}$$

where F_i^c is the weight of grains in the i-th interval of the particle size distribution curve of coarse fraction. D_i^c is the average diameter in the i-th interval of the particle size

distribution curve of coarse fraction.　The siliceous sand used here is mainly composed of quartz, categorized as sub-round to sub-angular.　Therefore, assuming an average shape coefficient $\alpha_D = 8$, the stress reduction factor α can be calculated as $\alpha_D = 0.58$.　Then i_{sc} becomes 0.60 from Eq. (6.42).　The corresponding critical hydraulic gradient are summarize in Table 6-1.

Table 6-1　　Assessment of critical hydraulic gradient

Method used to assess critical hydraulic gradient	Reduction factor α	Critical hydraulic gradient
Terzaghi's theory	—	1.03
Ke and Takahashi (2012)	0.25	0.25
Li (2008) based on the stress reduction factor α	0.58	0.60

Permeability tests are conducted on specimens with varying fines contents (FC = 2.5-30.0%) under a constant void ratio of the coarse skeleton (void ratio of the coarse skeleton $e_s = 0.885$, relative density of the coarse skeleton Dr_s =40%) in accordance with JIS and Japanese Geotechnical Society (JGS) standard.　In the tests, small hydraulic gradient is imposed so that the suffusion does not occur during the tests.　Figure 6-2 shows the obtained relationship between hydraulic conductivity and fines content.　In physical model tests described in Chapters 4, 5 and 8, the model embankment is made of partially saturated soil and tap water is used.　For these reasons, permeability tests are conducted on (a) partially saturated soil with tap water and (b) fully saturated soil with deaired water.　Figure 6-2 indicates that the hydraulic conductivity of specimen without deairing is lower than that of fully saturated ones.　It should be noted that, even at the same fines content, the packing of the fines may not be the same for these two conditions because the position of fines in the voids of the coarse skeleton are different depending on whether air bubble exists in a void or not.
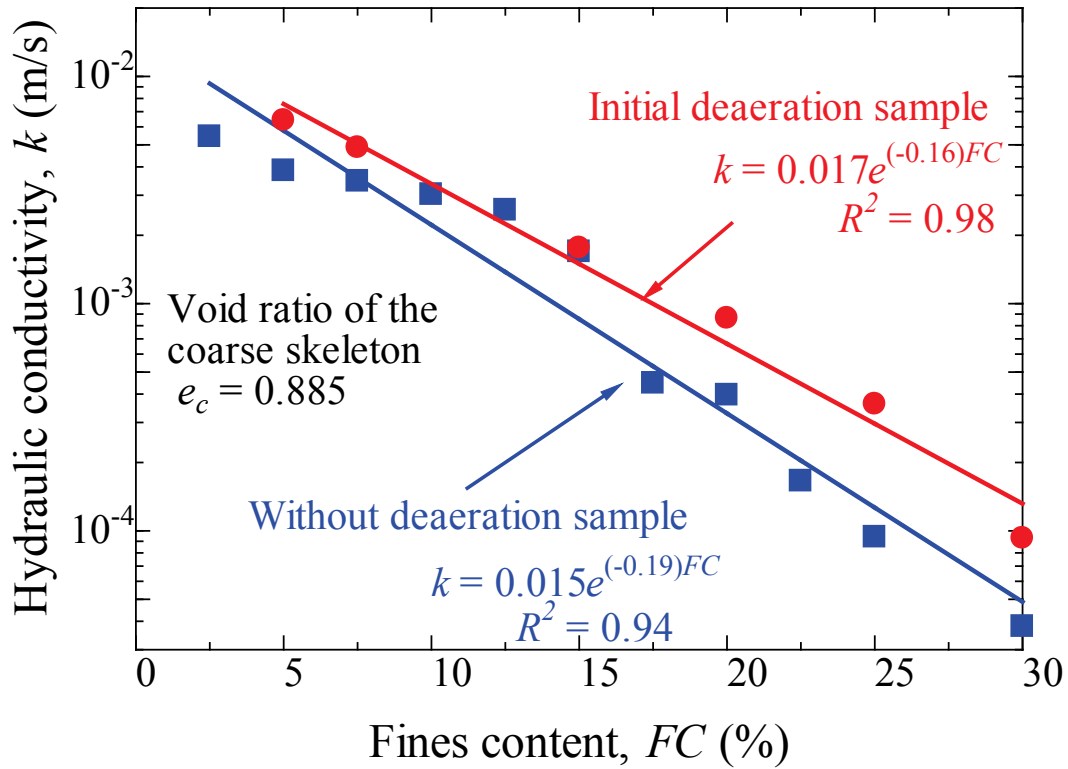
Figure 6-2 Relationship between fine content and permeability under constant void ratio of the coarse skeleton

6.3.2. Test apparatus and procedure

Constant head seepage test with upward water flow is performed under a controlled hydraulic gradient to investigate the erosion potential of soil. A schematic diagram of the seepage test apparatus is shown in Fig. 6-3. The apparatus has developed based on the same setup adopted in Sterpi (2003). The cylindrical seepage cell is 150 mm in internal diameter containing the soil sample to be tested. The inlet is connected to an upper water supply tank, which can be raised or lowered to control the hydraulic gradient across the specimen. The outlet is open to the atmosphere. To prevent material separation during preparation of the specimen, the moist tamping method (Ladd, 1978) is employed for the reconstituted 200 mm high specimen. This procedure was also found to give good control over the global density of specimen. The soil is compacted by layers with the thickness of 40 mm. The target dry density is 1.560 g/cm^3 (void ratio $e = 0.695$, relative density $Dr = 35\%$). The initial moisture content is 3.0%. The layer consisting of about 2.5 mm single-sized glass balls underneath the 200 mm-thick specimen serves to break up the incoming

flow to ensure a uniform water flow on the specimen.　A pore water pressure transducer (SSK Micro Pressure Transducer P306V-01, measurable range: 0 – 10 kPa, see Photo. 5-2) is put at the base of the glass balls layer to measure the inflow pore water pressure.　This allows apparatus to directly evaluate the hydraulic gradient and to avoid possible errors due to hydraulic head losses taking place at the nozzles or within the inlet tube.　The variation in water head within the specimen is measured by five pore water pressure transducers at three different depths, 20 mm (connected at the right and left side of cylinder, i.e. two), 70 mm and 120 mm (two).　A 0.025 mm opening size sieve (JIS Z 8801) is placed above the lower reservoir to collect fines washed out of the specimen.

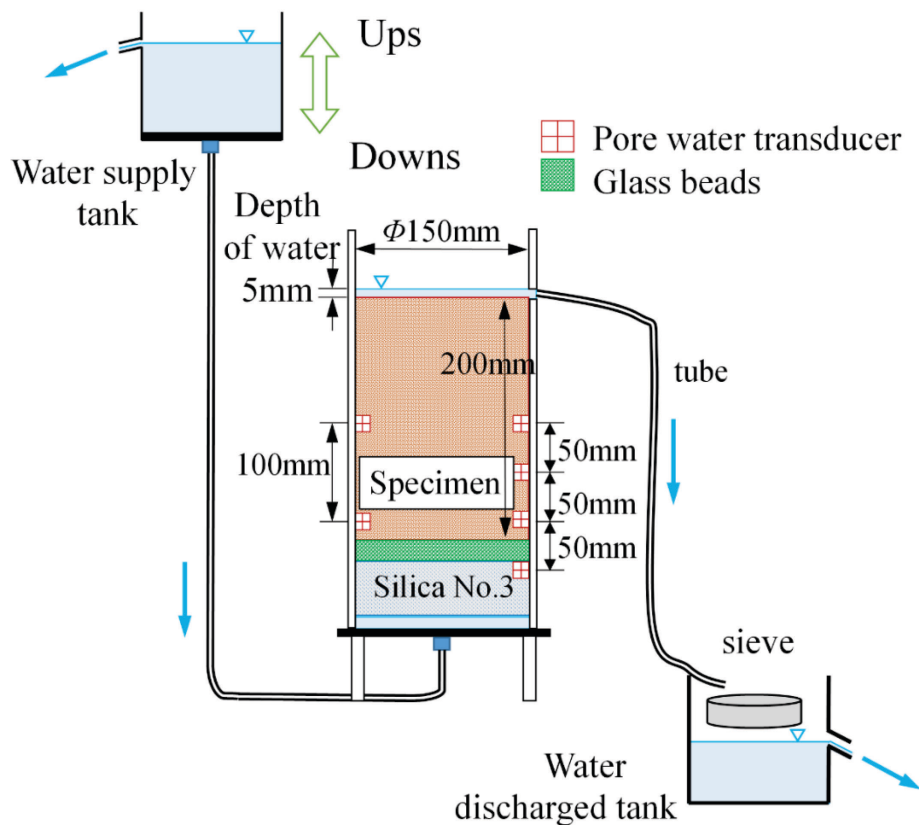Figure 6-3　　A schematic diagram of the seepage test apparatuses

To increase degree of saturation of the specimen, CO_2 was percolated up through the specimen using a pressure.　The CO_2 suppressing pushed out air trapped within the specimen voids.　After that, de-aired water is purged into the specimen from the bottom inlet at a slow rate with increasing the level of the upper water supply tank.

The applied water head is increased by elevation of upper water supply tank when the specimen reaches the hydrostatic conditions. The water level at the top of specimen (downstream) is fixed at the 5 mm from the top of specimen. The experiment is conducted for six days and applied hydraulic gradient is gradually increased step by step from 0.126 to 0.726 by uplifting the upper water supply tank with the time interval of 24 hours. The hydraulic gradient of each step is obtained by pore water pressure measurements recoded by pore water transduces. Eroded and washed out fines are collected, dried and weighted after the test. Due to the above, the cumulative eroded mass with time can be obtained. Estimate the discharge flow rate by measuring the volume of discharge of the water.

During this test, similar to the way Sterpi (2003)'s experiment, a gentle air flow is applied at the top of the specimen, through a thin tube, to avoid the redeposition of the eroded particles on the specimen head. Notice that the hydraulic gradient of sixth step is smaller than previous step due to errors by hydraulic head losses taking place at the nozzles and thin inlet tube.

6.3.3. Test result

Figure 6-4 shows the change in fines content with time. It indicates the relationships cumulative eroded mass and cumulative time. In this figure, dots denote the experimental results and the solid lines denote the fitting curve based on the erosion law described above. The current fines content are obtained by amount of eroded fines. From this figure, it can be seen that erosion rate decreases with time. There is a general trend that the larger imposed hydraulic gradient the larger fine particle loss with time. The higher the hydraulic gradient is, the more the decrease in the fines content fc.
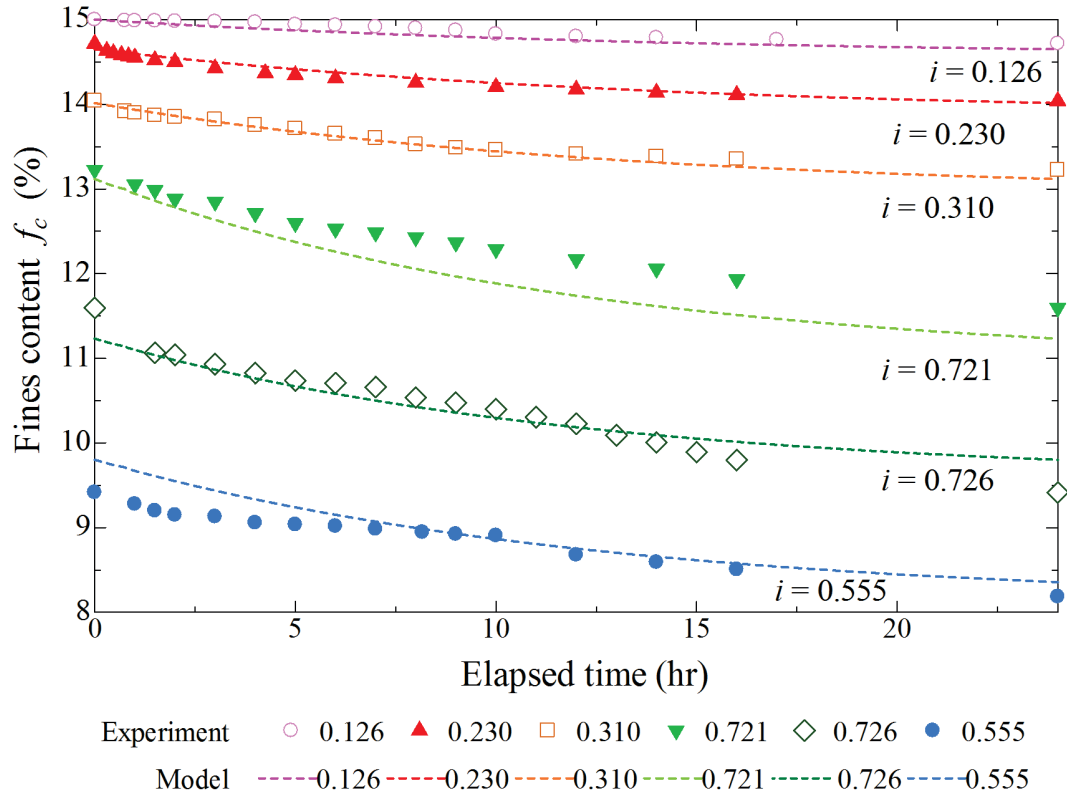
Figure 6-4   Variation of fines content with time

The parameters *a, b, c, d₁* and *d₂* in Eqs. (6.34) and (6.35) are obtained by non-linear least-square method with minimizing the between experiment results (dots) and integrated form of Eq. (6.34) under the constant hydraulic gradient (lines) (Fig. 6-4).   The fitting parameters controlling internal erosion are summarized in Table 6-2.

Table 6-2   Parameters of the erosion laws for mixture of
Silica No.3 and No.8 (*FC* = 15%)

a	1.1
b	1.2
c	0.67
d_1 (1/s)	0.000024
d_2	0.11

6.4. Analysis condition

In this subsection a physical model test described in Chapter 5 is simulated using the internal erosion model above.　Firstly, the distribution of pore water pressure under steady seepage flow in the model embankment is calculated by a separate seepage analysis program by the finite element method.　And then the mass conservation of eroded fines is considered and trapped fines density in pore fluid is calculated by using finite element analysis code developed by Akihiro Takahashi (Horikoshi *et al.*, 2015; Kokaki *et al.*, 2015).

6.4.1.　Geometric configuration and boundary conditions

Figure 6-5 depicts the analysis model geometric configuration and the finite element mesh. The configuration of embankment and its foundation is determined from a physical model test described in Chapter 5.　The number of element is 13735 and that of nodes is 13457. Same as the physical model tests, the water head is set at a height of 190mm from bottom of the foundation at the upstream boundary and is set at a height of 40mm from bottom of the foundation at the downstream boundary.　The bottom of the foundation is set as an impermeable.　The soil-water characteristic curve is obtained by gravity drainage column experiment (Nakano *et al.*, 1995) and is modeled by van Genuchten model (van Genuchten, 1980).　The van Genuchten model has the following form:

$$S_e = \frac{1}{\left[1+\left(\alpha_{VG}h_p\right)^{n_{VG}}\right]^m}$$

(6.47)

where h_p is the pressure head, and α_{VG}, n_{VG} and m are empirical parameters, respectively. S_e is the effective saturation and obtained following form:

$$S_e = \frac{\theta-\theta_r}{\theta_s-\theta_r}$$

(6.48)

where θ is the volumetric water content, θ_r is the residual water content, and θ_s is the saturated water content.　The corresponding unsaturated hydraulic conductivity, k_{wu}, is

$$k_{wu} = kS_e^{l_{us}}\left[1-\left(1-S_e^{1/m}\right)^m\right]^2$$

(6.49)

in which l_{us} is an empirical pore-connectivity parameter.　Commonly, this parameter is fixed at 0.5 (Mualem, 1976).　The parameters used in the finite element analyses on seepage flow are shown in Table 6-3 and soil-water characteristic curve of the mixture of Silica No.3 and 8 is shown in Fig. 6-6.

Table 6-3   Parameters used in seepage analysis

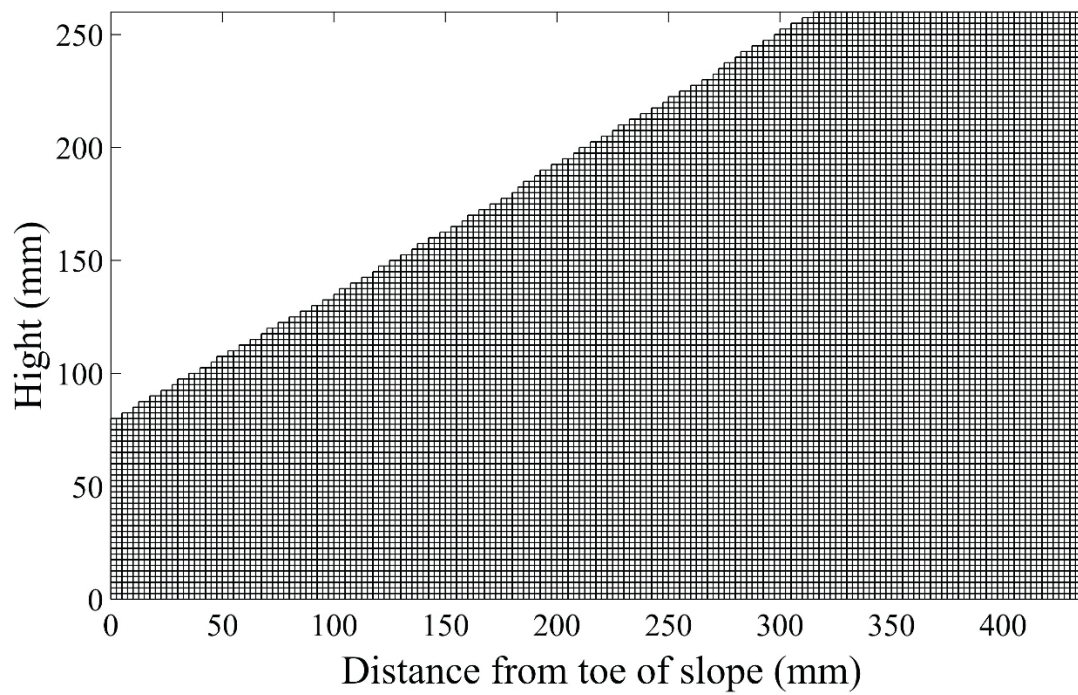|	
Specific gravity of soil particle, Gs (kg/m³)	2645
Initial fines content, f_{c0}	0.15
Initial hydraulic conductivity of saturated mixture ($FC=15\%$), k_{sr} (m/s)	1.695×10^{-3}
Initial porosity, n_0	0.376
Paramters for van Genuchten model	
θ_s	0.32553
θ_r	0
α_{VG}	57.938
n_{VG}	1.6205
m	0.3829

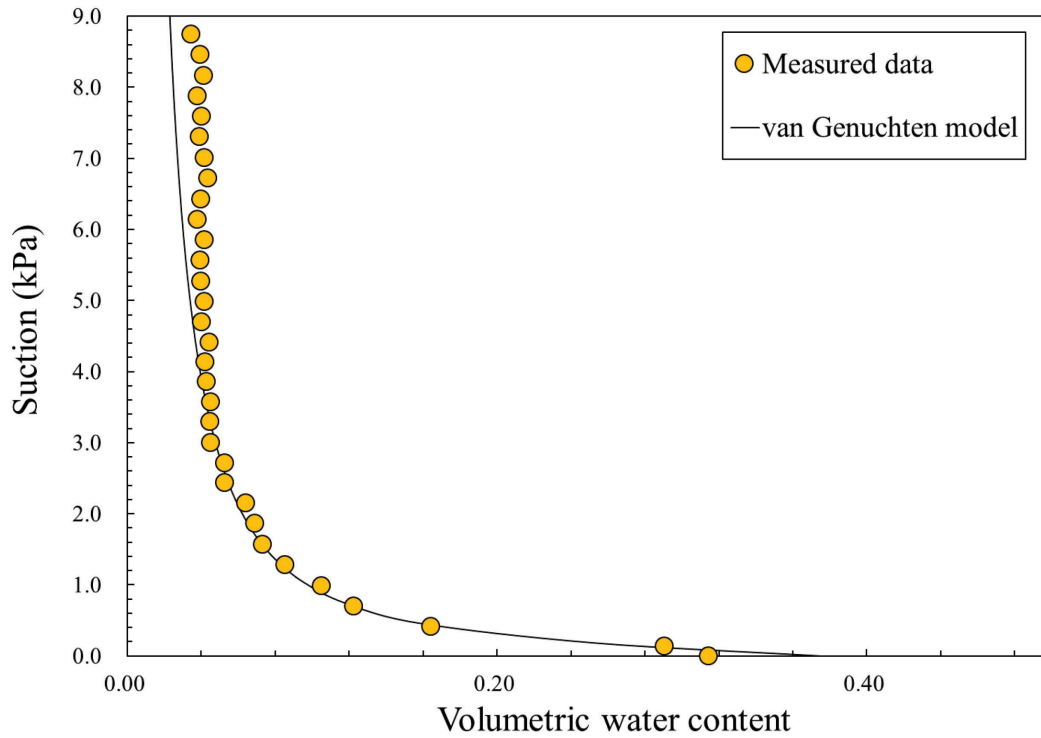Figure 6-5   Analysis finite element mesh

Figure 6-6　　Soil-water characteristic curve

In this internal erosion analysis, it is assumed that no fines are supplied from the upstream. This is the same as that in the physical model tests conducted in Chapter 5. It means that inflow of eroded fines from upstream is zero, that is, the density of fines in pore fluid at the upstream boundary is set to zero. Therefore, the boundary condition is set as the Dirichlet boundary condition, at which the fines density in pore fluid is known. The parameters used in the finite element analysis on internal erosion are shown in Table 6-2.

For coupling seepage flow analysis and internal erosion analysis, two conditions are considered; one is "Uncoupled analysis" and the other is "Weakly-coupled analysis" as shown in Fig 6-7. In the former, the steady seepage flow analysis is conducted at $t = 0$ only and it is assumed that the boundary flow velocity, hydraulic gradient and hydraulic conductivity in the analytical domain do not change throughout the calculation, from $t = 0$ to $t = a$ in the internal erosion analysis. In the real situation, porosity, hydraulic conductivity, and hydraulic gradient change with time because of seepage-induced internal erosion. To consider these changes in the internal erosion analysis, coupling of the seepage flow analysis and internal erosion analysis is made. Strictly speaking, the state parameters

mentioned above have to be consistent in both the analyses at any moment. However, as these state parameters gradually change with time, the weak-coupling is considered in the coupled analysis and its calculation procedure is as follow: the procedure by applying the results of seepage flow analysis (SF-1) as the input values for internal erosion analysis is same as the uncoupled analysis but the internal erosion analysis (IE-1) is conducted from $t = 0$ to $t = T$. Next, the values of hydraulic conductivity at each element are calculated from the final values of fines content in IE-1 by using correlation shown in Fig.6-2 as:

$$k = 0.0015 \exp(-0.19\,fc) \quad [\text{m/s}] \tag{6.50}$$

The second seepage flow analysis (SF-2) is conducted by using the updated values of hydraulic conductivity. By applying the results of SF-2 as the input values and the final condition of IE-1 as the initial condition, the second internal erosion analysis (IE-2) is conducted from $t = T$ to $t = 2T$. This procedure is repeated until $t = a$ (SF-n and IE-n). In "Weakly-coupled analysis", the seepage condition is updated every 1800 seconds (0.5 hours) and $a = 360000$ (100 hours). "Uncoupled analysis" is also conducted until $a = 360000$.
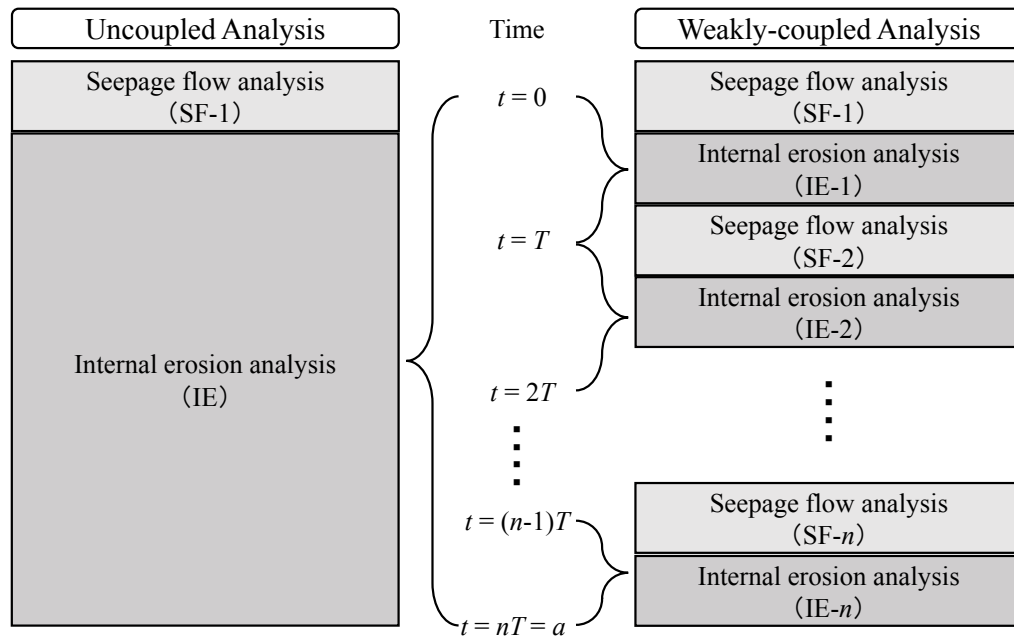

Figure 6-7   Uncoupled analysis and weakly-coupled analysis (Kokaki, 2015)

6.5. Results and discussion

6.5.1. Initial seepage condition

The initial condition of spatial distributions of water head, hydraulic gradient, degree of saturation and flow velocity in the embankment obtained by steady seepage analysis are shown in Fig. 6-8. As describe above, the seepage condition is updated every 1800 seconds in weakly coupled analysis. The concentration of hydraulic gradient and flow velocity can be confirmed from the middle of the foundation near the downstream boundary as shown in Fig. 6-8(b), (d). The maximum value of hydraulic gradient is 1.468. This value is greater than Terzaghi's critical gradient (1.03).

6.5.2. Results of internal erosion analysis

The evolutions of the fines content inside the embankment for uncoupled and weakly-coupled analyses are shown in Figs. 6-9 and 6-10, respectively. In these results, the fines content f_c' defined by Eq. (6.18) are shown. The calculated phreatic surface by finite element method at initial condition is indicated by a solid line. The fines content decrease is apparent in elements contacted by the water surfaces at the downstream boundary (Figs. 6-9(a), 6-10(a)). After certain elapsed times, fines content continues to decrease with time (Figs. 6-9(b)-(d), 6-10(b)-(d)). It seems that decrease of fines develops from middle of the foundation near downstream boundary in accordance with the magnitude of velocity. That is, the suffusion starts from downstream side and progress toward upstream side. The results of uncoupled analysis shows the larger decrease in fines near the downstream boundary, compare to results of weakly-coupled analysis (see Figs. 6-9 and 6-10). That is, the loss of fines can be overestimated in the uncoupled analysis at active seepage zone. However, larger decrease in fines is observed at upstream side in case of weakly-coupled analysis. In this case, area of decrease in fines is extended more upward at upper part of phreatic surface. This trend is because of large increase in hydraulic conductivity against suffusion. Figures 6-11 shows the evolution of the hydraulic conductivity inside the embankment with different elapsed seepage time in case of weakly-coupled analysis. It can be seen that increase of hydraulic conductivity also develops from middle of the foundation near downstream boundary in accordance with the loss of fines content in the saturated area. At the element located middle of the foundation near downstream boundary, the hydraulic conductivity increase to almost double ($1.695\times10^{-3}\rightarrow2.900\times10^{-3}$ m/s) after 100 hours seepage.

(a)   Water head

(b)   Hydraulic gradient

(c)   Effective degree of saturation

(d)   Velocity
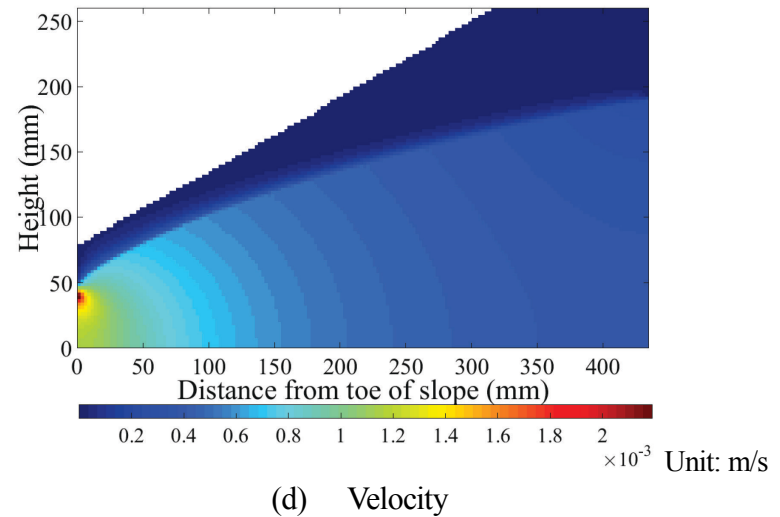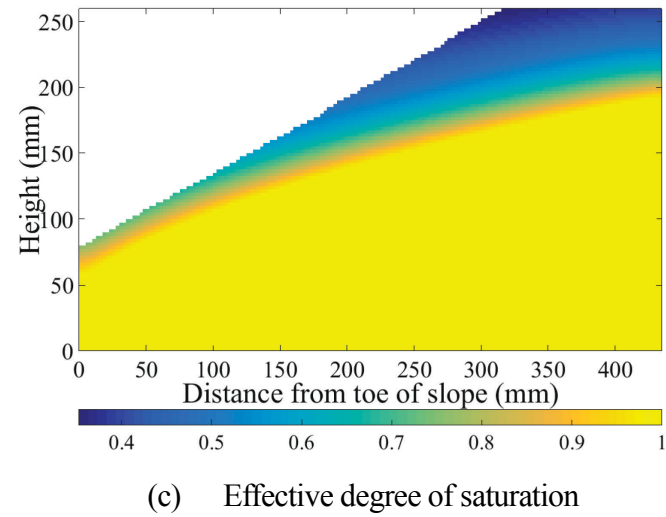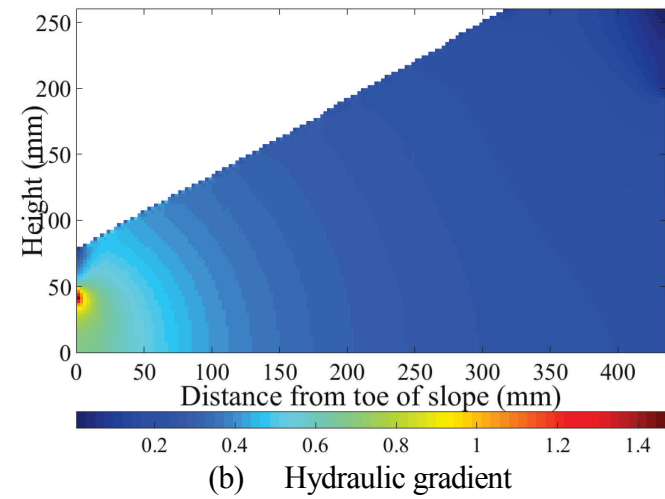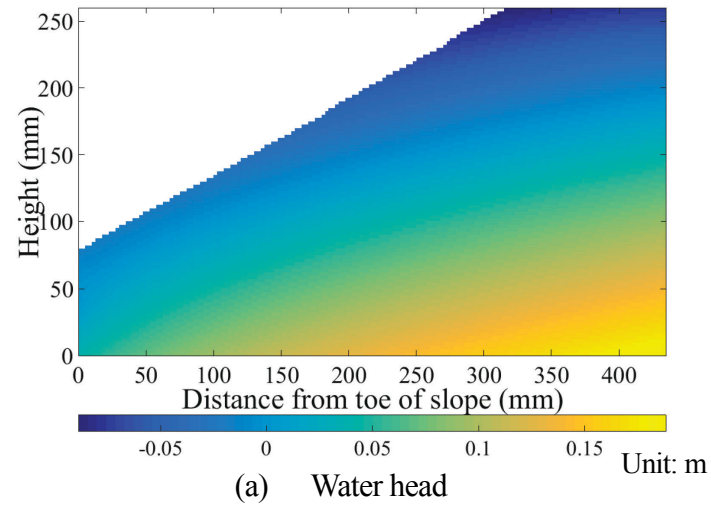
Figure 6-8   Initial hydraulic condition in the embankment
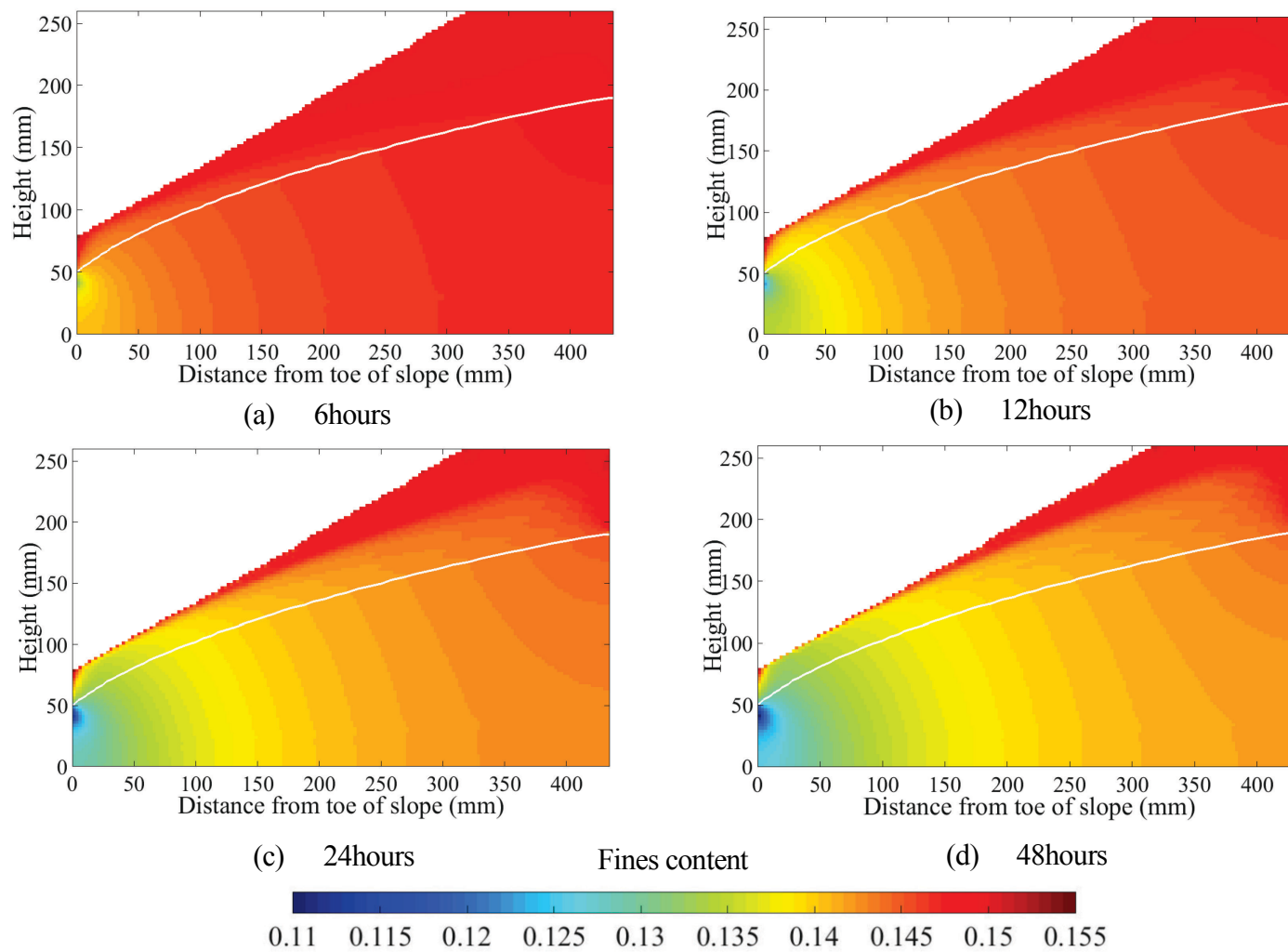
Figure 6-9   Spatial distribution of fines content in the embankment at different time in uncoupled analysis
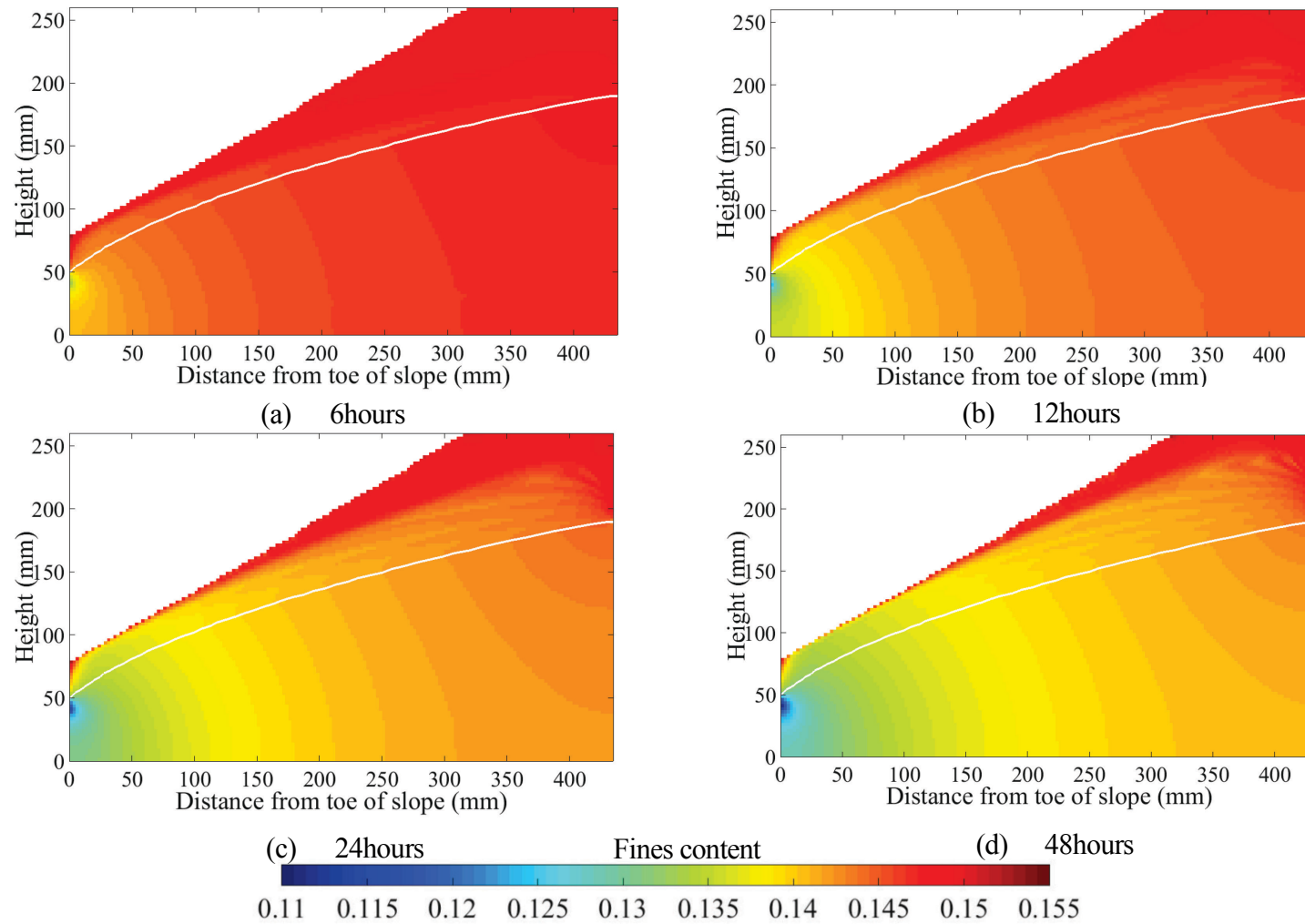
Figure 6-10   Spatial distribution of fines content in the embankment at different time in weakly-coupled analysis

(a)   Initial

(b)   6hours

(c)   24hours

Hydraulic conductivity, m/s

(d)   48hours

Figure 6-11   Spatial distribution of hydraulic conductivity in the embankment at different time in Weakly-coupled analysis

To investigate effect of hydraulic conductivity change in erosion potential of embankments, (1) detailed comparisons between "Uncoupled analysis" and "Weakly-coupled analysis" and (2) comparisons with the experimental results are made. Figure 6-12(a) shows evolutions of the normalized cumulative eroded soil mass for uncoupled and coupled analyses. From this figure, it can be seen that the eroded soil mass from the embankment in the coupled an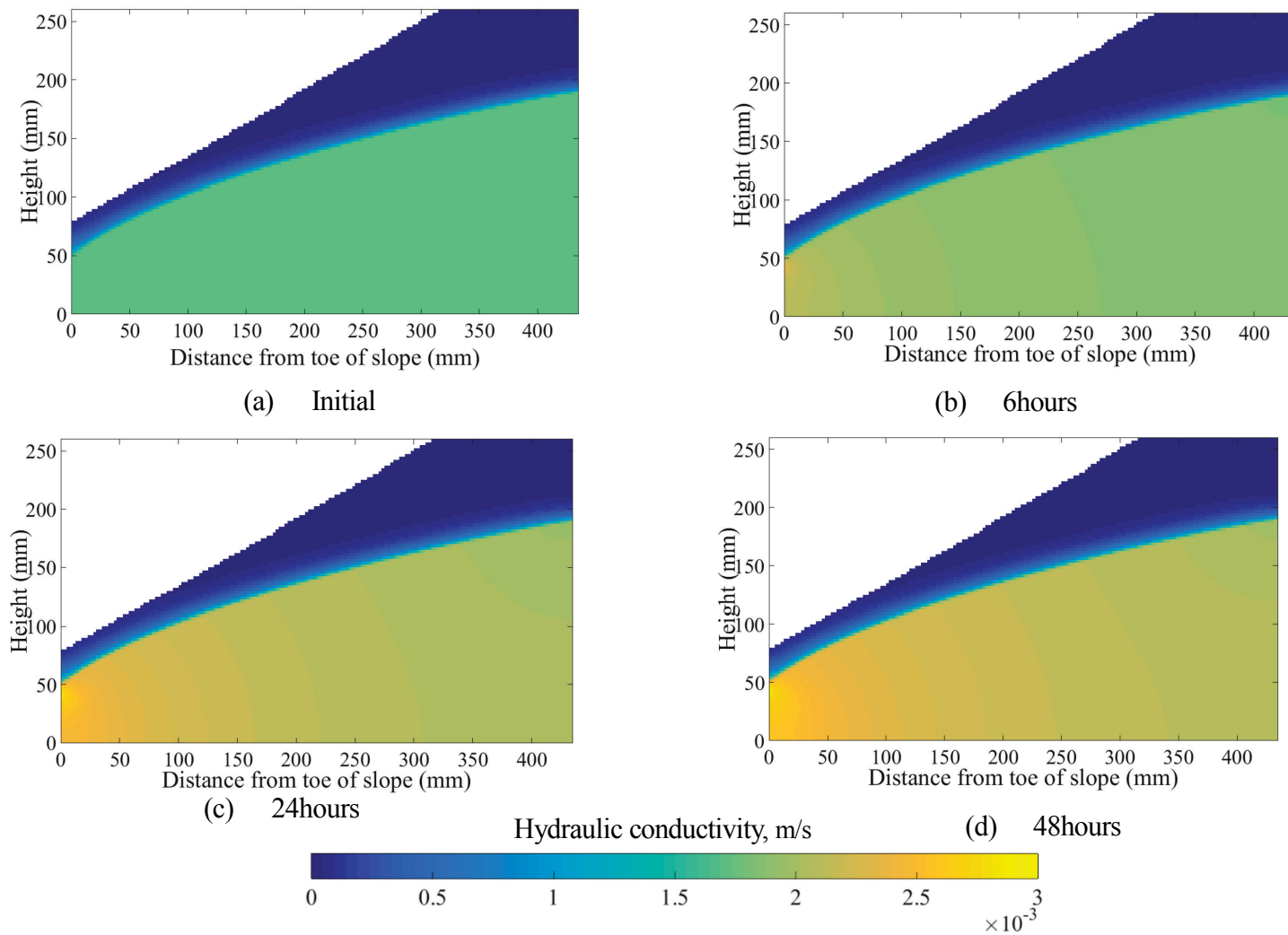alysis is slightly larger than that in the uncoupled analysis. The normalized cumulative eroded soil masses from Foundation zone and Slope zone are also plotted in Fig. 6-12(b). It can be seen that the eroded soil masses in the coupled analysis are slightly larger than that in the uncoupled analysis in Slope and Foundation zone. Firstly, the major coupling effect appears gradually in Foundation zone. Secondly, that effect begins to gradually appear in Slope zone.

Figure 6-13 shows a comparison between the calculated cumulative eroded soil mass and the measured values in physical model tests described in Chapter 5. The right vertical axis is for the normalized mass of erosion. It can be noted that the measured values is larger than the calculated values until around 2 hour. As described in Chapter 5, seepage conditions in physical model tests are unsteady before reaching the near steady state. Major fines erosion takes place in physical model tests during this transient seepage stage. After an elapsed time 2 hour, the calculated values become larger than the measured values. The calculated values continue to increase until the end of the simulation.

Figure 6-14 shows the evolutions of the discharge rate of water at the toe in the experiments described in Chapter 5 and calculated ones in the numerical analyses. In the uncoupled analysis, the hydraulic conductivity and hydraulic gradient are kept constant during the simulation. Therefore, the discharge rate of water is constant. As described in Chapter 5, the discharge rate in the experiments is relatively large in the early stage of the seepage tests. After that, the erosion rate gets smaller and the discharge rate also gradually decreases with time to 0.4-0.6 *L/min* due to local concentration of fines in the embankment. On the other hand, discharge rate of water calculated by the coupled analysis gradually increases with time to 0.8 *L/min* due to erosion-induced increase in the hydraulic conductivity. Since decrease in the hydraulic conductivity due to clogging or redeposition of fines in the soil cannot be modeled in the analysis, the coupled analysis shows opposite tendency compared to the experiments.
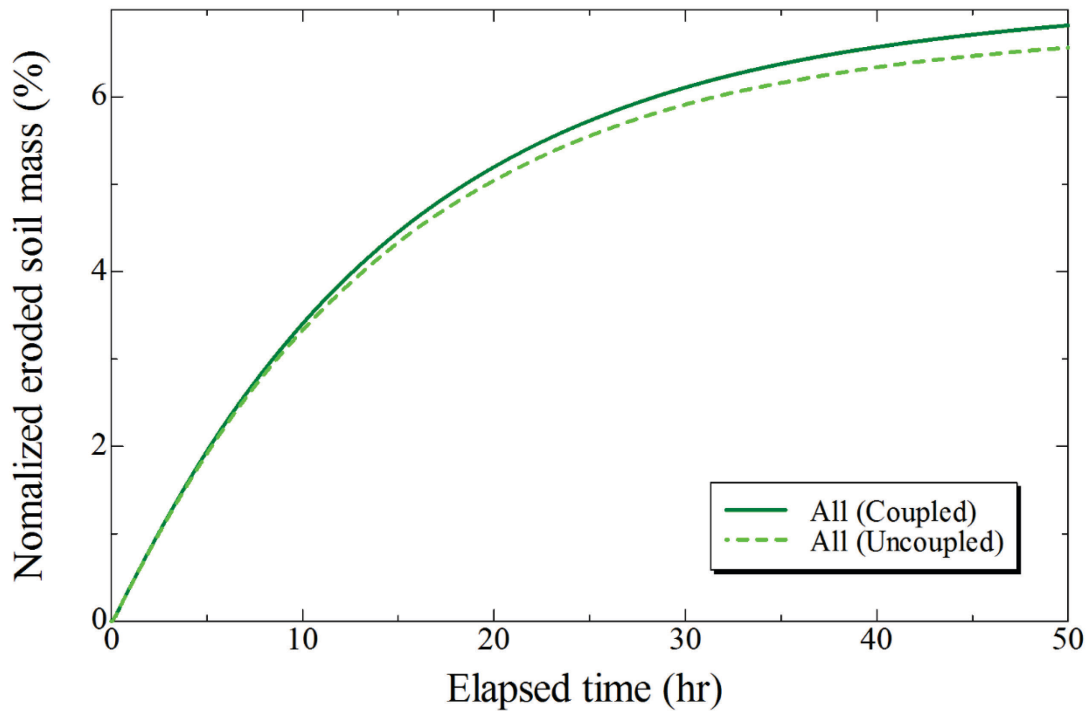
(a) Evolutions of cumulative eroded soil mass from whole embankment model
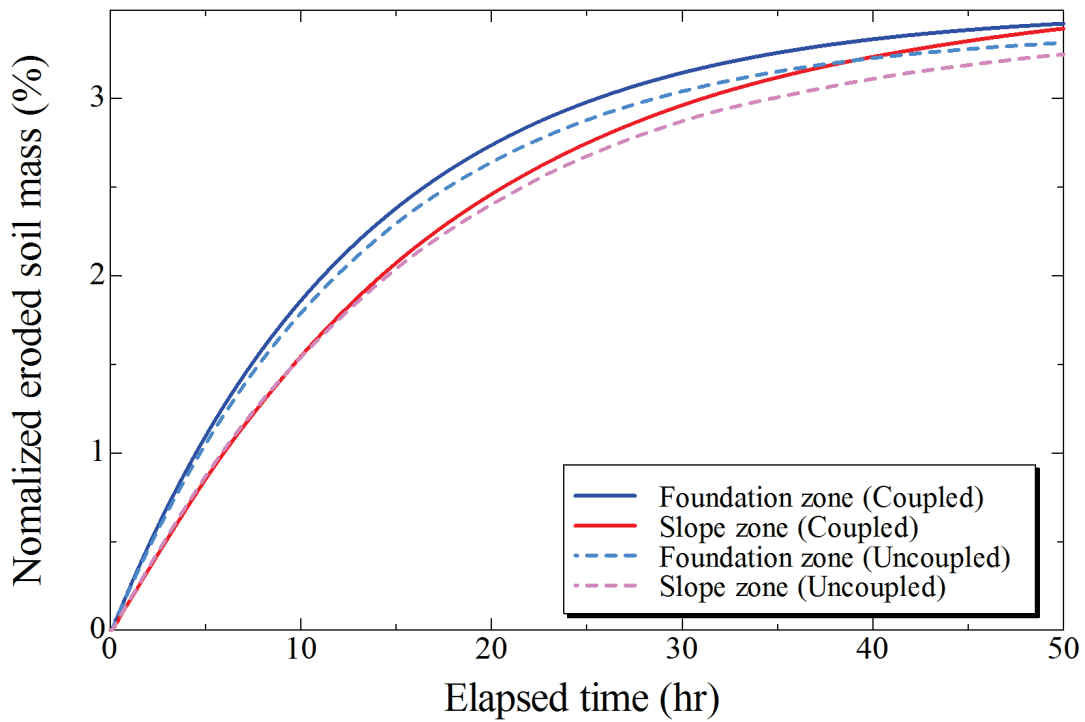
(b) Evolutions of cumulative eroded soil masses from Foundation zone and Slope zone

Figure 6-12   Evolutions of cumulative eroded soil mass for numerical analyses
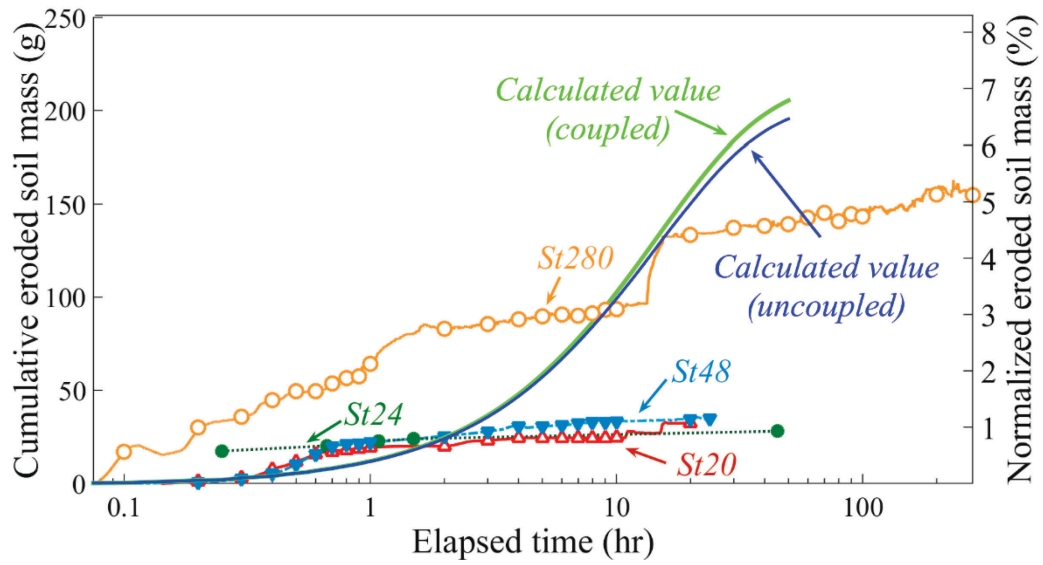
Figure 6-13   Evolutions of cumulative eroded soil mass for physical model tests and numerical analyses
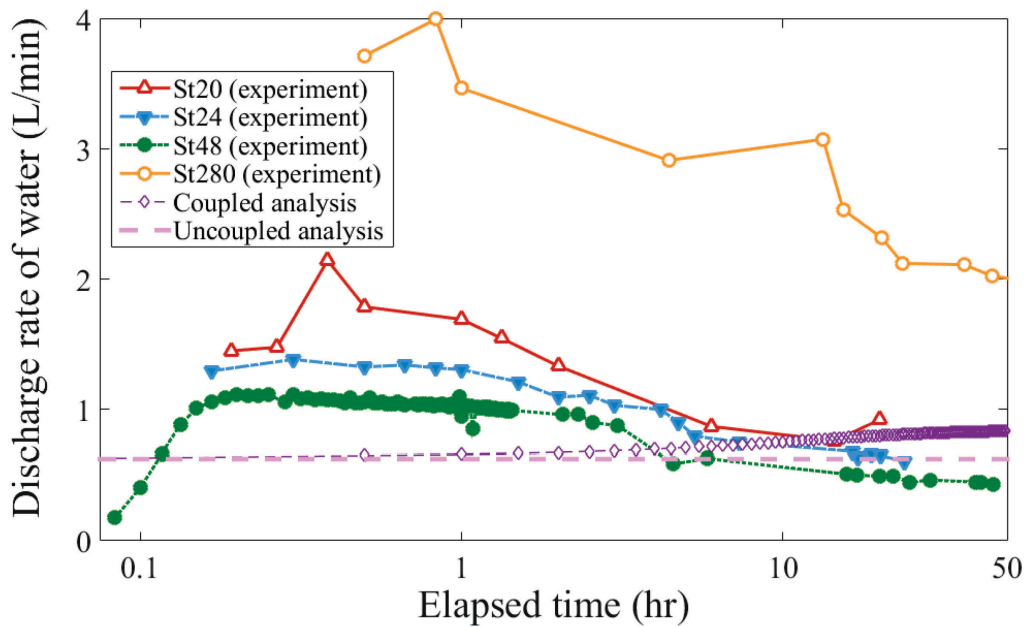
Figure 6-14   Evolutions of discharge rate of water for physical model tests and numerical analyses

111

The variations of fines content fines content contained both trapped fines in pore fluid and fines remaining in the soil skeleton f_c', hydraulic conductivity k and hydraulic gradient i with time at selected elements are focused. Figure 6-15 shows locations of focused Elements A to C. Element A is located at the middle of the foundation near the downstream boundary (at a height of 40 mm from the bottom). Hydraulic gradient and flow velocity are relatively large near Element A. Elements B is located at the horizontally 170 mm distant from toe of slope and vertically 60 mm distant from the base of the model. Elements C is located at the horizontally 315 mm distant from toe of slope vertically 60 mm distant from the base of the model. Hydraulic gradient and flow velocity are large at Element A, while they are relatively small at Element C. The variations of fines content f_c', hydraulic conductivity k and hydraulic gradient i with time at these elements are plotted in Fig. 6-16. It can be seen that reduction of fines contents at Elements B and C in the coupled analysis is slightly larger than that in the uncoupled analysis (Fig. 6-16 (c) (e)). In Fig. 6-16 (d) (f), it can be observed slightly increase in hydraulic conductivity and hydraulic gradient in the coupled analysis. On the other hand, reduction of fines contents in the uncoupled analysis is larger than that in the coupled analysis at Element A (Fig. 6-16 (a)). In coupled analysis, hydraulic conductivity at Element A increases with time due to the coupling (Fig. 6-16 (b)). However, hydraulic gradient at Element A decrease with time.
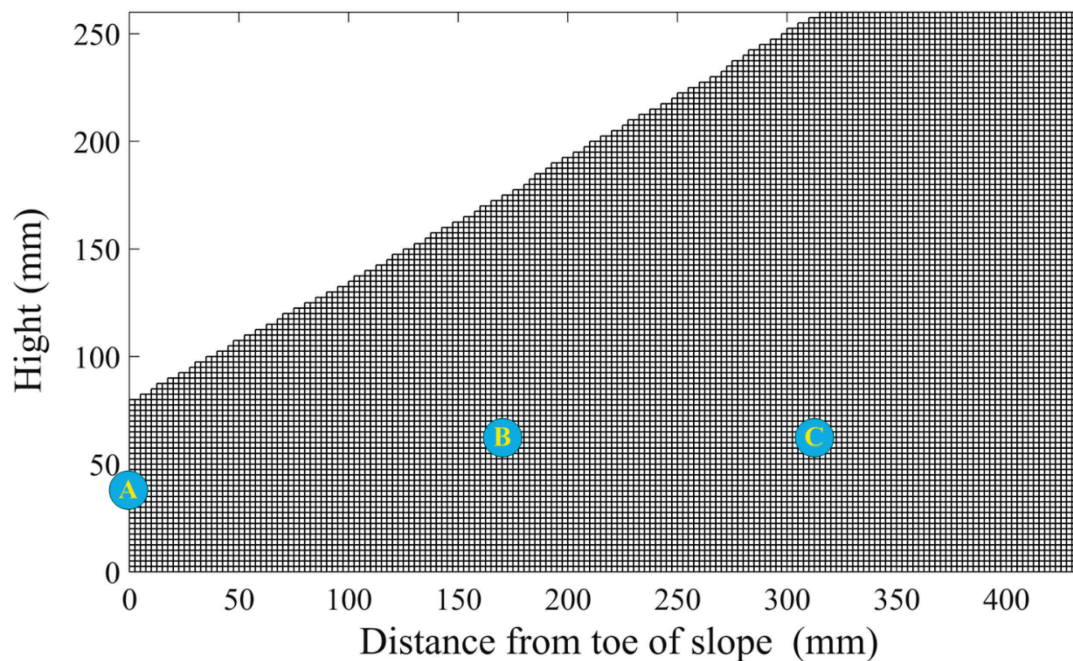
Figure 6-15   Locations of selected elements
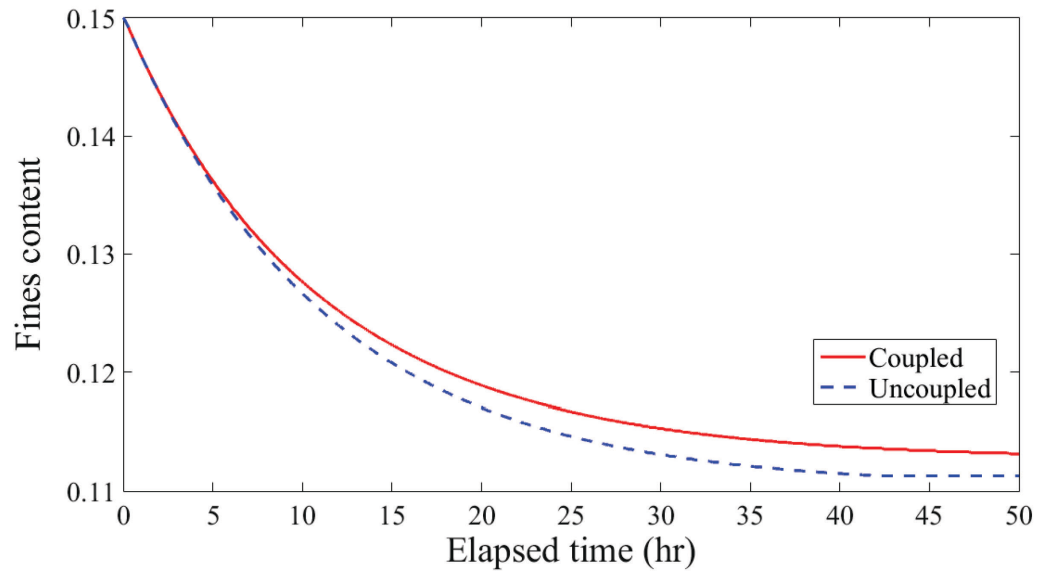
(a) Variation of fines content at Element A
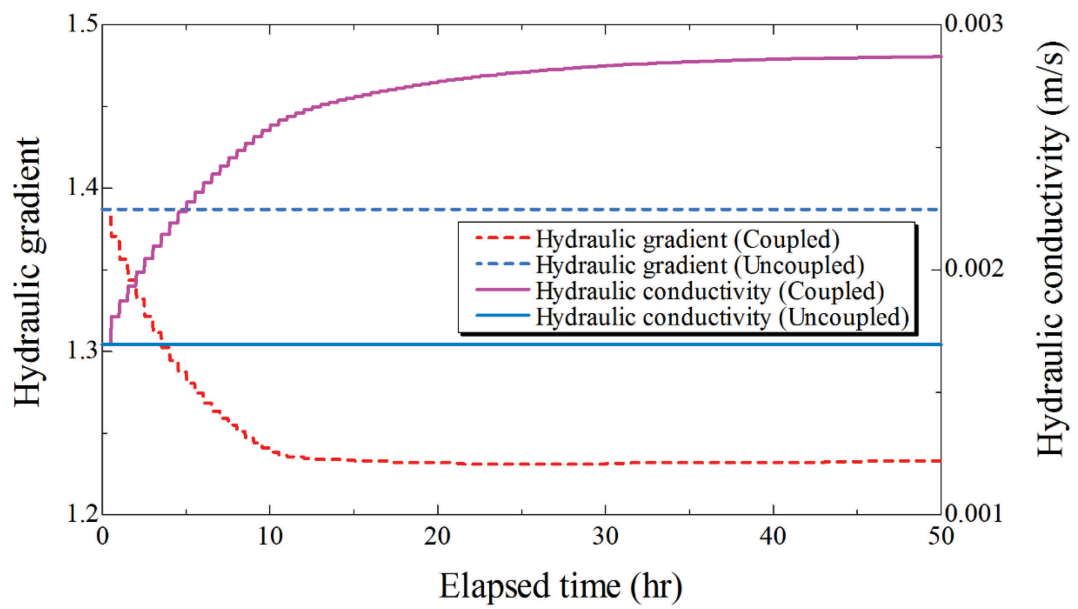
(b) Variations of hydraulic gradient and hydraulic conductivity at Element A

113
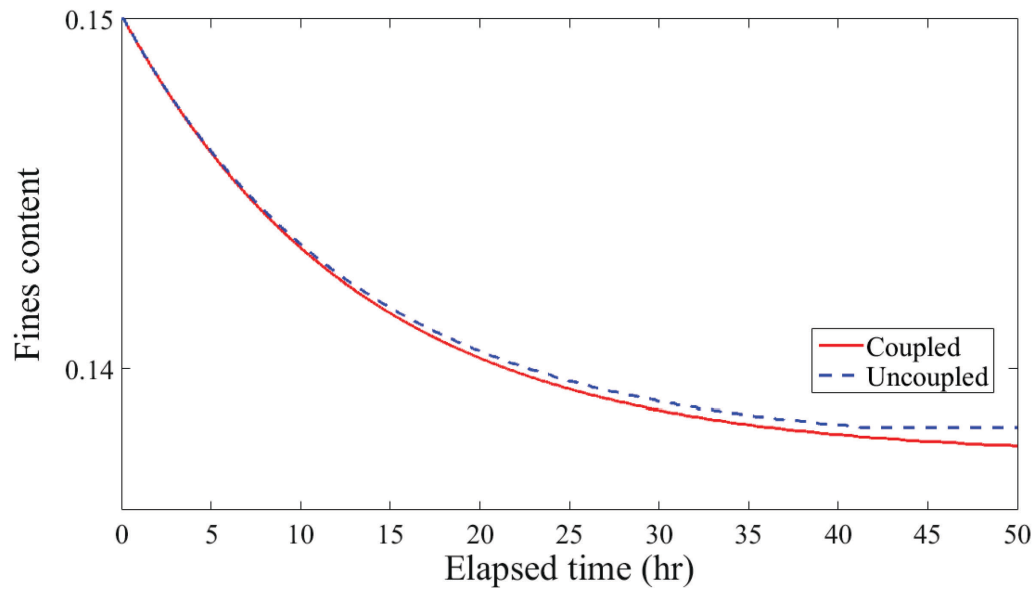
(c) Variation of fines content at Element B
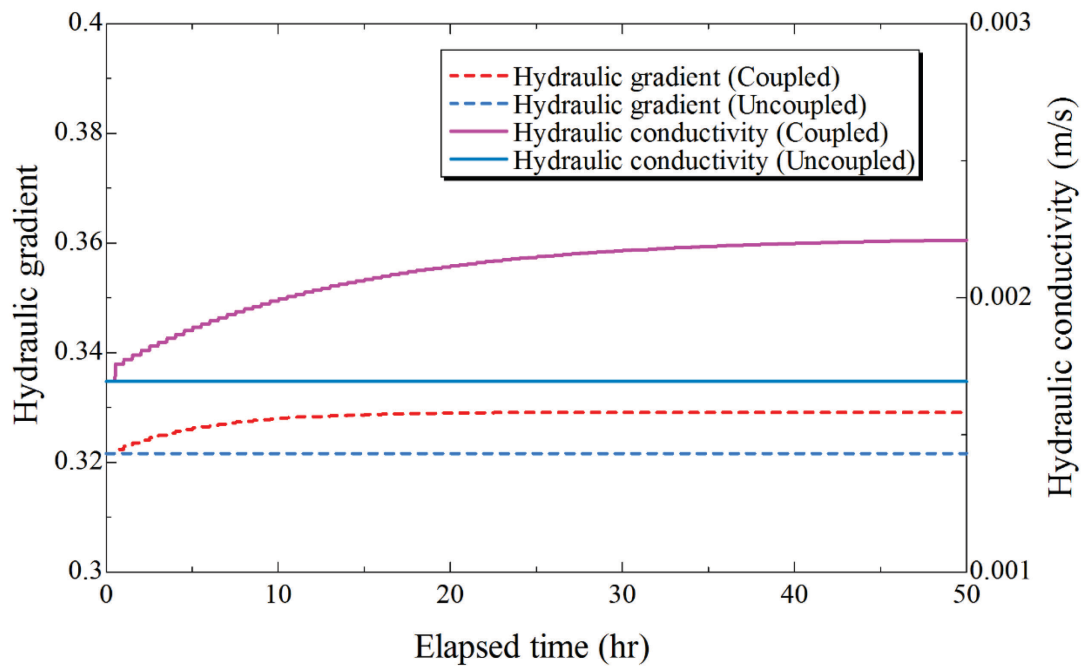
(d) Variations of hydraulic gradient and hydraulic conductivity at Element B
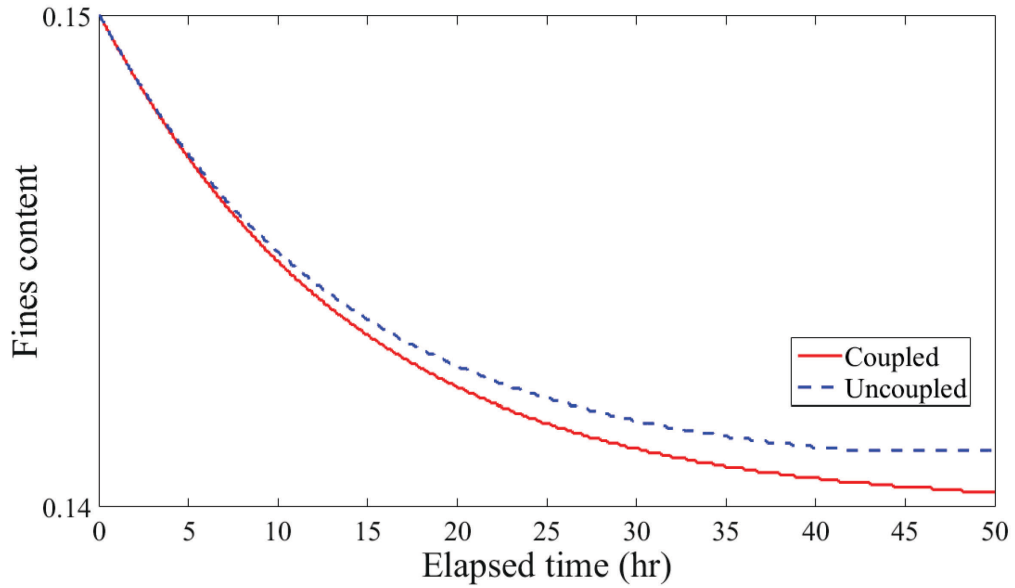
(e) Variation of fines content at Element C
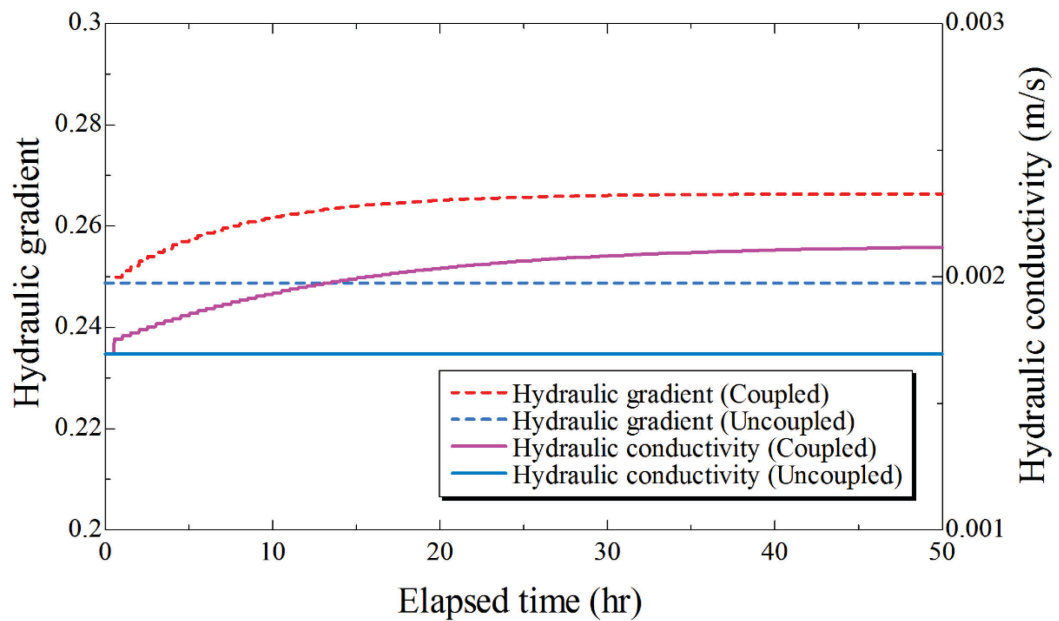
(f) Variations of hydraulic gradient and hydraulic conductivity at Element C

Figure 6-16   Variations of fines content fc, hydraulic conductivity k

and hydraulic gradient i with time

6.6. Discussion on seepage-induced downward transport of fine particle

Comparison with the physical model test described in Chapter 5 is made here. To eliminate the spatial fines content change during the transient stage, i.e., before the seepage flow becomes stable, the incremental change of the normalized fines content with time is calculated and plotted in Fig. 6-17 (a) by making *Case St1* as a reference. This figure is same as Fig. 5-10 (c). Similarly, distributions of change in the fines content obtained by numerical analysis normalized by the initial value are plotted in Fig. 6-17 (b) for 48 hours seepage.

(a) Results of physical model test (b) Results of numerical analysis
(after 48 hours) (after 48 hours)
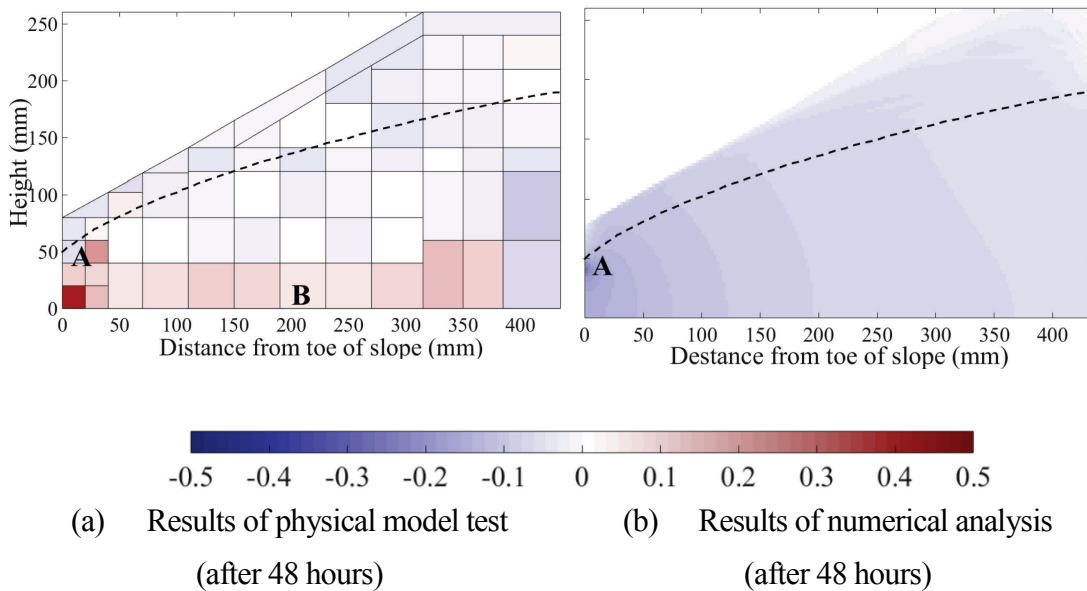
Figure 6-17 Spatial distribution of fines content
in the physical model test and numerical analysis

Observation in the model tests with the constant boundary heads, which is described in details in Chapter 5, can be summarized as follows:

1) A decrease of fines propagates backwardly along the phreatic surface from the middle of the foundation near the downstream (A in Fig. 6-17 (a)) in the embankments under long-term seepage flow.

2) Below the phreatic surface, some erodible fines move vertically and are deposited in the bottom of the foundation (B in Fig. 6-17 (a)).

By comparing spatial changes in the fines content for physical model test and numerical analysis result (Fig. 6-17), it can be said that the numerical simulation can reproduce a backward decrease in fines from downstream.   However, the numerical analysis cannot capture the increase of fines in the bottom of foundation in the physical model tests.   The causes of this deference might be mainly attributable to:

(1) Fluctuation of the phreatic surface promotes the downward movement of fines around the phreatic surface and (2) gravitational vertical force, which is not considered in the numerical analysis, transports the fines downward and fines deposit in the bottom of the foundation.

Therefore, change in the spatial distribution of fines in the embankments in Figs. 5-10 and 6-17 (a) would be result of the above-mentioned two factors, i.e., vertical fines migration due to the gravitational force and migration of fines by seepage force (i.e. tractive force attributable to flow velocity or hydraulic gradient) displayed in Fig. 6-17(b).

The used internal erosion model cannot express increase in fines because the erosion test used in the model calibration gives only positive erosion rate expressed as the sum of detachment and deposition (and/or clogging) of fines.   Though the other internal erosion models (sand production model) developed by Vardoulakis et al. (1996, 2001, 2004) and Papamichos and Vardoulakis (2005) include the term for the redeposition of fines in the equations, the term is neglected or is not considered in a simulation by assuming that the seepage flow is large enough to seep through the erodible fines.   However, some previous one-directional seepage tests showed a decrease in hydraulic conductivity with elapsed time (e.g. Lafleur, 1999; Bendahmane et al., 2008; Marot et al., 2012).   This decrease in hydraulic conductivity is the result of the suffusion-induced clogging in the soil specimen. The physical model tests in this study and the previous studies mentioned above demonstrate the considerable effect of the fines redepodition, i.e. increase in fines in a certain area of interest, on flow field change, which should be considered if detailed modeling of the erosion process is required.

6.7. Summary

Two dimensional finite element analyses are carried out to examine the seepage-induced suffusion process in an embankment on foundation ground in this Chapter. Numerical results show the decrease of fines develops from middle of the foundation near downstream boundary in accordance with the magnitude of flow velocity. Influence of update of hydraulic condition, i.e., coupling effect of the seepage and internal erosion is also examined because porosity, hydraulic conductivity, and hydraulic gradient change with time due to the seepage-induced internal erosion in the real condition. It is noticed that the loss of fines can be overestimated in the uncoupled analysis at active seepage zone within the scope of this study.

Applicability and limitations of used erosion method are summarized by comparing with results of physical model test as follows:

1. The numerical simulation can reproduce overall erosion response of the embankment, i.e. backward decrease in fines from the downstream.

2. Since the fines redeposition-induced clogging has considerable effects on flow field change as demonstrated in the physical model tests and previous studies, this should be considered if detailed modeling of erosion process is required.

To elaborate the cause of redeposition of fines in the seepage-induced suffusion, further physical model tests are conducted in the next Chapter.

REFERENCES

Bendahmane, F., Marot, D. & Alexis, A. 2008. Experimental parametric study of suffusion and backward erosion. *Journal of Geotechnical and Geoenvironmental Engineering,* 134(1)**,** pp. 57-67.

Bonelli, S. & Brivois, O. 2008. The scaling law in the hole erosion test with a constant pressure drop. *International Journal for Numerical and Analytical Methods in Geomechanics,* 32(13)**,** pp. 1573-1595.

Cividini, A., Bonomi, B., Vignati, G. C. & Gioda, G. 2009. Seepage-induced erosion in granular soil and consequent settlements. *International Journal of Geomechanics,* 9(4)**,** pp. 187-194.

Cividini, A. & Gioda, G. 2004. Finite-element approach to the erosion and transport of fine particles in granular soils. *International Journal of Geomechanics,* 4(3)**,** pp. 191-198.

Done, J. 1984. A Taylor-Galerkin method for convective transport problems. *International Journal for Numerical Methods in Engineering,* 20(1)**,** pp. 101-119.

Fujisawa, K., Murakami, A. & Nishimura, S. 2010. Numerical analysis of the erosion and the transport of fine particles within soils leading to the piping phenomenon. *Soils and Foundations,* 50(4)**,** pp. 471-482.

Horikoshi, K., Takeyama, T. & Takahashi, A. 2015. Numerical simulation on seepage-induced change of spatial distribution of fines in embankment. Symposium on Applied Mechanics, JSCE., Kanazawa, Japan (In Japanese).

Ke, L. & Takahashi, A. 2012. Strength reduction of cohesionless soil due to internal erosion induced by one-dimensional upward seepage flow. *Soils and Foundations,* 52(4)**,** pp. 698-711.

Kokaki, H., Maruyama, T., Horikoshi, K. & Takeyama, T. 2015. Numerical and physical modelling of seepage-induced internal erosion around permeable sheet pile. Symposium on Applied Mechanics, JSCE, Kanazawa, Japan. (In Japanese).

Kovács, G. 1981. *Seepage Hydraulics*: Elsevier.

Ladd, R. S. 1978. Preparing test specimens using undercompaction. *Geotechnical Testing Journal,* 1(1)**,** pp. 16-23.

Lafleur, J. 1999. Selection of geotextiles to filter broadly graded cohesionless soils. *Geotextiles and Geomembranes,* 17((5‑6))**,** pp. 299-312.

Li, M. 2008. *Seepage induced instability in widely graded soils.* Doctor of Philosophy ph.D. Thesis, The University of Columbia.

Li, M. & Fannin, R. J. 2008. Comparison of two criteria for internal stability of granular soil. *Canadian Geotechnical Journal,* 45(9)**,** pp 1303-1309.

Marot, D., Bendahmane, F. & Nguyen, H. H. Influence of angularity of coarse fraction grains on internal erosion process. *Proceedings of the 6th International Conference on Scour and Erosion*, 2012 Paris. pp. 887-894.

Mualem, Y. 1976. A new model for predicting the hydraulic conductivity of unsaturated porous media. *Water resources research,,* 12(3)**,** pp. 513-522.

Nakano, M., Miyazaki, T., Shiozawa, M. & Nishimura, T. 1995. *Soil Physics Measurement Methods*, Tokyo: University of Tokyo Press,(in Japanese).

Papamichos, E. & Vardoulakis, I. 2005. Sand erosion with a porosity diffusion law. *Computers and Geotechnics,* 32(1)**,** pp. 47-58.

Reddi, L. N., Lee, I.-M. & Bonala, M. 2000. Comparison of internal and surface erosion using flow pump tests on a sand-kaolinite mixture. *Geotechnical Testing Journal,* 23(1)**,** pp. 116-122.

Skempton, A. W. & Brogan, J. M. 1994. Experiments on piping in sandy gravels. *Géotechnique,* 44(3)**,** pp. 449-460.

Sterpi, D. 2003. Effects of the erosion and transport of fine particles due to seepage flow. *International Journal of Geomechanics,* 3(1)**,** pp. 111-122.

Uzuoka, R., Ichiyama, T., Mori, T. & Kazama, M. Hydro-mechanical analysis of internal erosion with mass exchange between solid and water. *Proceedings of the 6th International Conference on Scour and Erosion*, 2012 Paris. pp. 655-662.

van Genuchten, M. T. 1980. A closed form equation for predicting the hydraulic conductivity of un-saturated soils. *Soil Science Society of America Journal,* 44, pp. 892-898.

Vardoulakis, I. 2004. Fluidisation in artesian flow conditions: Hydromechanically unstable granular media. *Géotechnique,* 54(3)**,** pp. 165-177.

Vardoulakis, I., Papanastasiou, P. & Stavropoulou, M. 2001. Sand erosion in axial flow conditions. *Transport in Porous Media,* 45(2)**,** pp. 267-280.

Vardoulakis, I., Stavropoulou, M. & Papanastasiou, P. 1996. Hydro-mechanical aspects of the sand production problem. *Transport in Porous Media,* 22, pp. 225-244.

Zienkiewicz, O. C., Taylor, R. L. & Nithiarasu, P. 2013. *The Finite Element Method for Fluid Dynamics*, Seventh Edition: Butterworth-Heinemann.

Chapter 7   Experimental observation of seepage-induced fines transport and redeposition in embankments

7.1.   Introduction

The physical model tests described in Chapter 5 noted that fines redeposition-induced clogging in the bottom of the foundation of the embankment is not only caused by quasi-horizontal seepage flow but also is caused by the gravitational force.   It is inferred that this fines migration depends on (1) force balance between the seepage-induced drag force and gravitational force and (2) void distribution around a moving fine.   Among them, effects of void distribution at the bottom of the foundation on the overall migration tendency of fines in embankment are investigated in this Chapter.   Several physical model tests on the seepage-induced suffusion in the small-scaled model embankment built on the foundation ground with different fines content are performed.

7.2.   Soil specimens

Same as the tests described in Chapters 4 and 5, Silica sand No. 3 and Silica sand No.8 are used as the model materials in this series of tests.   In the tests, Silica sand No. 3 also models the soil skeleton, while Silica sand No.8 is used as the erodible fine particles in the voids of the coarse skeleton.   The grain size distribution curves of both Silica sands and basic properties of the materials were shown in Fig. 4-2 and Table 4-1 in Chapter 4, respectively.

The chosen fines contents of the mixture at the base of the foundation are 5%, 15 % and 25 %.   The grain size distributions curves of the mixtures and basic properties of each material are shown in Fig. 4-3 and Table 4-2, respectively.

The vulnerability of these mixtures to suffusion is estimated by several criterion internal instability.   The details of the assessment and vulnerability against suffusion are shown in Table 7-1.

Table 7-1   Assessment of vulnerability to suffusion

Criteria	Specimen $f_c = 5\%$	Specimen $f_c = 15\%$	Specimen $f_c = 25\%$
Istomina (1957) [Ref. Kovacs (1981)]	S[*1]	S	S
Burenkova (1993) [Ref. e.g. Wan and Fell (2004)]	U	U	U
Li and Fannin (2008)	U	U	U
Wan and Fell (2008) [*2]	U	U	U
Chang and Zhang (2013)	U	U	S

*1: "U" means Unstable; "S" means Stable.

*2: Combined method of Kezdi (1979) criterion and Kenney and Lau (1985, 1985) criteron

The calculated critical hydraulic gradient for zero effective stress is 1.0 according to Terzaghi's equation.   From linear relationship in previous one-dimensional seepage tests on a similar mixture by Ke and Takahashi (2012) described in Chapter 4.2, the expected critical gradients against suffusion for the mixtures used (5, 15 and 25% fines content) are 0.28, 0.25 and 0.21.

In a series physical model tests described in this Chapter, the configuration of the embankment and its foundation are the same as that described in Chapter 5.   However, various colored Silica No. 8 sands are used in the model (Fig. 7-1).   The green colored Silica No.8 sand is placed at bottom of the foundation (D in Fig. 7-1).   The blue colored Silica No.8 sand is placed top of the foundation (C in Fig. 7-1).   In the slope zone, original Silica No.8 sand (white color) is mainly used (A in Fig. 7-1).   The red colored Silica No.8 sand is used in the lower section of crown (B in Fig. 7-1).   The yellow colored Silica No.8 is used at the area where the phreatic surface supposedly locates at the boundary between the slop zone and lower section of the crown under the controlled steady seepage condition (E in Fig. 7-1).   Each colored Silica No.8 sands are artificially coated by pigment and then stabilized by baking.   Ouyang and Takahashi (2015) estimated the aspect ratio, convexity and sphericity of each colored Silica No.8 sand by the image analysis, quantitatively.

Figure 7-2 shows indices for shape of colored Silica No.8 sands.   The black colored Silica
No. 8 sand is not used.   The results of this image analysis show that the colored Silica No.8
sands have similar morphologies with that of commonly used white one.
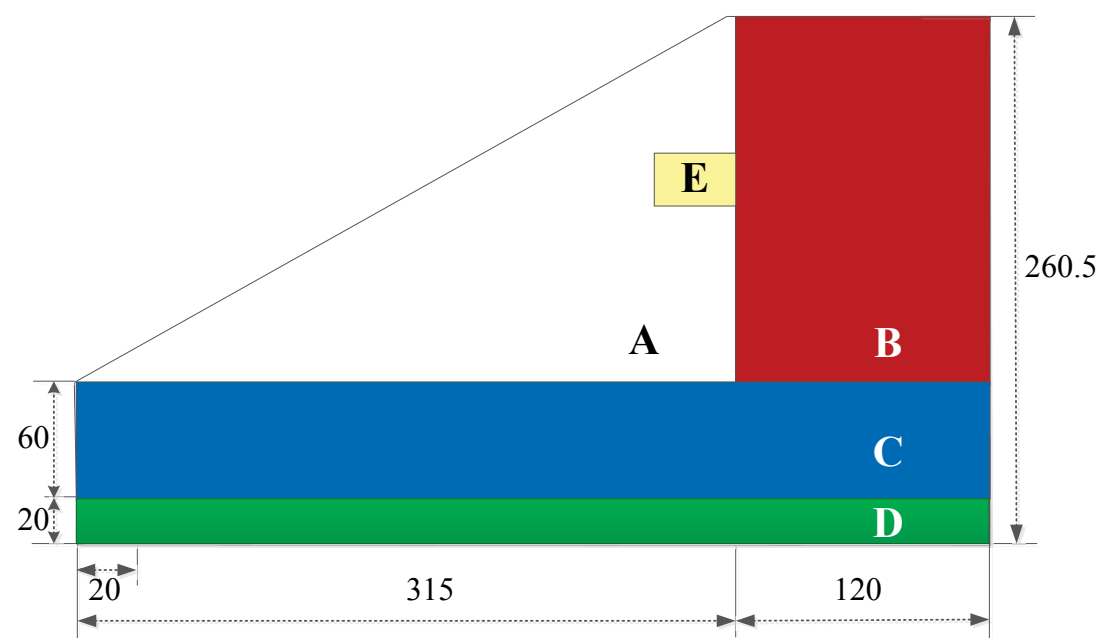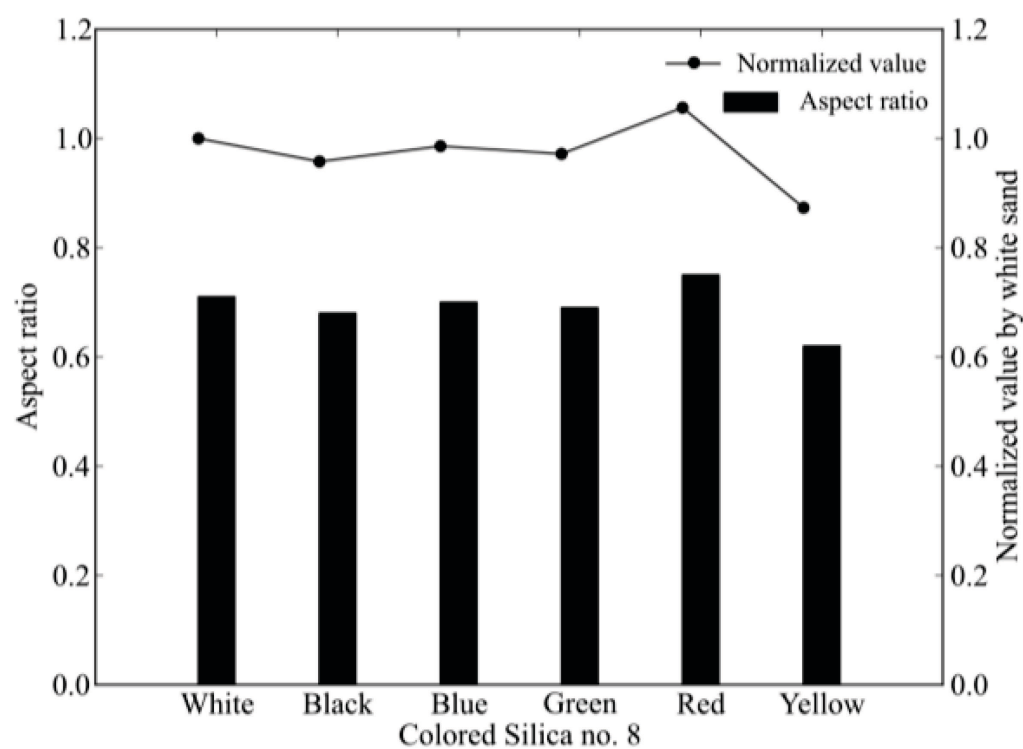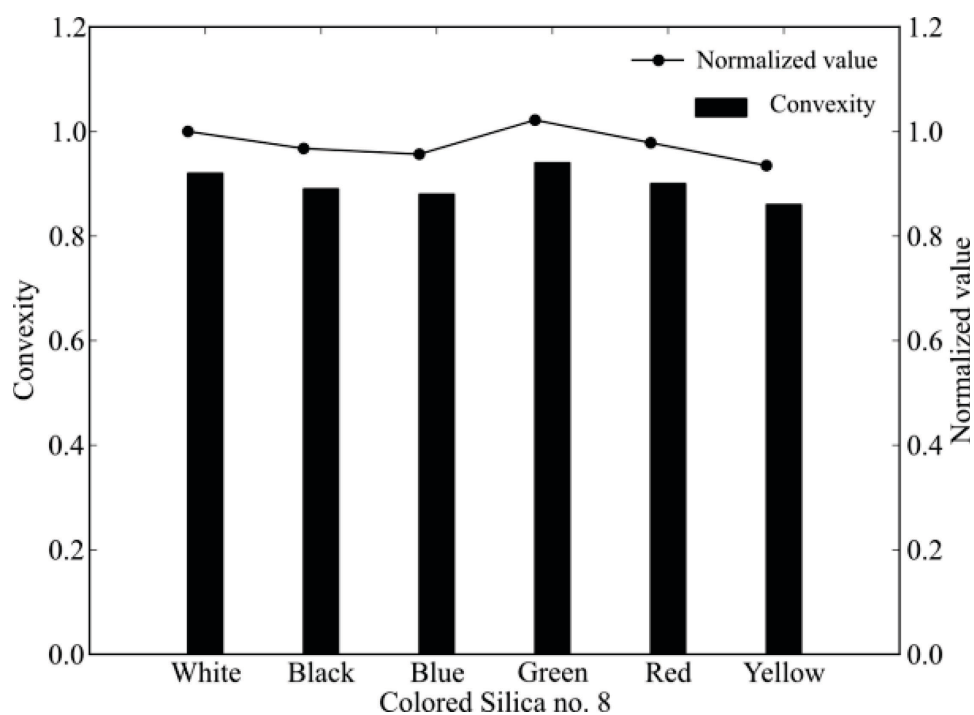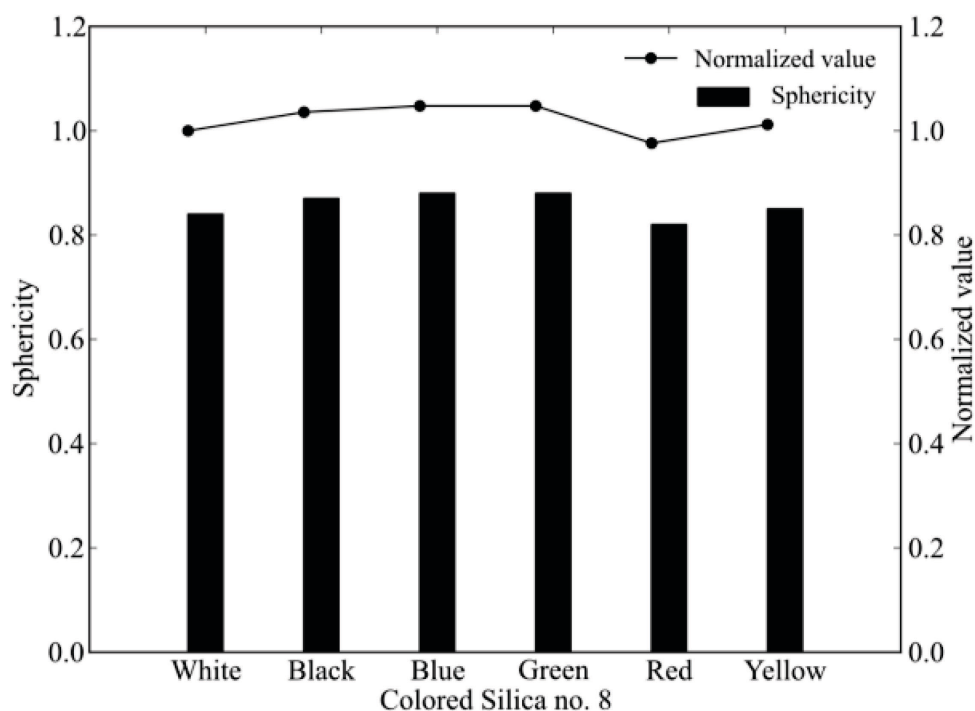

Figure 7-1   Initial position of each fines

(a)   Aspect ratio and its normalized value of colored Silica No. 8

(b)   Convexity and its normalized value of colored Silica No. 8

(c)   Sphericity and its normalized value of colored Silica No. 8

Figure 7-2   Indices for shape of colored Silica No.8

(Ref. Ouyang and Takahashi (2015))

7.3. Test system

In order to investigate the effects of void distribution at the bottom of the foundation on the overall migration tendency of the fines in the embankment, the physical model tests are conducted using almost the same system as described in Chapter 5. The difference between the test system in this Chapter and that in Chapter 5 is that the eroded fines mass is not recorded automatically in the tests of this Chapter. Eroded and washed out fines are collected by a suspended bowl on wires underwater in the small container at a certain interval of time. To prevent the outflow of fines to the outside of the bowl and to help the sedimentation of fines, it is covered with filter paper on the side surface. The collected fines are dried and weighted after the tests. The discharge flow rate is measured by the volume of discharge of the water in a certain period.

The target relative density of the coarse skeleton is 40% (the void ratio of the coarse skeleton $e_s = 0.885$, relative density $Dr = 35$ %). Therefore, the target dry density for the mixtures used (5, 15 and 25% fines content) are 1.360, 1.560 and 1.717g/cm³, respectively. The initial moisture content is 3.0 %. After making the level ground, the model ground is scraped off with a shaped frame and formed to be a 260.5 mm high embankment. The fines content of material for the embankment zone (Areas A, B and E in Fig. 7-1) and top of the foundation (Area C in Fig. 7-1) are 15%. The fines content at the bottom of the foundation (Area D in Fig. 7-1) is 5%, 15%, or 25% in each experimental case respectively.

7.4. Experiment procedures and conditions

To investigate the cause of redeposition of fines, a series of physical model tests on seepage-induced suffusion in the small-scaled model embankment is performed. Elapsed time is measured from the start of pouring of water into the water supply tank. Seepage flow in the embankment also reaches a near steady condition in 30-40 minutes and the boundary heads reach 190 mm and 40 mm in 30-40 minutes at the upstream and downstream sides, respectively.

In total three tests are conducted. The seepage is continued for 48 hours with keeping the water heads at the boundaries constant. Detailed test conditions are summarized in Table 7-2. The experimental parameter is the fines content at the bottom of the foundation (Area

D in Fig. 7-1).   Here, homogenous model with 15% fines content mixtures are used in *Case 2* and it is refer to the test described in Chapter 5 as *Case St48*.

Table 7-2   Test cases of seepage testing

Case	Dry density (Mg/m³)	Fines content at the bottom of foundation (%)	Seepage time (min)	Division number	Eroded soil ratio (%)
Case 1	1.560	5	2880	118	0.951
Case 2	1.567	15	2880	66	0.913
Case 3	1.560	25	2880	118	0.976

After the seepage testing, sieve analyses on subdivided areas of the model embankment are conducted to estimate the spatial variation of fines content.   And then, particle analyses on (a) eroded particles and (b) the remaining particles in the subdivided areas are conducted to estimate the initial position of transported fines or redeposited fines in *Cases 1* and *3*.   In the particle analyses, eroded particles and remaining particles are sieved and these particles are classified by several particle size ranges; 150-250, 106-150, 75-106, 25-75μm and less than 25μm.   The images of classified particles are record by the digital microscope (HIROX Co., Ltd., VCR-800) with a low-magnification lens (20 magnifications, HIROX Co., Ltd., VCR-209).   The color of particles is examined for more than 1000 particles in each size range.   Finally, the initial positon of transported fines can be obtained by reference to Fig. 7-1.

Change of the initial fines content at Area D either increases or decreases the amount of fines in the void of the coarse skeleton, i.e. decreasing or increasing in porosity, in this corresponding area.   In case with the larger fines content, i.e., the smaller porosity, at the bottom of the foundation, the less percolation of the fines into this area is expected.   Thus, the less sedimentation or reposition of the fines due to the gravitational force is expected in

Case 3, while the more in *Case 1*.   Through the comparison among the cases, effects of the gravitational force on migration of fines can be observed.   However, it should be noted that the distribution of seepage velocity in the model embankment is also changed when the fines content at Area D is changed.   Figure 7-3 shows the initial horizontal velocity profiles calculated by steady seepage analysis using finite element method at the horizontally 0 mm, 50 mm and 100mm distant from toe of slope.   In all the cases, flow velocity increases with depth in the unsaturated zone, i.e., above the phreatic surface.   In the saturated zone, except at the downstream boundary, the flow velocity is very uniform.   At the boundary between Areas C and D, clear gap in the velocity is observed in *Cases 1* and *3*, since the hydraulic conductivity in Area D is different from those in Areas A and C.   In *Case 3* where the fines content at Area D is large, the hydraulic conductivity and hence the flow velocity is small at this zone, while the reverse in *Case 1*.   There is no much difference in the magnitude of the flow velocity among the cases in Areas A and C, but somewhat larger in *Case 1* where the flow velocity in Area D is smaller than the other cases and somewhat smaller in *Case 3* where the flow velocity in Area D lager than the other cases.   By taking these in consideration, experimental results are discussed in the following section.
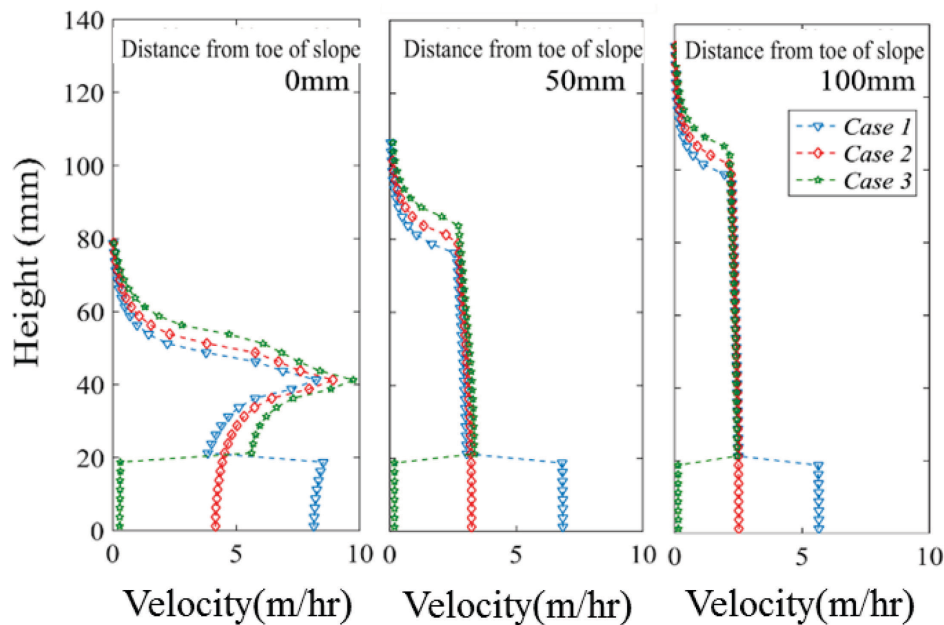

Figure 7-3   Horizontal velocity profiles

7.5. Results and discussion

Figure 7-4 shows evolutions of the cumulative eroded soil mass and discharge rate of water at the toe. In this figure, the calculated discharge rates of water without erosion by finite-element method are also plotted. The amount of discharged fines is normalized by the initial total amount of Silica No.8 in the model and it is defined as the eroded soil ratio. The final total eroded soil mass and eroded soil ratio are summarized in Table 7-2. By comparing the results, except the eroded soil mass at the first measurement point in Case 2, the larger the fines content at the bottom of the foundation the larger the eroded soil mass. It can be also noted that the larger the fines content at the bottom of the foundation, the less the discharge rate of water. Figure 7-4 also shows that major fines erosion takes place in the early stage of the seepage tests (until around 3 hour). In this period, the discharge rate is relatively large. After that, erosion rate gets smaller and the discharge rate also gradually decreases with time. These indicate that decreasing in flow velocity causes reduction in the tractive force to transport the fines.

Distributions of change in the fines content normalized by the initial value are plotted in Fig. 7-5 for all the cases. Position of the calculated phreatic surface by the finite element method is indicated by the dashed line in Fig. 7-5. In all the cases, marked decrease in the fines content is observed at the elements located at 20-60 mm height from the base of the model at the downstream boundary (point **a** in Figure 7-5). This location coincides with the element at which the flow velocity is the largest as showed in Figure 7-3. Observation for each case can be summarized as follows:

- In *Case 1* (Fig. 7-5 (a)), the clear boundary that separates the fines increasing zone from the decreasing zone is observed at the boundary between Areas C and D where the initial fines content is 5%. A number of fines in the decreasing zone moves right below or obliquely downward. An increase in fines can be observed at the element located vertically 0-20 mm distant from the base of the model at the downstream boundary (point b in Figure 7-5 (a)).
- In *Case 2*, a regressive decrease of fines along the phreatic surface is observed from the middle of the foundation near the downstream boundary. It also shows an increase in fines in the foundation round horizontally 270-380 mm distant from the toe of the slope (point **c** in Fig. 7-5 (b)).
- In *Case 3*, less redeposition of fines into bottom of the foundation is observed.
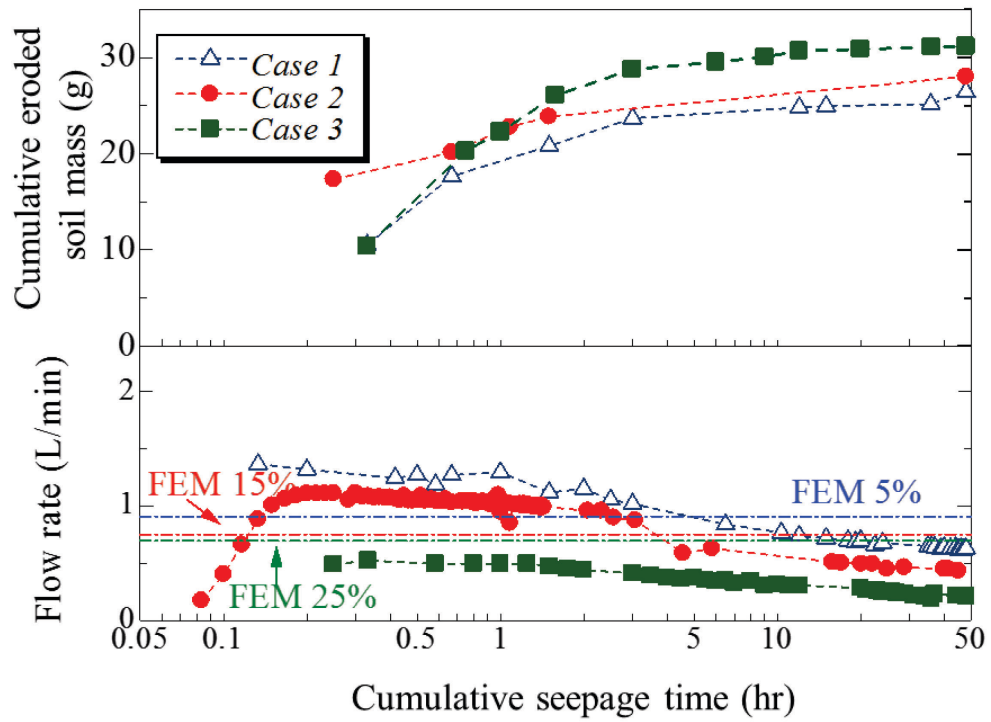
129

Figure 7-4　Evolutions of cumulative eroded soil mass and evolutions of discharge
rate of water

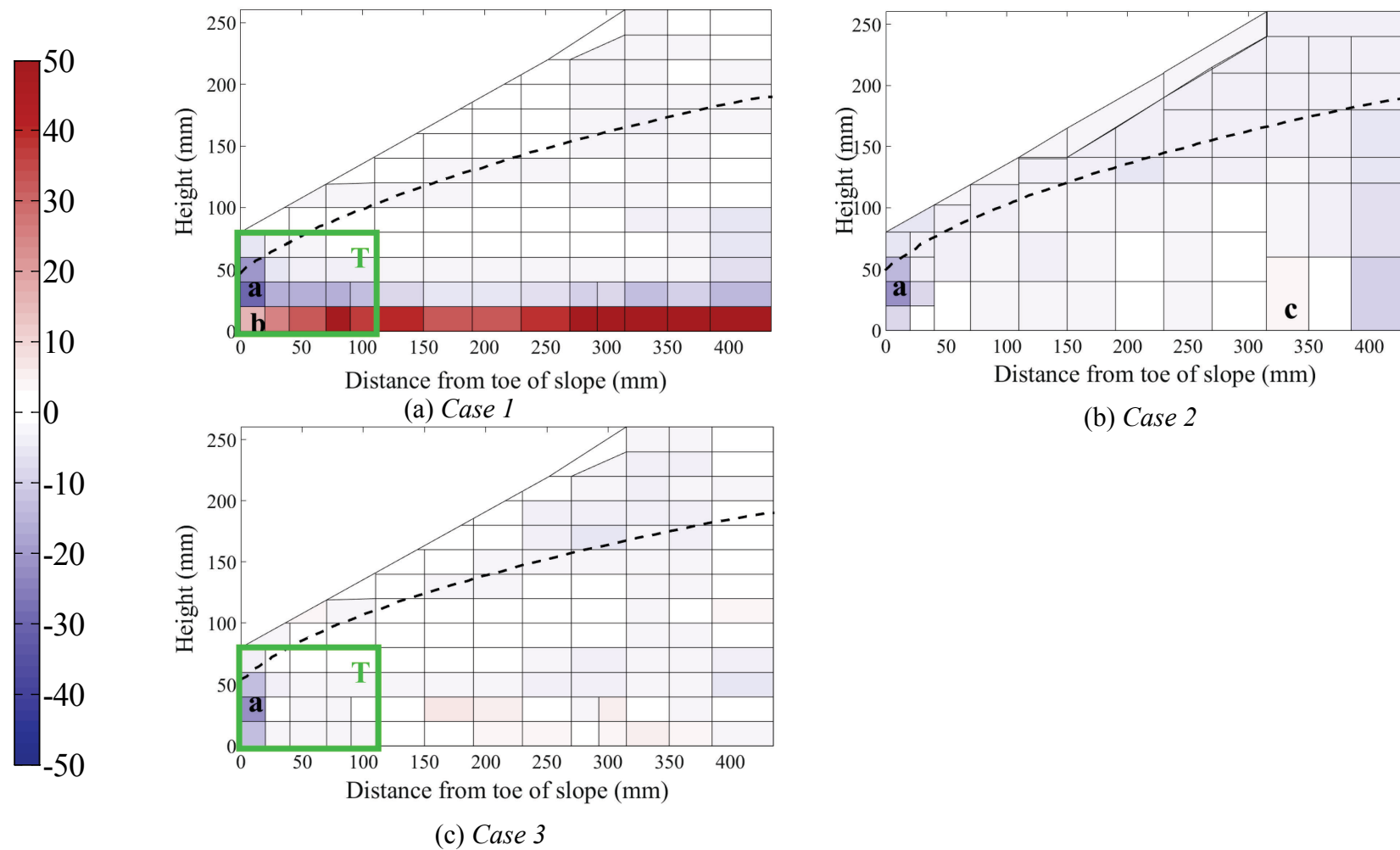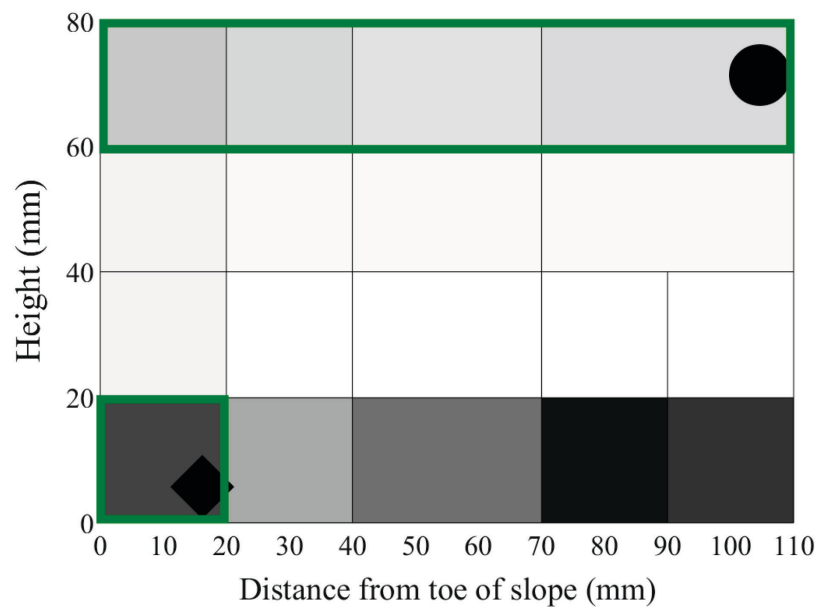(a) *Case 1*

(b) *Case 2*

(c) *Case 3*

Figure 7-5   Distributions of change in fines content normalized by initial value

131

In *Cases 1* and *3*, the origin of remaining particles in the subdivided areas is estimated by the color of each. The ratio of influx of fines from other areas is estimated in Zone *T* framed in by the green line in Figs. 7-5 (a) and (c) as shown in Fig. 7-6. This influx ratio is calculated as follows: The ratio of influx of fines from other areas is firstly estimated from the microscope image for each particle size range. The ratio is secondly weighted by the content ratio of each particle size range obtained by sieve analysis. The influx ratio of all particle size range is finally given by using the weighted ratio of the influx of each particle size range.

In Areas C (top of the foundation) and D (bottom of the foundation), most of influx fines by seepage are originally located just above the corresponding area, i.e., the fines migrated from Area A dominates the influx fine in Area C, the fines migrated from Area C dominates the influx fines in Area D. From Fig. 7-6, the ratio of influx fines from other areas in Area D for *Cases 1* and *3* are 0.157-0.406 and 0.013-0.077, respectively. The influx ratio in Case 3 is smaller than that in *Case 1* as expected.

As Fig. 7-3 shows, flow velocity at Area C in the initial condition is almost same for all the cases. This means that the magnitude of the seepage-induced tractive force on fines is also almost the same in this area for all the cases. However, the ratio of influx fines from other areas (mainly from Area A) in the subdivided elements ● is larger in *Case 1* as compared to *Case 3*. In addition, the ratios of influx from Area A in the element marked ◆ are 0.047 and 0.002 for *Cases 1* and *3*. These denote that the fines migration does not only depend on the magnitude of the seepage force, but also the void size at the bottom of the foundation. In other words, the larger the void at the bottom of the foundation ground, the more the downward fines transport by gravitation.

(a) *Case 1*
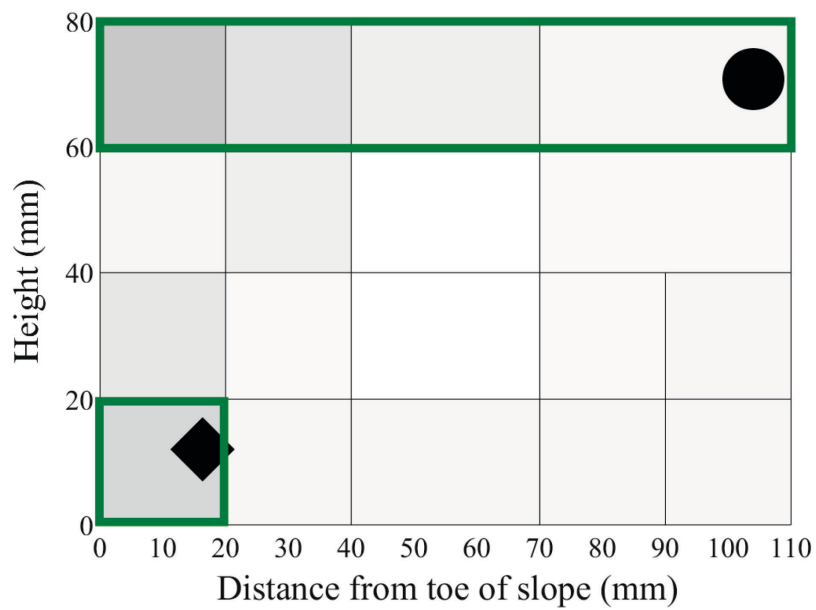
(b) *Case 3*

Figure 7-6   Ratio of influx of fines from other area near the toe

Figure 7-7 shows that the horizontal distributions of increment of content of fines originated from each area (color) and sum of all in Area D after the seepage testing. The plotted positions are corresponded the intermediate position of each subdivided element. From this figure, it can be observed that sum of the fines originated from each area is increased over the whole area of the bottom of the foundation in *Case 1*. Increment is larger in the element closer to the upstream boundary. In this case, the marked contribution of the influx from Area C is noted. Near the downstream, at around horizontally 30-100 mm distant from toe of the slope (Place *I* in Fig. 7-7), increase of fines originated from Area D is observed, while decrease of fines originated from Area D is observed from midstream to upstream, at elements located around horizontally 130-280 mm distant from toe of the slope (Place *II* in Fig. 7-7). Based on these postmortem observations in *Case 1* and the fact that the fines at the bottom of the foundation is increased with time in the homogeneous model (see Chapter 5), possible explanation of evolution of fines migration is given below:

- Firstly, the fines originally located at Place *I* are transported to outside of the model and then voids are increased in these elements.
- After that the fines originally located at Place *II* inflow horizontally into these enlarged voids.
- The fines located at Area C gradually inflow vertically with time into the whole area of bottom of the foundation during the seepage.

As mentioned above, increment is larger in the element closer to the upstream boundary, especially due to the influx from Area C. This is because of the relatively smaller seepage force, i.e., the smaller flow velocity, in upstream, compared to the gravitational force.

In *Case 3*, content of fines originally located at Area D decreases from 25.0 % to 18.7 % at the downstream boundary. In the other elements, no marked change is observed, due to the smaller voids in Area D. As seen in *Case 1*, increment is relatively larger in the element closer to the upstream boundary (Place *III* in Fig. 7-7), especially due to the influx from Area C. The reason for this may be the same as in *Case 1*.
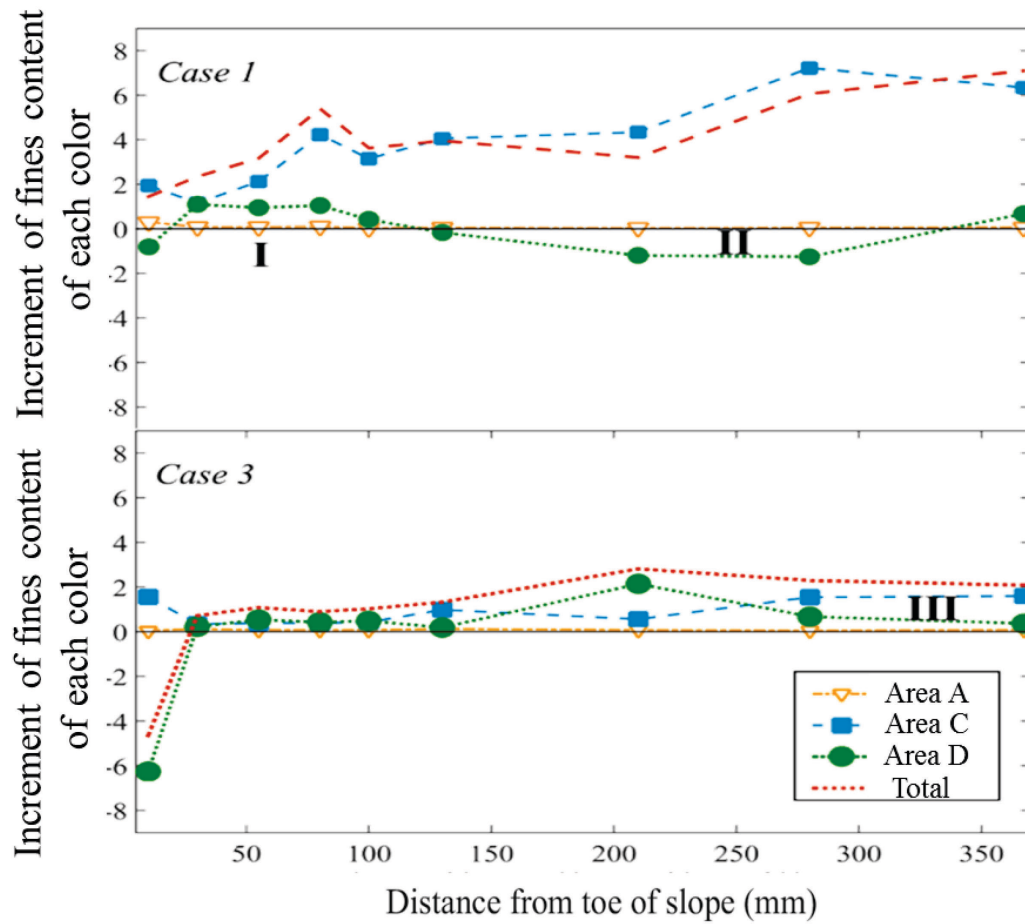
Figure 7-7   Increment of fines from each area at the bottom of foundation

In *Cases 1* and *3*, particle analyses on eroded particles, i.e., the soil that seeps out from the model, are also conducted by counting the number of particles for each color.   The evolution of the ratio of the fines originated from each area (color) to the total amount of eroded particles for *Cases 1* and *3* is shown in Fig. 7-8.   The cross sectional area ratio of Area C and Area D to the total area at the downstream boundary is indicated by dashed line in this figure.   The time at which arrival of the seeping water is detected by the pore water pressure transducer at P1 in Fig. 7-1 and that at which the seepage flow gets steady are also indicated in the figure.

In *Case 1*, it can be observed that almost all the fines (ratio is 0.77 to 0.91) are originated from Area C for each measurement interval (Fig. 7-8 (a)).   In *Case 3*, about 80 % eroded fines (ratio is 0.74 to 0.82) are originated from Area C except the first measurement interval (Fig. 7-8 (b)).   These indicate that majority of the eroded fines are originated from Area C.
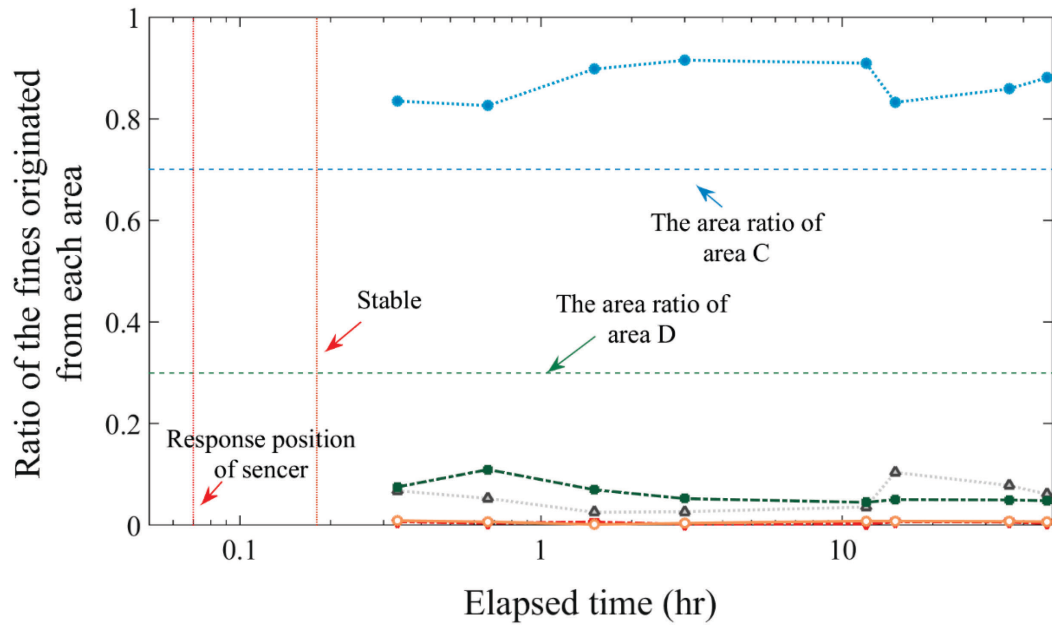
(a) *Case 1*
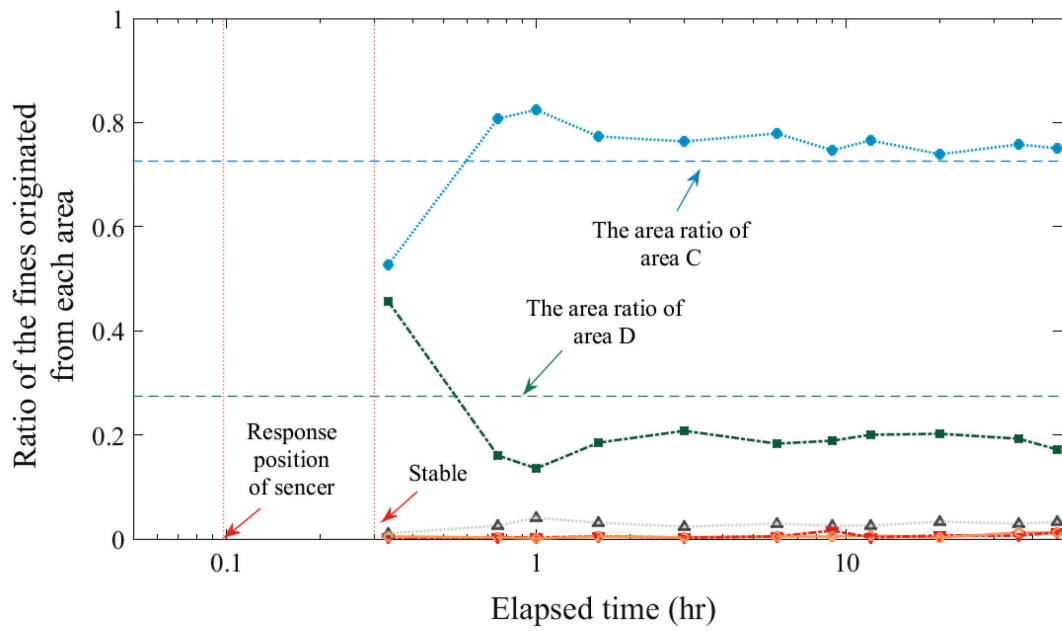
(b) *Case 3*

Figure 7-8   The evolution of the ratio of the fines originated from each area

As shown in Fig. 7-5, the fines content is predominantly decreased in elements located 20-60 mm height from the base of the model near the downstream boundary, which corresponds to Area C in Fig. 7-1. This is in accord with the results from Fig. 7-8. In *Case 2*, the estimation of the initial positon of the eroded particles and the remaining particles in the subdivided areas cannot be made because the colored Silica No. 8 sands are not used in the model. However, as seen in *Cases 1* and *3*, it is supposed that almost all the eroded fines are originated from top of the foundation, which corresponds to Area C.

Amount of the fines originated from Area D is less in the outflow of fines. From the Fig. 7-8, the ratio of fines originated from Area D in all the eroded fines is 0.08-0.110 for *Case 1* and is 0.13-0.20 for *Case 3*, except the first measurement interval. Eroded fines also contain fines originated from Area A. Its ratio is 0.05-0.10 and 0.01-0.04 for *Cases 1* and *3*, respectively. They are considerably smaller than the fines originated from Areas C and D. Here, eroded fines originated from Areas B and E are negligibly small (less than 0.01).

The ratio of fines originated from Areas C and D in all the eroded fines are close to the cross sectional area ratio of Area C and Area D to the total area at the downstream boundary are displayed by dashed lines in *Case 3*.(Fig.7-8 (c)). In *Case 1*, the ratios of the outflow of fines from Areas C and D are comparable to the area ratios, but the ratio of fines originated from Area C is relatively larger and that from Area D is relatively small, compared to *Case 3*. From the Fig. 7-7, in Case 1 the fines content increase of 1.94% at the bottom of the foundation comes from top of the foundation (Area C in Fig.7-1) at the downstream boundary. It is notes that at the upstream side, a large amount of fines is transported into bottom of the foundation (Area D in Fig.7-1) compared to *Case 3*. It is inferred that part of fines originated from Area C is deposited into Area D and then is transported laterally through this area and is discharged from the embankment. This means that the discharged fines from downstream boundary at Area D are not only from Area D, but also from Area C. This is the possible reason for the large ratio of fines originated from Area C in Fig. 7-8 (a).

This erosion mode observed in this series of tests, whose model has different fines content in the same void size at the bottom of the foundation, is similar to the contact erosion. As

described in Chapter 2, the contact erosion is the erosion of particles at the interface between fine and coarse layers due to a quasi-horizontal groundwater flow.

Experimental studies on the contact erosion have been examined by element tests (Cyril *et al.*, 2010; Beguin *et al.*, 2013) and physical model test with the small-scaled model (Saito *et al.*, 2014) and large-scaled model (Beguin *et al.*, 2012). In these experiments on the contact erosion showed that a part of fines initially located above the coarser material layer is vertically deposited and then is transported horizontally. Fines finally clog at the downstream of the bottom layer consisted of coarser material (Beguin *et al.*, 2012), which is comparable to the observation in this study.
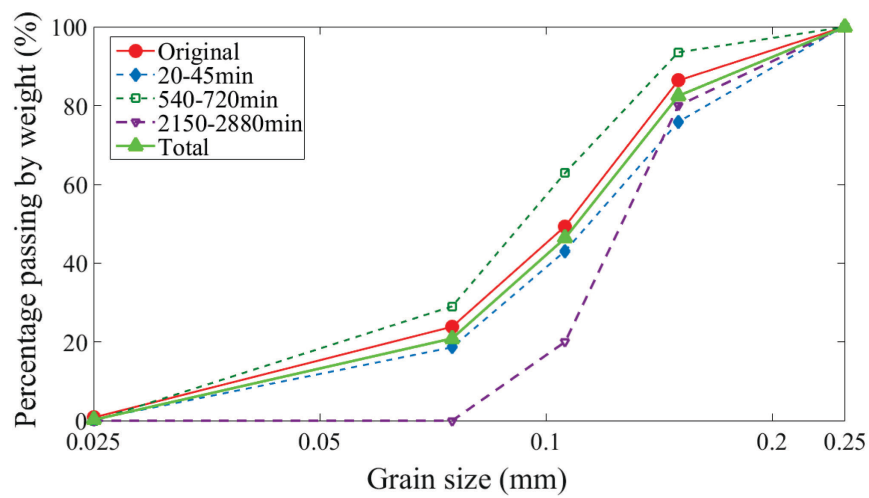
The grain size distribution of eroded fines collected for each measurement interval is examined to investigate which particle size ranege is more erodible. The grain size distribution curves for the eroded fines collected in selected intervals and total of eroded fines are shown in Fig. 7-9. As described above, it is supposed that almost all the eroded fines are originated from top of the foundation, which corresponds to Area C. In Fig. 7-9, the initial grain size distribution for material of Area C (original Silica No.8 in *Case 2*, blue colored Silica in Cases 1 and 3) is also shown by the red line. By comparing the grain size distribution of the eroded fines collected over an entire period of tests with the initial grain size distribution of fines of Area C, it can be said that both grain size distribution is similar. In addition, the grain size distribution curves for eroded fines collected in the selected intervals (the time corresponds to the measure point in Fig.7-4) are similar to the initial grain size distribution of fines of Area C when certain fines erosion is confirmed in Fig. 7-4. These indicate the horizontal fines migration near the downstream boundary is developed regardless of the size of particles. According to the studies on the bed transport in sand-gravel river, it is known that soil is transported regardless of the size of particles if the tractive force is large (Sekine, 2005). The test results suggest that erosion of internally instable material occurs independent from particle size of fines if the tractive force by seepage flow is sufficiently large.
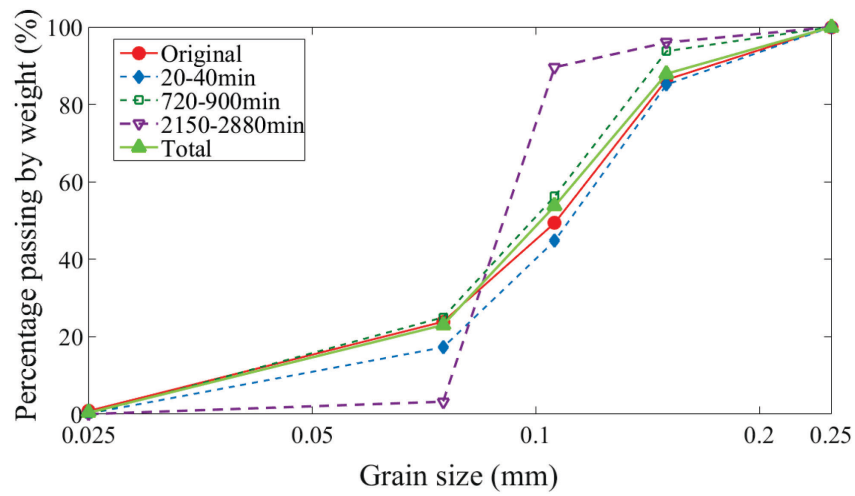
(a) *Case 1*
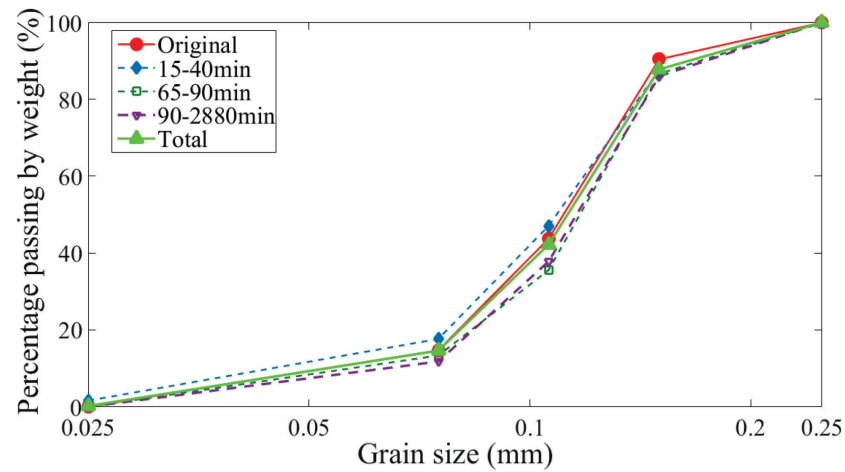
(b) *Case 2*

(c) *Case 3*

Figure 7-9   Grain size distribution curve or eroded fines

7.6. Summary

In this chapter, a series of physical model tests on seepage-induced suffusion in the small-scaled model embankment built on the foundation ground with different fines content is performed to investigate the cause of redeposition of fines.   To examine temporal and spatial variation of the fines content, sieve analyses on subdivided areas of the model embankment and particle analyses on (a) eroded particles and (b) remaining particles in the subdivided areas are also conducted and the following conclusions are drawn:

1. The larger the void at the bottom of the foundation ground, the more the downward fines transport by gravitation across the embankment.
2. Marked downward transport of the fines is observed in the upstream because of relatively small seepage force.
3. Fines migrate actively in the area where the hydraulic gradient or velocity is large.
4. Erosion of internally instable material occurs independent from particle size of fines if the tractive force by seepage flow is sufficiently large.

REFERENCES

Beguin, R., Fry, J. J., Picault, C., Courivaud, J. R., Faure, Y. H. & Philippe, P. Control of the risk of dike failure caused by contact erosion. *Proceding of 6th International Conference on Scour and Erosion*, 2012 Paris. pp. 1551-1558.

Beguin, R., Philippe, P. & Faure, Y.-H. 2013. Pore-scale flow measurements at the interface between a sandy layer and a model porous medium: Application to statistical modeling of contact erosion. *Journal of Hydraulic Engineering,* 139(1)**,** pp. 1-11.

Chang, D. S. & Zhang, L. M. 2013. Extended internal stability criteria for soils under seepage. *Soils and Foundations,* 53(4)**,** pp. 569-583.

Cyril, G., Yves-Henri, F., Beguin, R. & Chia-Chun, H. 2010. Contact erosion at the interface between granular coarse soil and various base soils under tangential flow condition. *Journal of Geotechnical and Geoenvironmental Engineering,* 136(5)**,** pp. 741-750.

Ke, L. & Takahashi, A. 2012. Strength reduction of cohesionless soil due to internal erosion induced by one-dimensional upward seepage flow. *Soils and Foundations,* 52(4)**,** pp. 698-711.

Kenney, T. C. & Lau, D. 1985. Internal stability of granular filters. *Canadian Geotechnical Journal,* 22(2)**,** pp. 215-225.

Kenney, T. C. & Lau, D. 1986. Internal stability of granular filters: Reply. *Canadian Geotechnical Journal,* 23(3)**,** pp. 420-423.

Kezdi, A. 1979. *Soil Physics: Selected Topics (Developments in Geotechnical Engineering)*, Amsterdam,New York: Elsevier Science.

Kovács, G. 1981. *Seepage Hydraulics*: Elsevier Science.

Li, M. & Fannin, R. J. 2008. Comparison of two criteria for internal stability of granular soil. *Canadian Geotechnical Journal,* 45(9)**,** pp. 1303-1309.

Ouyang, M. & Takahashi, A. Image-based quantification of size and shape of colored siliceous sand. 50th Japan National Conference on Geotechnical Engineering, 2015, Sapporo, Japan.

Saito, H., Maeda, K., Imase, T., Ito, Y. & Wakasa, A. Influence of sequential action of high-water levelon the stability of a dike. THe 49th Japan National Conference on Geotechnical Engineering, 2014, Kitakyusyu. pp. 979-980. (In Japanese).

Sekine, M. 2005. *Hydraulic of movable bed*, Kyoritsu Shuppan.(In Japasese)

Wan, C. F. & Fell, R. 2004. Experimental investigation of internal instability of soils in embankment dams and their foundations, Wales, U. o. N. S. (Sidney).

Wan, C. F. & Fell, R. 2008. Assessing the potential of internal instability and suffusion in embankment dams and their foundations. *Journal of Geotechnical and Geoenvironmental Engineering,* 134(3)**,** pp. 401-407.

Chapter 8　Conclusions

8.1.　Main conclusions

The goal of this dissertation is to examine the seepage-induced suffusion process in an embankment with foundations during the phases of initiation and continuation of erosion. To this end, firstly, preliminary physical tests in small-scaled model were conducted to find the ways to reproduce suffusion in the small model and to determine experimental conditions for further tests.　It is described in Chapter 4 and is concluded as follows:

1. Seepage-induced suffusion in embankments can be reproduced with the small-scaled loosely compacted embankment models in the laboratory.

2. The larger the fines content, the less the suffusion in the early stage of seepage tests. After a certain elapsed time, decrease of the fines due to suffusion can widen the flow channel and the internal erosion rate can increase.

3. The increase of flow velocity by suffusion makes tractive force larger.　In addition, suffusion is progressively broadened from the toe to center of the embankment.

4. Hydraulic boundary condition at the downstream has a significant effect on amount of eroded fines.

In Chapter 5, the suffusion process under the transient and steady seepage conditions in embankments are presented. Based on the finding in Chapter 4, test apparatus was improved and a series of physical model test were conducted on a homogenous embankment with the foundation.　The spatial extent of erosion-induced fines content variation is discussed through sieve analyses on subdivided areas of the model embankment after seepage testing. The obtained conclusions are:

1. Sieve analyses in each area of the embankment allow to observe the spatial distribution of fines with in the model embankment.

2. Under the transient seepage in the first permeation, major fines erosion takes place due to rising phreatic surface.　Disappearance of suction and the transportation of fines with the seepage flow change the fines content distribution in the embankment.

3. After a certain elapsed time, suffusion develops backward along the phreatic surface

143

from downstream in the embankments.   Below the phreatic surface, the erodible fines not only move laterally by seepage flow but also move vertically due to the gravitational force and are deposited in the foundation.   This deposition of the fines results in the expansion of the fine-rich region in the foundation and causes decrease in the permeability of the whole embankment.   In addition, it is confirmed that the repeated permeation leads to the prominent vertical transportation of fines from the slope zone to the foundation zone.

In Chapter 6, a physical model test on the seepage-induced suffusion on a small-scale homogeneous model embankment described in Chapter 5 was numerically simulated using existing simple erosion model based on elemental erosion tests.   The applicability and limitations of the numerical model used are discussed by comparison results of the physical model tests and numerical simulation and these are summarized as follows:

1. The numerical simulation can reproduce overall erosion response of the embankment, i.e. backward decrease in fines from the downstream.

2. Since the fines redeposition-induced clogging has considerable effects on flow field change as demonstrated in the physical model tests and previous studies, this should be considered if detailed modeling of erosion process is required.

To elaborate the cause of redeposition of fines in the seepage-induced suffusion, further physical model tests were also conducted with embankment built on the foundation ground with different fines content to investigate the cause of redeposition of fines in Chapter 7. To examine temporal and spatial variation of the fines content, sieve analyses on subdivided areas of the model embankment and particle analyses on (a) outflow particles and (b) remaining particles in the subdivided areas were also conducted after seepage testing.   The following conclusions are drawn:

1. The larger the void at the bottom of the foundation ground, the more the downward fines transport by gravitation across the embankment.

2. Marked downward transport of the fines is observed in the upstream because of relatively small seepage force.

3. Fines migrate actively in the area where the hydraulic gradient or velocity is large.

4. Erosion of internally instable material occurs independent from particle size of fines if the tractive force by seepage flow is sufficiently large.

144

8.2. Recommendations for future study

Currently, increase in fines, i.e. clogging, can be not expressed by existing internal erosion model because the erosion test used in the model calibration gives only positive erosion rate or measurement of clogging are very hard to evaluate. However, physical model tests in Chapter 5 and the previous studies (*e.g.* Lafleur, 1999; Bendahmane *et al.*, 2008; Marot *et al.*, 2012) demonstrate the considerable effect of the fines redepodition on suffusion development.

If extreme fines decreasing zone develops, the hydraulic structure becomes more vulnerable to seepage failures because of high possibility in formation of piping or backward erosion. Furthermore, extreme fines increases zone develops, the drainage system of the hydraulic structure might be deteriorated due to clogging at the downstream. This may lead to elevation of water level at the upstream and may make the hydraulic structure more vulnerable to seepage failures and/or earthquake. If the performance of an eroded hydraulic structure is of interest, detailed modeling of the erosion process is required and increase in fines in a certain area of interest should be properly considered.

REFERENCES

Bendahmane, F., Marot, D. & Alexis, A. 2008. Experimental parametric study of suffusion and backward erosion. *Journal of Geotechnical and Geoenvironmental Engineering,* 134(1)**,** pp. 57-67.

Marot, D., Bendahmane, F. & Nguyen, H. H. Influence of angularity of coarse fraction grains on internal erosion process. *Proceedings of the 6th International Conference on Scour and Erosion*, 2012 Paris. pp. 887-894.

Lafleur, J. 1999. Selection of geotextiles to filter broadly graded cohesionless soils. *Geotextiles and Geomembranes,* 17((5‑6))**,** pp. 299-312.